



JAEA-Data/Code

2018-014

DOI:10.11484/jaea-data-code-2018-014

Nuclear Data Processing Code FRENDY Version 1

Kenichi TADA, Satoshi KUNIEDA and Yasunobu NAGAYA

Nuclear Data and Reactor Engineering Division
Nuclear Science and Engineering Center
Nuclear Science Research Institute
Sector of Nuclear Science Research

January 2019

Japan Atomic Energy Agency

日本原子力研究開発機構

JAEA-
Data/
Code

本レポートは国立研究開発法人日本原子力研究開発機構が不定期に発行する成果報告書です。
本レポートの入手並びに著作権利用に関するお問い合わせは、下記あてにお問い合わせ下さい。
なお、本レポートの全文は日本原子力研究開発機構ホームページ (<https://www.jaea.go.jp>)
より発信されています。

国立研究開発法人日本原子力研究開発機構 研究連携成果展開部 研究成果管理課
〒319-1195 茨城県那珂郡東海村大字白方 2 番地4
電話 029-282-6387, Fax 029-282-5920, E-mail:ird-support@jaea.go.jp

This report is issued irregularly by Japan Atomic Energy Agency.
Inquiries about availability and/or copyright of this report should be addressed to
Institutional Repository Section,
Intellectual Resources Management and R&D Collaboration Department,
Japan Atomic Energy Agency.
2-4 Shirakata, Tokai-mura, Naka-gun, Ibaraki-ken 319-1195 Japan
Tel +81-29-282-6387, Fax +81-29-282-5920, E-mail:ird-support@jaea.go.jp

Nuclear Data Processing Code FRENDY Version 1

Kenichi TADA, Satoshi KUNIEDA and Yasunobu NAGAYA

Nuclear Data and Reactor Engineering Division
Nuclear Science and Engineering Center
Nuclear Science Research Institute
Sector of Nuclear Science Research
Japan Atomic Energy Agency
Tokai-mura, Naka-gun, Ibaraki-ken

(Received November 12, 2018)

Abstract

A new nuclear data processing code FRENDY has been developed in order to process the evaluated nuclear data library JENDL. Development of FRENDY helps to disseminate JENDL and various nuclear calculation codes.

FRENDY is developed not only to process the evaluated nuclear data file but also to implement the FRENDY functions to other calculation codes. Users can easily use many functions *e.g.*, read, write, and process the evaluated nuclear data file, in their own codes when they implement the classes of FRENDY to their codes. FRENDY is coded by considering maintainability, modularity, portability and flexibility.

The processing method of FRENDY is similar to that of NJOY. The current version of FRENDY treats the ENDF-6 format and generates the ACE file which is used for the continuous energy Monte Carlo codes such as PHITS and MCNP.

This report describes the nuclear data processing methods and input instructions for FRENDY.

Keywords: FRENDY, JENDL, Nuclear Data Processing, User's Manual

核データ処理システム FRENDY 第1版

日本原子力研究開発機構
原子力科学研究所 原子力基礎工学研究センター
核工学・炉工学ディビジョン
多田 健一、国枝 賢、長家 康展

(2018年11月12日 受理)

要旨

評価済み核データライブラリーJENDL を適切に処理するため、日本原子力研究開発機構において、核データ処理システム FRENDY を開発した。FRENDY の開発は、JENDL や日本原子力研究開発機構が提供する粒子輸送計算コードの普及に役立つことが期待される。

FRENDY 開発では、評価済み核データファイルを処理するだけでなく、他の計算コードに FRENDY の機能を実装することも念頭に置いた。利用者は FRENDY の読み書きや各処理機能について、他のコードに容易に取り込むことができる。FRENDY は保守性、簡潔性、移植性、拡張性などを考慮して作られた。

FRENDY の核データ処理手法は米国ロスアラモス国立研究所が開発した NJOY と同様である。現バージョンの FRENDY は ENDF-6 形式の評価済み核データから連続エネルギーモンテカルロ輸送計算コード PHITS や MCNP が利用する断面積ライブラリ形式である ACE ファイルを生成することができる。

本報告書では FRENDY で用いられている核データ処理手法と FRENDY の入力について説明する。

Contents

1	Introduction.....	1
1.1	Background.....	1
1.2	Overview of FRENDY	2
2	Resonance Reconstruction	5
2.1	Tasks of Resonance Reconstruction.....	5
2.1.1.	Unionization of Energy Grid.....	5
2.1.2.	Linearization of All Cross-Sections Given in File 3	5
2.1.3.	Reconstruction of Resolved and Unresolved Resonance Cross-Sections	6
2.2	Calculation Flow of Linearization and Resonance Reconstruction	7
2.2.1	Algorithm of Linearization	8
2.2.2	Linearization of All Cross-Sections without Resonance Cross-Section.....	10
2.2.3	Resonance Reconstruction and Linearization in Resonance Region	11
2.2.4	Merge and Output Cross Sections.....	12
2.3	Cross-Section Formulae in Resolved Resonance Region	12
2.3.1	Single-Level Breit-Wigner Resonance Formula	12
2.3.2	Multi-Level Breit-Wigner Resonance Formula	15
2.3.3	Adler-Adler Resonance Formula	16
2.3.4	Reich-Moore Resonance Formula.....	16
2.4	Cross-Section Formulae in Unresolved Resonance Region.....	17
3	Doppler Broadening.....	22
3.1	Task of Doppler Broadening.....	22
3.2	Calculation Flow of Doppler Broadening.....	23
3.3	Doppler Broadening Formula	25
3.3.1	Doppler Broadening Theory	25
3.3.2	Speed-Up of Doppler Broadening.....	31
3.4	Calculation of Thermal Quantities	32
4	Thermal Scattering Cross-section Calculation.....	35
4.1	Thermal Scattering Law Data	35
4.2	Calculation Flow of Thermal Scattering Cross-Sections	35
4.2.1	Coherent Elastic Scattering	36
4.2.2	Incoherent Elastic Scattering	38
4.2.3	Incoherent Inelastic Scattering.....	39
5	Probability Table Generation	45

5.1	Treatment of Self-Shielding Effect in Unresolved Resonance Region	45
5.2	Calculation Flow of Probability Table Generation.....	45
5.2.1	Determination of resonance energy.....	46
5.2.2	Determination of resonance width	47
5.2.3	Determination of Energy Grid Points.....	48
5.2.4	Calculation of Cross Sections	48
5.2.5	Calculation of the probability	52
5.3	Investigation of Appropriate Number of Ladders	53
6	Gas Production Cross-Section Calculation	63
7	ACE File Generation.....	64
8	Input Instructions	66
8.1	Input Format.....	66
8.2	FRENDDY Original Input Format.....	66
8.2.1	Processing Mode.....	67
8.2.2	Input Parameters	69
8.3	NJOY99 Compatible Format	87
8.4	Sample Input Data.....	88
8.4.1	Simplest Input Data.....	88
8.4.2	Input Data to Modify Default Input Parameters.....	89
8.4.3	Input Data to Reproduce NJOY99 Input.....	90
9	Installation of FRENDDY	98
9.1	Directory Structure.....	98
9.2	How to Install FRENDDY on Linux, UNIX, or MacOS Platforms.....	98
9.3	How to Execute FRENDDY	100
9.4	Test Calculation with Samples	100
9.5	Test Programs for Boost test Library	100
Acknowledgements.....		102
References.....		103

目 次

1	はじめに	1
1.1	背景	1
1.2	FRENZY の概要.....	2
2	共鳴再構成	5
2.1	断面積再構成の目的.....	5
2.1.1	エネルギー格リッドの統一化.....	5
2.1.2	断面積の線形化.....	5
2.1.3	分離・非分離共鳴断面積の再構成.....	6
2.2	線形化及び共鳴再構成の計算フロー.....	7
2.2.1	線形化アルゴリズム.....	8
2.2.2	断面積の線形化.....	10
2.2.3	共鳴領域の共鳴再構成と線形化.....	11
2.2.4	断面積の結合と出力.....	12
2.3	分離共鳴領域の共鳴公式.....	12
2.3.1	Breit-Wigner の一準位公式.....	12
2.3.2	Breit-Wigner の多準位公式.....	15
2.3.3	Adler-Adler の共鳴公式	16
2.3.4	Reich-Moore の共鳴公式	16
2.4	非分離共鳴領域の共鳴公式.....	17
3	ドップラー拡がりの計算.....	22
3.1	ドップラー拡がりの目的.....	22
3.2	ドップラー拡がりの計算フロー.....	23
3.3	ドップラー拡がりの計算で用いられる計算式.....	25
3.3.1	ドップラー拡がりの理論.....	25
3.3.2	ドップラー拡がりの計算の高速化.....	31
3.4	熱定数の計算.....	32
4	熱中性子散乱断面積の計算.....	35
4.1	熱中性子散乱則.....	35
4.2	熱中性子散乱断面積の計算フロー	35
4.2.1	干渉性弹性散乱断面積.....	36
4.2.2	非干渉性弹性散乱断面積.....	38
4.2.3	非干渉性非弹性散乱断面積.....	39
5	確率テーブルの生成.....	45

5.1	非分離共鳴領域での自己遮蔽効果の取り扱い.....	45
5.2	確率テーブル生成の計算フロー.....	45
5.2.1	共鳴エネルギーの決定.....	46
5.2.2	共鳴幅の決定.....	47
5.2.3	エネルギー格リッドの決定.....	48
5.2.4	断面積の計算.....	48
5.2.5	確率の計算.....	52
5.3	適切なラダー数に関する検討.....	53
6	ガス生成断面積の計算.....	63
7	ACE ファイル生成.....	64
8	入力説明	66
8.1	FRENDY で取り扱う入力形式.....	66
8.2	FRENDY 独自の入力形式.....	66
8.2.1	処理モード.....	67
8.2.2	入力パラメータ.....	69
8.3	NJOY99 互換の入力形式	87
8.4	サンプル入力.....	88
8.4.1	最も単純な入力例.....	88
8.4.2	主要パラメータを変更した入力例.....	89
8.4.3	NJOY99 の入力を再現した入力例.....	90
9	FRENDY のインストール／実行方法.....	98
9.1	ディレクトリ構造.....	98
9.2	Linux、UNIX、MacOS への FRENDY のインストール方法.....	98
9.3	FRENDY の実行方法.....	100
9.4	サンプル入力のテスト	100
9.5	Boost test Library を用いたテスト	100
謝辞	102
参考文献	103

List of Tables

Table 2.4.1 Ten Point Quadrature Weights and Abscissa for Statistical Integration ($\mu=1, 2$)	20
Table 2.4.2 Ten Point Quadrature Weights and Abscissa for Statistical Integration ($\mu=3, 4$)	21
Table 3.3.1 The relation of $\sqrt{\beta}v_t$ and the Maxwell-Boltzmann distribution $P(v_t, T)$	29
Table 5.2.1 Chi-squared random numbers $R_{\chi^2}(k)$ in PURR	48
Table 5.3.1 RMS value of probability table difference in each number of ladders (293.6 K)	54
Table 5.3.2 RMS value of probability table difference in each number of ladders (1000 K)	57
Table 5.3.3 RMS value of probability table difference in each number of ladders (2000 K)	60
Table 7.1 ACE data classes and suffixes	65
Table 8.2.1 Available processing mode	68
Table 8.2.2 Input parameter name and recommended value for common parameter	71
Table 8.2.3 Input parameter name and recommended value which are used only for thermal scattering law data.....	74
Table 8.2.4 Input parameter name and recommended value for resonance reconstruction	75
Table 8.2.5 Input parameter name and recommended value for Doppler broadening	77
Table 8.2.6 Input parameter name and recommended value for gas production cross-section calculation	79
Table 8.2.7 Input parameter name and recommended value for probability table generation	81
Table 8.2.8 Input parameter name and recommended value for thermal scattering law data	83
Table 8.2.9 Input parameter name and recommended value for ACE file generation	85

List of Figures

Figure 1.2.1 The system structure of FRENDY.....	3
Figure 2.1.1 Example of resolved, unresolved, and smooth regions	5
Figure 2.1.2 Difference of resolved and unresolved resonance regions	7
Figure 2.2.1 Calculation flow of linearization and resonance reconstruction.....	8
Figure 2.2.2 Example of the linearization flow	9
Figure 2.2.3 Example of the middle point addition and the relation of σ and σ' , and x	9
Figure 2.2.4 Example of the discontinuity treatment.....	10
Figure 2.2.5 Example of the unionization of the energy grid	11
Figure 3.1.1 Example of Doppler broadened cross-sections.....	22
Figure 3.2.1 Calculation flow of the Doppler broadening	24
Figure 3.2.2 Example of the difference of energy grids in each temperature	24
Figure 3.3.1 The relation between the neutron velocity vector v_n and the target nucleus velocity vector v_t	28
Figure 3.3.2 The relation of $\sqrt{\beta}v_t$ and the Maxwell-Boltzmann distribution $P(v_t, T)$	28
Figure 4.2.1 Calculation flow of the thermal scattering cross-sections	36
Figure 4.2.2 Example of Bragg diffraction	36
Figure 4.2.3 Example of coherent elastic scattering cross-section for a crystalline material	37
Figure 4.2.4 Example of incoherent elastic scattering cross-section	39
Figure 4.2.5 Example of incoherent inelastic scattering cross-section	42
Figure 4.2.6 Example of incoherent inelastic scattering cross-section	42
Figure 5.2.1 Example of pseudo resonance structure generation for the ladder method	46
Figure 8.2.1 Processing flow to generate ACE files	67
Figure 8.2.2 Example of input file for continuous-energy neutron data	86
Figure 8.2.3 Example of input file for thermal scattering law data	86
Figure 8.2.4 Example of input file for dosimetry data.....	86
Figure 9.1.1 Directory structure.....	98

1 Introduction

1.1 Background

The Japan Atomic Energy Agency (JAEA) has developed the evaluated nuclear data library JENDL¹⁾ and many nuclear calculation codes including a general purpose Monte Carlo code MVP²⁾, a versatile reactor analysis code system MARBLE2³⁾, and a particle and heavy-ion transport code system PHITS⁴⁾. Though JAEA developed some nuclear data processing codes a few decades ago^{5,6)}, these codes cannot treat the current nuclear data format. The current nuclear data processing code in JAEA uses the foreign processing codes, *i.e.*, NJOY^{7,8)} and PREPRO⁹⁾, and an in-house nuclear data processing code to prepare cross-section data libraries for these nuclear calculation codes. It is very difficult for users to create cross-section data libraries for these nuclear calculation codes. The users have to wait for the release of the new or the revised cross-section data library if an evaluated nuclear data library is newly released or revised.

Modification of the nuclear data processing code is required if a new nuclear data representation, *e.g.*, a new resonance format, cannot be treated by the code. The foreign processing codes are developed to process their own evaluated nuclear data libraries. If the new nuclear data representation is adopted in ENDF¹⁰⁾ or JEFF¹¹⁾, a high priority is assigned to modify NJOY and PREPRO. However, if the new nuclear data representation was used only by JENDL, the priority of modification would be low and these codes might be modified by ourselves.

Recently, the introduction of the Generalized Nuclear Data Structure (GNDS) has been considered¹²⁾ as a new nuclear data format. The current processing codes cannot treat the GNDS format without extremely large revision of the processing codes since the format uses eXtensible Markup Language (XML) and it is quite different from the current nuclear data format, *i.e.*, the ENDF-6 format¹³⁾.

JAEA has developed a new nuclear data processing code FRENDY (FRom Evaluated Nuclear Data librarY to any application) to overcome such problems¹⁴⁾. The processing method of FRENDY is similar to that of NJOY. The current version of FRENDY treats only the ENDF-6 format and generates A Compact ENDF (ACE) file which is used for the continuous energy Monte Carlo codes including PHITS, MCNP¹⁵⁾, and Serpent¹⁶⁾. Treatment of the GNDS format and generation of the other cross-section data library for the JAEA's nuclear calculation codes including multi-group cross-section data library will be implemented in the future.

This report describes an overview of the nuclear data processing methods and input instructions. As described before, the processing method of FRENDY is similar to that of NJOY. The difference of the processing method is mainly described in this report.

1.2 Overview of FRENDY

FRENDY is developed by considering maintainability, modularity, portability and flexibility. FRENDY is written in the object-oriented language C++ to achieve these requirements. The maintainability and modularity are better than the conventional codes written in FORTRAN since all classes in FRENDY were encapsulated. Each class is designed to be compact and independent for portability and flexibility. FRENDY is developed not only to process the evaluated nuclear data file but also to implement the FRENDY functions to other calculation codes. Users can easily employ many functions *e.g.*, read, write, and process the evaluated nuclear data file, in their own codes when they implement the classes of FRENDY to their codes.

The version control system Git¹⁷⁾ is used to ensure traceability and quality assurance. The version control system enables us to easily create and manage the sources. The Boost test library¹⁸⁾ is used for the test program of FRENDY. The test programs are prepared to confirm the verification of capabilities. It would be helpful to confirm each capability and avoid possible problems. For example, when a developer modifies class A and this modification affects class B, the test program of class B will alert the developer.

The system structure of FRENDY is shown in Fig. 1.2.1. The modules with solid-lined shapes have been already implemented, while the ones with dashed-lined shapes have not been developed yet. FRENDY can treat not only the ENDF-6 format but also other nuclear data formats. FRENDY converts the nuclear data from each nuclear data format to NuclearDataObject. FRENDY can treat the other nuclear data formats when parser, writer and converter modules are implemented. Each module can be easily improved, extended and modified to satisfy future needs since each module is encapsulated and is not affected by other modules. FRENDY keeps all data on NuclearDataObject and uses NuclearDataObject for the data transfer between different processing modules, *e.g.*, the resonance reconstruction and Doppler broadening, to reduce the effect of rounding errors and overhead by file access. NJOY uses an intermediate file, which is called the Point-wise Evaluated Nuclear Data Format (PENDF) file or Group-wise Evaluated Nuclear Data Format (GENDF) file, for the data transfer. Because the memory capacity of old computers was limited, the intermediate file was required to reduce the memory size. This limitation is not so meaningful from the view point of the current computational resources.

FRENDY has parser and writer modules to handle ACE file. These modules are useful for generation and modification of the ACE file. There are some cases where users want to modify a cross-section data library by themselves in order to estimate the impact of the modification of the cross-section data library on the nuclear calculation results. The ACE file uses random access with pointers to the various parts of the data. If the number of energy grid points is modified, modification of the pointer data is also required. To modify the pointer data is difficult for the nuclear calculation code users who do not know well about the ACE format. FRENDY automatically

adjusts the pointer data by the ACE data writer module. Users can modify the ACE file when they write a main (control) program with the ACE data parser and writer modules in FRENDY.

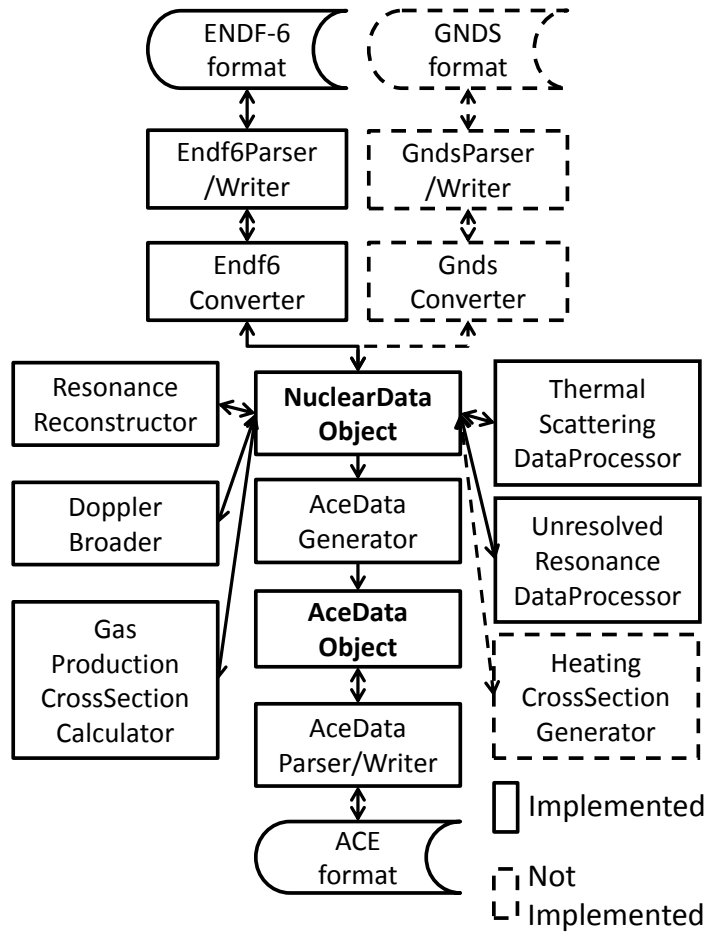


Figure 1.2.1 The system structure of FRENDY

Some modules have not been implemented yet in the current version of FRENDY. The main purpose of the first version is generation of ACE files for neutronics calculation codes which calculate multiplication factors and neutron flux distributions. Though the heating cross-section generator module is very important to calculate radiation damage, it is not so important for the neutronics calculation codes. The development priority of the GNDS treatment modules, *i.e.*, parser, writer and converter modules of the GNDS format, is not so high since the evaluated nuclear data library which is only prepared in the GNDS format has not been released yet. These modules will be developed in the near future.

FRENDY can treat the input file for NJOY and the PENDF file. NJOY is widely used in many laboratories and companies to generate the cross-section data library for their nuclear calculation codes. The NJOY users can easily use FRENDY without modification of their processing

environment, *e.g.*, running shell scripts, input files, and post processing programs. Though the current version of FRENDY processes only the ACE files, users can generate the other cross-section data libraries such as a multi-group one when they couple the NJOY modules, *e.g.*, GROUPR.

2 Resonance Reconstruction

2.1 Tasks of Resonance Reconstruction

2.1.1. Unionization of Energy Grid

Generally, the evaluated nuclear data file contains cross sections for many reactions, such as total, elastic scattering, first chance fission, second chance fission, and radiative capture cross-sections. The energy grid of cross sections is not necessarily the same for the different reactions in the evaluated nuclear data file. Considering the post process for the Doppler broadening and the cross-section data library generation, the energy grid should be unified for all the reactions.

As shown in Fig. 2.1.1, the cross-section data given in the evaluated nuclear data file is divided into three energy-regions, *i.e.*, resolved resonance, unresolved resonance, and smooth regions. In the ENDF-6 format^{[13)}, File 2 contains resonance parameters which are used to reconstruct point-wise cross sections (exceptional cases may be found for the typical light-nuclei where only File 3 is used to give the excitation functions^{[1)}). In many cases, the evaluated nuclear data file contains the resonance parameters for the total, elastic scattering, fission, and radiative capture reaction. The cross sections of other reactions and cross sections in smooth region are given in File 3, together with background cross sections which are used to supplement the cross sections in resonance region.

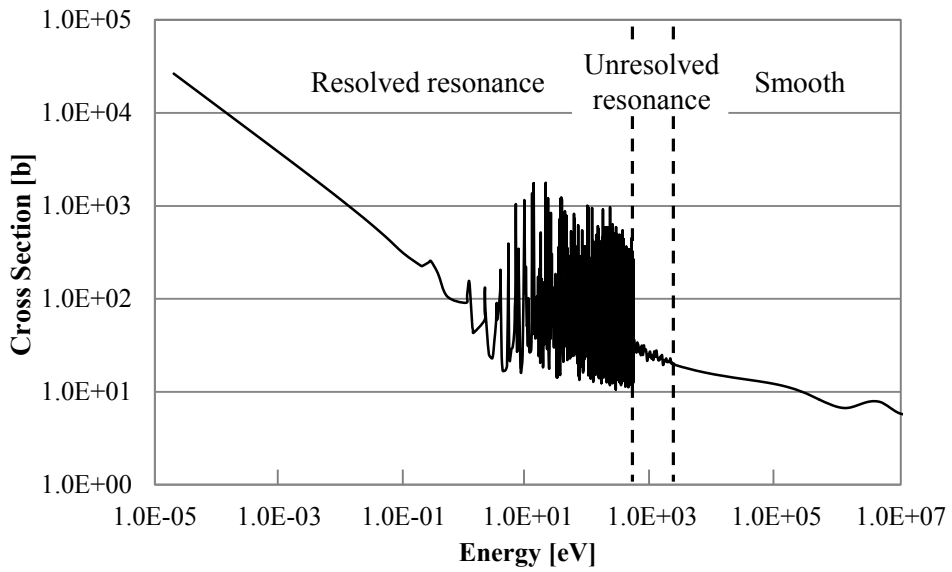


Figure 2.1.1 Example of resolved, unresolved, and smooth regions

2.1.2. Linearization of All Cross-Sections Given in File 3

The interpolation scheme is not necessarily the same for the different reactions and energy regions to describe smooth cross section curves with a minimized number of the energy grid points. For

example, the radiative capture cross-section obeys the $1/v$ law in the low energy region where it could be described with a few energy grid points by the log-log interpolation rather than the linear-linear interpolation. In contrast, the elastic scattering cross-sections are constant due to potential scattering at the low energy region. In such a case, the linear-linear interpolation is appropriate. Different interpolation schemes are usually used for each reaction in order to reduce the data size of the evaluated nuclear data file, which is inconvenient for nuclear calculation codes. Therefore, unification of the interpolation scheme is desirable for easy handling by nuclear calculation codes.

2.1.3. Reconstruction of Resolved and Unresolved Resonance Cross-Sections

A significant number of energy grid points are required to describe a resonance cross-section curve especially for heavier nuclei due to many resonance peaks. The evaluated nuclear data file provides the parameters of the cross-section formulae, *e.g.*, the Single- and Multi-Level Breit-Wigner¹⁹⁾, Adler-Adler^{20,21)}, Reich-Moore^{22,23)}, and R-matrix limited¹³⁾. The explanation of these formulae is described in Sec. 2.3.

As shown in Fig. 2.1.2, the resonance region is divided into two regions, *i.e.*, the resolved and unresolved resonance regions²⁴⁾. The resonance peaks correspond to the excited levels of a compound nucleus. As the excitation energy increases, the level spacing becomes so narrow that each excitation level cannot be separated. The region where each excited level can be resolved is called a “resolved” resonance region, whereas the region where each excited level cannot be resolved is called an “unresolved” resonance region. At the higher energy, the resonance cannot be observed. This region is called a smooth region.

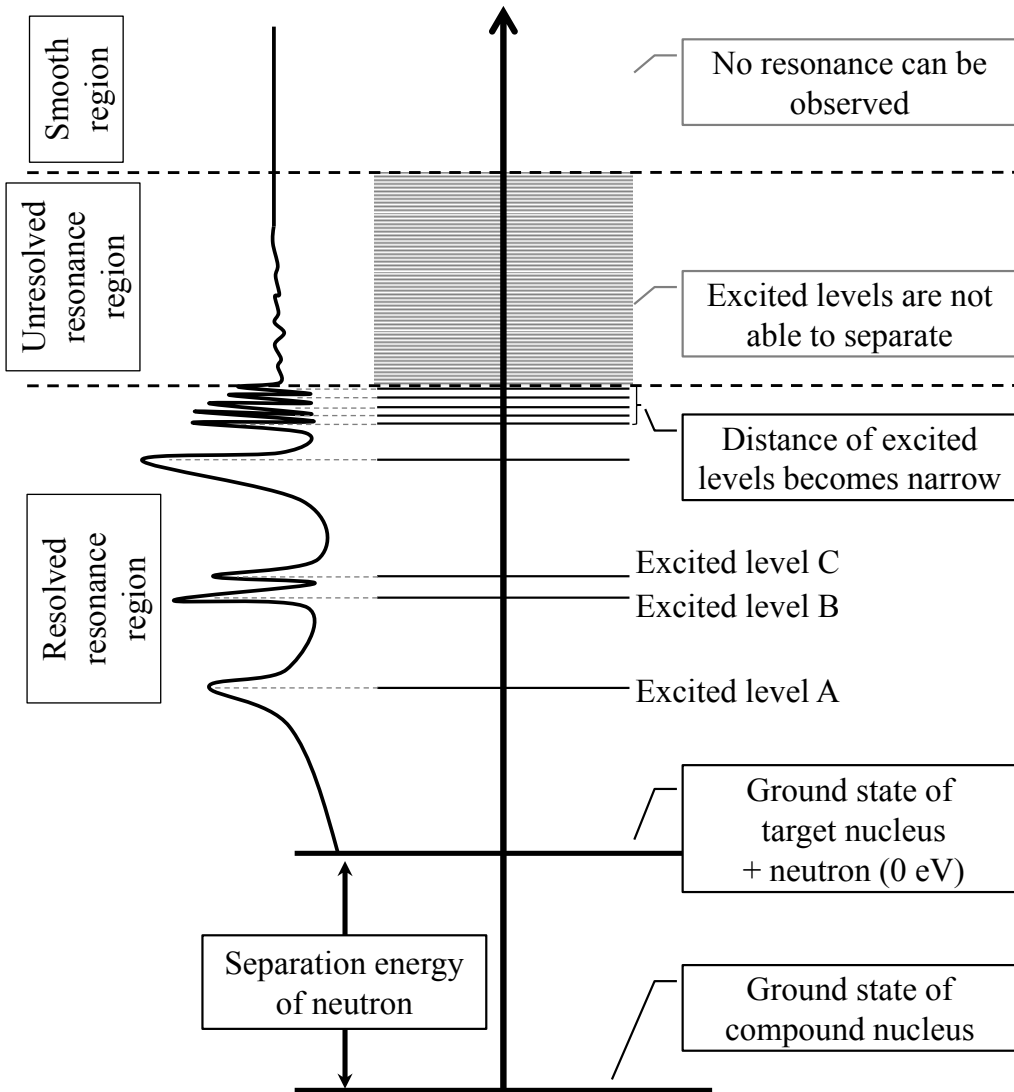


Figure 2.1.2 Difference of resolved and unresolved resonance regions

2.2 Calculation Flow of Linearization and Resonance Reconstruction

A calculation flow of the cross-section linearization and resonance reconstruction is shown in Fig. 2.2.1. The evaluated nuclear data file uses the table data for all cross-sections without resonance cross-section and the parameter of the cross-section formulae in the resonance region to describe the cross section of these regions. Therefore, the linearization process is divided into two processes, *i.e.*, the linearization of all cross-sections given in File 3 and that of the resolved and unresolved resonance cross-sections given in File 2. The evaluated nuclear data file might contain background cross-sections in the resolved and unresolved resonance regions in File 3. The background cross-sections are also linearized in the former process.

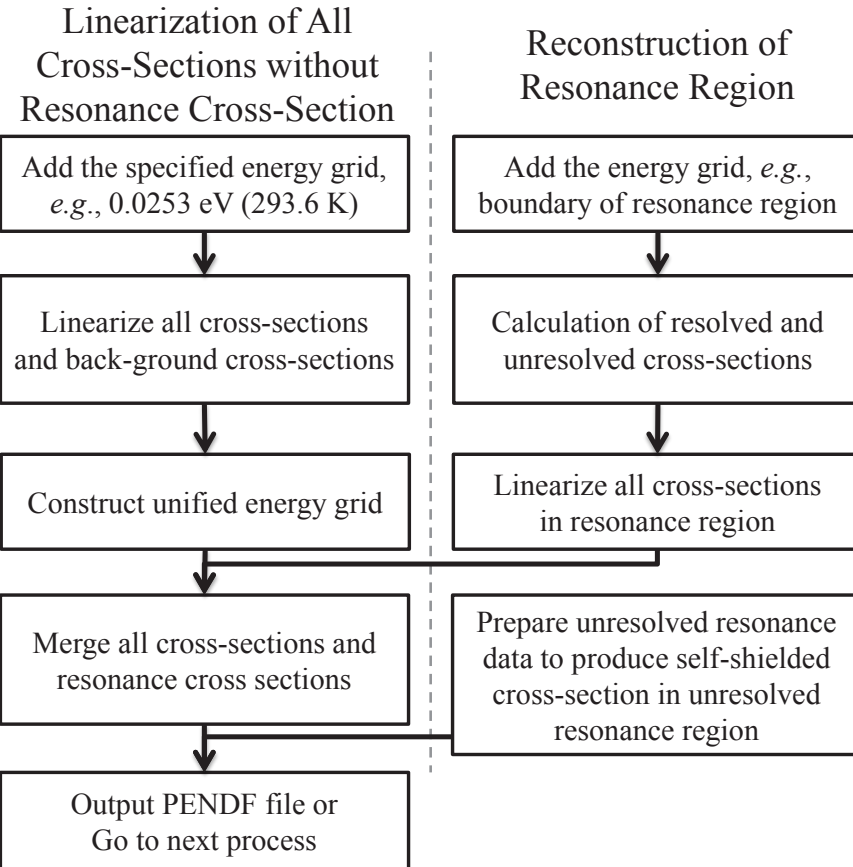


Figure 2.2.1 Calculation flow of linearization and resonance reconstruction

2.2.1 Algorithm of Linearization

An algorithm of the linearization is shown in Fig. 2.2.2. The linearization flow is as follows:

1. If the distance of energy grid points is large, a middle energy grid point is added.
2. Calculate the cross sections $\sigma_{i+1/2}$ and $\sigma'_{i+1/2}$ at the middle point $x_{i+1/2}$.
3. If $\sigma'_{i+1/2}$ does not satisfy Eqs. (2.2.2) and (2.2.3), the middle energy grid point is added.
4. If $\sigma'_{i+1/2}$ satisfies Eqs. (2.2.2) and (2.2.3), go to next energy grid point ($i=i+1$).

Here, σ is a cross section in the original interpolation, σ' a cross section interpolated by the linear-linear interpolation, i an index of energy grid point, and x an incident particle energy. They are shown in Fig. 2.2.3. FRENDY uses three criteria for linearizing the cross section, *i.e.*, the distance of energy grid points (dif_1), relative difference of $\sigma_{i+1/2}$ and $\sigma'_{i+1/2}$ (dif_2), and integral difference of $\sigma_{i+1/2}$ and $\sigma'_{i+1/2}$ (dif_3), where

$$dif_1 = \frac{x_{i+1}}{x_i} > 1.0 + \sqrt{5.3 \times err}, \quad (2.2.1)$$

$$dif_2 = \frac{|\sigma'_{i+1/2} - \sigma_{i+1/2}|}{\sigma_{i+1/2}} \leq err, \quad (2.2.2)$$

$$dif_3 = \left(\frac{x_{i+1} - x_i}{2} \right) |\sigma'_{i+1/2} - \sigma_{i+1/2}| \leq err_{int} \times x_{i+\frac{1}{2}}, \quad (2.2.3)$$

err and err_{int} are the tolerance value and maximum integral error for linearization. These values are input for nuclear data processing codes.

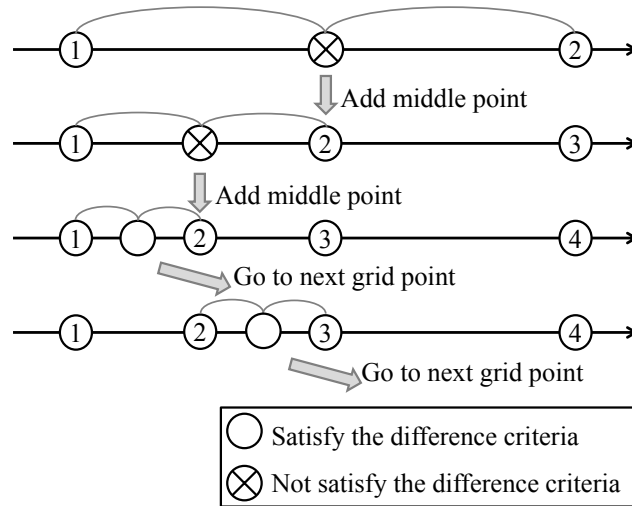


Figure 2.2.2 Example of the linearization flow

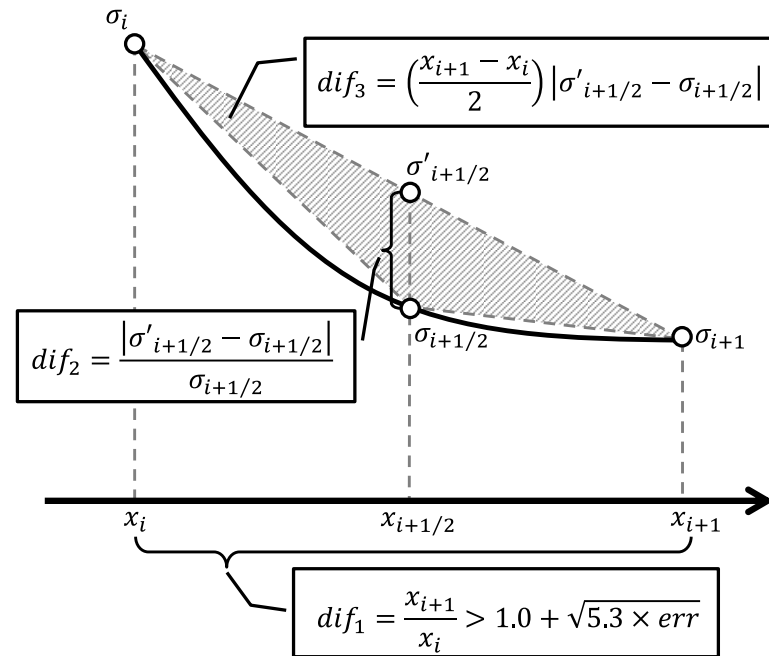


Figure 2.2.3 Example of the middle point addition and the relation of σ and σ' , and x

2.2.2 Linearization of All Cross-Sections without Resonance Cross-Section

FRENODY adds the specified energy grid points to all the reaction types before linearization. FRENODY automatically adds energy grid points, *i.e.*, $1.0 \times 10^{\pm n}$, $2.0 \times 10^{\pm n}$, and $5.0 \times 10^{\pm n}$ eV, where, n is an integer. Cross sections are measured at 293.6 K in most cases. At 293.6 K, the most probable neutron energy E is

$$E = k_B T = \frac{1.3806488 \times 10^{-23} [\text{J/K}]}{1.6021766 \times 10^{-19} [\text{J/eV}]} \times 293.6 [\text{K}] = 0.0253 [\text{eV}], \quad (2.2.4)$$

where, k_B is the Boltzmann constant. The most probable neutron energy $E = 0.0253$ eV is automatically added in the grid points. FRENODY is also able to add the arbitrary energy grid points specified in the input file by users.

As shown in Fig. 2.2.4, FRENODY modifies discontinuity points. In the evaluated nuclear data file, the discontinuities are often found at the energy where two different values are given. For instance, the discontinuities are found at the boundary of the resonance region. When the discontinuity is found, FRENODY deletes the energy grid point E_0 , and adds the energy grid points $E_0 \pm \Delta E$ to obtain a continuous curve of the cross section. ΔE is determined so that

$$\Delta E = \frac{E_0 \times 10^{-7}}{\text{Significand of } E_0}. \quad (2.2.5)$$

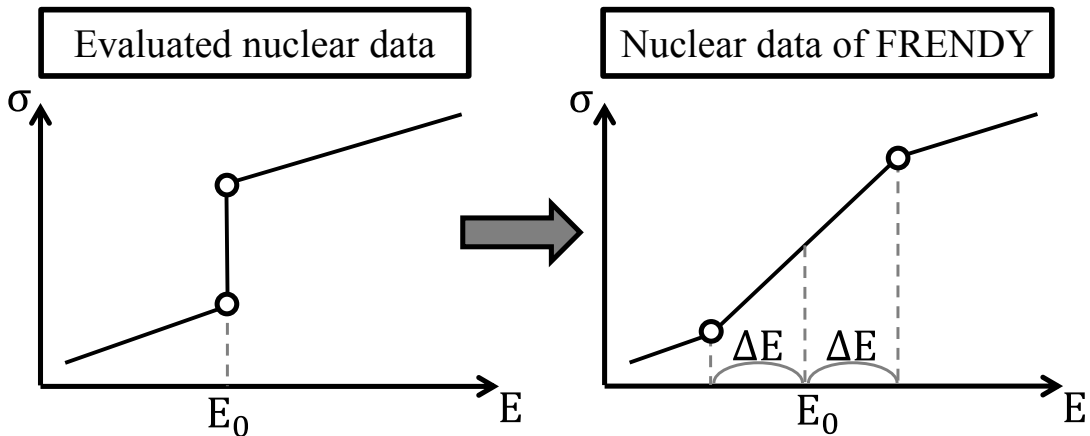


Figure 2.2.4 Example of the discontinuity treatment

The energy grid points in each reaction are unionized as shown in Fig. 2.2.5. In the unionized energy grid, a cross section is calculated by the interpolation when the corresponding energy grid is not found in the original energy grid. If the relative difference of the energy grid point is less than 1.0×10^{-10} eV, FRENODY assumes that both energy grid points are identical.

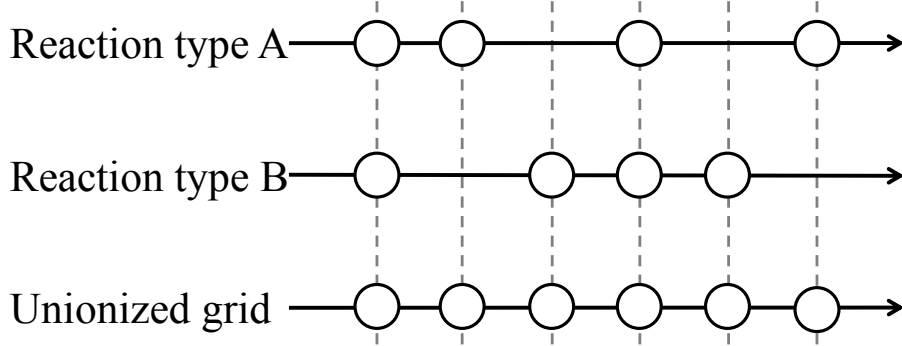


Figure 2.2.5 Example of the unionization of the energy grid

2.2.3 Resonance Reconstruction and Linearization in Resonance Region

FRENODY uses the energy grid points obtained in Sec. 2.2.2 as initial grid points. FRENODY adds energy grid points before linearization, *i.e.*, $1.0 \times 10^{\pm n}$, $2.0 \times 10^{\pm n}$, $5.0 \times 10^{\pm n}$, and 0.0253 eV, in the resolved resonance region, and also adds 13 energy grid points per decade, *i.e.*, $1.0 \times 10^{\pm n}$, $1.25 \times 10^{\pm n}$, $1.5 \times 10^{\pm n}$, $1.7 \times 10^{\pm n}$, $2.0 \times 10^{\pm n}$, $2.5 \times 10^{\pm n}$, $3.0 \times 10^{\pm n}$, $3.5 \times 10^{\pm n}$, $4.0 \times 10^{\pm n}$, $5.0 \times 10^{\pm n}$, $6.0 \times 10^{\pm n}$, $7.2 \times 10^{\pm n}$, and $8.5 \times 10^{\pm n}$ eV, in the unresolved resonance region.

The boundary of the resolved and unresolved resonance regions is the discontinuity point. As shown in Fig. 2.2.4, FRENODY splits the energy grid at the boundaries of the resonance regions, *i.e.*, $E_{low}^{reso} \rightarrow E_{low}^{reso} + \Delta E$, $E_{high}^{reso} \rightarrow E_{high}^{reso} - \Delta E$, $E_{low}^{unreso} \rightarrow E_{low}^{unreso} + \Delta E$, and $E_{high}^{unreso} \rightarrow E_{high}^{unreso} - \Delta E$ to modify the discontinuities at the boundary of the resolved and the unresolved resonance regions. E_{low}^{reso} and E_{high}^{reso} are the lower and upper limit energies of the resolved resonance region, respectively. E_{low}^{unreso} and E_{high}^{unreso} are the lower and upper limit energies of the unresolved resonance region, respectively.

In the unresolved resonance region, the ENDF-6 format contains the interpolation scheme to represent the cross section¹³⁾. NJOY calculates the unresolved resonance cross-section using the cross-section formulae on the fixed energy grid points and the other energy grid points between the fixed energy grid points are calculated by the log-log interpolation. FRENODY does not use the interpolation and calculates the unresolved resonance cross-sections on all energy grid points using the cross-section formulae to rigorously reproduce the unresolved resonance cross-sections.

The resonance cross-sections are also linearized using the similar method which is described in Sec. 2.2.1. If $\sigma'_{r,i+1/2}$ does not satisfy Eq. (2.2.6), a middle energy grid point is added so that

$$E \times [dif_{1,r}]_{max} < err \cup \left(dif_{1,r} \leq err_{max} \cap dif_{2,r} \leq err_{int} \times x_{i+\frac{1}{2}} \right)_{r \in All}, \quad (2.2.6)$$

where r is the type of a reaction and err and err_{int} are the tolerance value and maximum integral error for linearization, and

$$dif_{1,r} = \frac{|\sigma'_{r,i+1/2} - \sigma_{r,i+1/2}|}{\sigma_{r,i+1/2}}, \quad (2.2.7)$$

$$dif_{2,r} = \frac{1}{2}(x_{i+1} - x_i)|\sigma'_{r,i+1/2} - \sigma_{r,i+1/2}|. \quad (2.2.8)$$

In the ENDF-6 format file (MT 151 section of File 2 except for LRF=3 and 7), the resonance parameters for the total, elastic scattering, fission and radiative capture cross-sections are stored. The symbol $[dif_{1,r}]_{max}$ indicates the maximum relative difference in each reaction.

2.2.4 Merge and Output Cross Sections

The linearized cross sections in the smooth and resonance regions are merged. FRENDY checks the consistency of the cross sections and corrects the total and total inelastic scattering cross-sections when the cross sections are merged. The total (MT 1) and total inelastic scattering cross-sections (MT 4) obtained by evaluated nuclear data file may be different from the sum of each component cross-section. Thus, FRENDY makes the total and total inelastic scattering cross-sections from the sum of each component cross-section.

Though the reconstruction of the resonance cross-sections is appropriately carried out, the resonance cross-sections occasionally become negative due to a limitation of resonance formulae. In such a case, FRENDY sets the cross section as 1.0×10^{-15} b.

As described in Sec. 1.3, FRENDY can treat and write PENDF file. The PENDF file contains the self-shielded cross-sections in the unresolved resonance region in MT 152 section of File 2.

2.3 Cross-Section Formulae in Resolved Resonance Region

This section describes the cross-section formulae in the resolved resonance region^{8,13)}. The derivation of the cross-section formulae is written in References 25 and 26.

The ENDF-6 format adopts the Single- and Multi-Level Breit-Wigner, Adler-Adler, Reich-Moore, and R-matrix limited and FRENDY can treat all resonance formulae. FRENDY uses the AMUR code²⁷⁾ to calculate the R-matrix limited.

2.3.1 Single-Level Breit-Wigner Resonance Formula

The Single-Level Breit-Wigner (SLBW) resonance formula is as follows:

$$\sigma_{n,n}(E) = \sigma_p + \frac{4\pi}{k^2} \sum_J g_J \sum_l \sum_r \frac{\Gamma_{n,r}(E)}{\Gamma_r} \left\{ \begin{aligned} & \left[\cos 2\phi_l - \left(1 - \frac{\Gamma_{n,r}(E)}{\Gamma_r} \right) \right] \psi(x) \\ & + [\sin 2\phi_l] \chi(x) \end{aligned} \right\}, \quad (2.3.1)$$

$$\sigma_f(E) = \frac{4\pi}{k^2} \sum_J g_J \sum_r \frac{\Gamma_{n,r}(E) \Gamma_{f,r}}{\Gamma_r^2} \psi(x), \quad (2.3.2)$$

$$\sigma_\gamma(E) = \frac{4\pi}{k^2} \sum_J g_J \sum_r \frac{\Gamma_{n,r}(E)\Gamma_{\gamma,r}}{\Gamma_r^2} \psi(x), \quad (2.3.3)$$

$$\sigma_t(E) = \sigma_{n,n}(E) + \sigma_f(E) + \sigma_\gamma(E), \quad (2.3.4)$$

$$\sigma_p = \frac{4\pi}{k^2} \sum_l (2l+1) \sin^2 \phi_l, \quad (2.3.5)$$

where $\sigma_{n,n}$ is the elastic scattering cross-section, σ_p the potential scattering cross-section, σ_f the fission cross-section, σ_γ the radiative capture cross-section, E the incident neutron energy [eV], g_J the spin statistical factor, k the neutron wave number, Γ the total width, Γ_n the neutron width, Γ_f the total width, Γ_γ the capture width, ϕ_l the phase shift, and

$$k = \frac{2\pi}{h} \sqrt{2m_n E} \frac{A}{A+1} = (2.196771 \times 10^{-3}) \frac{A}{A+1} \sqrt{E}, \quad (2.3.6)$$

$$g_J = \frac{2J+1}{2(2I+1)} = \frac{2J+1}{4I+2}, \quad (2.3.7)$$

$$\Gamma_{n,r}(E) = \frac{P_l(E)\Gamma_{n,r}}{P_l(|E_r|)}, \quad (2.3.8)$$

$$\psi(x) = \frac{1}{1+x^2}, \quad (2.3.9)$$

$$\chi(x) = \frac{x}{1+x^2}, \quad (2.3.10)$$

$$x = \frac{2(E - E'_r)}{\Gamma_r}, \quad (2.3.11)$$

$$E'_r = E_r + \frac{S_l(|E_r|) - S_l(E)}{2P_l(|E_r|)} \Gamma_{n,r}(|E_r|). \quad (2.3.12)$$

Here h is Planck's constant, m_n the mass of the neutron, A the ratio of the mass of the isotope to that of the neutron, I the target spin, P_l the penetration factor, S_l the shift factor, and E_r the resonance energy [eV]. The phase shift ϕ_l is given by^{13,25,28,29}

$$\phi_l = \phi_{l-1} - \tan^{-1} \left(\frac{P_{l-1}}{l - S_{l-1}} \right), \quad (2.3.13)$$

$$\phi = \hat{\rho}, \quad (2.3.14)$$

$$\phi_1 = \hat{\rho} - \tan^{-1} \hat{\rho}, \quad (2.3.15)$$

$$\phi_2 = \hat{\rho} - \tan^{-1} \frac{3\hat{\rho}}{3 - \hat{\rho}^2}, \quad (2.3.16)$$

$$\phi_3 = \hat{\rho} - \tan^{-1} \frac{\hat{\rho}(15 - \hat{\rho}^2)}{15 - 6\hat{\rho}^2}, \quad (2.3.17)$$

$$\phi_4 = \hat{\rho} - \tan^{-1} \frac{\hat{\rho}(105 - 10\hat{\rho}^2)}{105 - 45\hat{\rho}^2 + \hat{\rho}^4}. \quad (2.3.18)$$

The penetration factor P_l is given by^{13,25,28,29)}

$$P_l = \frac{\rho^2 P_{l-1}}{(l - S_{l-1})^2 + P_{l-1}^2}, \quad (2.3.19)$$

$$P_0 = \rho, \quad (2.3.20)$$

$$P_1 = \frac{\rho^3}{\rho^2 + 1}, \quad (2.3.21)$$

$$P_2 = \frac{\rho^5}{\rho^4 + 3\rho^2 + 9}, \quad (2.3.22)$$

$$P_3 = \frac{\rho^7}{\rho^6 + 6\rho^4 + 45\rho^2 + 225}, \quad (2.3.23)$$

$$P_4 = \frac{\rho^9}{\rho^8 + 10\rho^6 + 135\rho^4 + 1575\rho^2 + 11025}. \quad (2.3.24)$$

The shift factor S_l is given by^{13,25,28,29)}

$$S_l = \frac{\rho^2(l - S_{l-1})}{(l - S_{l-1})^2 + P_{l-1}^2} - l, \quad (2.3.25)$$

$$S_0 = 0, \quad (2.3.26)$$

$$S_1 = -\frac{1}{\rho^2 + 1}, \quad (2.3.27)$$

$$S_2 = -\frac{3\rho^2 + 18}{\rho^4 + 3\rho^2 + 9}, \quad (2.3.28)$$

$$S_3 = -\frac{6\rho^4 + 90\rho^2 + 675}{\rho^6 + 6\rho^4 + 45\rho^2 + 225}, \quad (2.3.29)$$

$$S_4 = -\frac{10\rho^6 + 270\rho^4 + 4725\rho^2 + 44100}{\rho^8 + 10\rho^6 + 135\rho^4 + 1575\rho^2 + 11025}, \quad (2.3.30)$$

where

$$\rho = ka, \quad (2.3.31)$$

$$\hat{\rho} = k\hat{a}. \quad (2.3.32)$$

Here a and \hat{a} are the channel radii in units of 10^{-12} cm. In the ENDF-6 format, the meaning of a and \hat{a} varies with the value of NRO and $NAPS$ in MT 151 section of File 2 as follows:

$$a = \begin{cases} 0.123A^{\frac{1}{3}} + 0.08 & (NAPS = 0) \\ \hat{a} & (NAPS = 1), \\ AP & (NAPS = 2) \end{cases} \quad (2.3.33)$$

$$\hat{a} = \begin{cases} AP & (NRO = 0) \\ AP(E) & (NRO = 1). \end{cases} \quad (2.3.34)$$

The quantities AP and $AP(E)$ are given in File 2 if required.

The SLBW resonance formulae can represent the Doppler broadened cross-section using the ψ - χ

method³⁰⁾. In the ψ - χ method, the cross-section at T K is calculated as follows^{8,26,29)}:

$$\sigma_{n,n}(E) = \sigma_p + \frac{4\pi}{k^2} \sum_J g_J \sum_l \sum_r \frac{\Gamma_{n,r}(E)}{\Gamma_r} \left\{ \left[\cos 2\phi_l - \left(1 - \frac{\Gamma_{n,r}(E)}{\Gamma_r} \right) \right] \psi(\theta, x) \right. \\ \left. + [\sin 2\phi_l] \chi(\theta, x) \right\}, \quad (2.3.35)$$

$$\sigma_f(E) = \frac{4\pi}{k^2} \sum_J g_J \sum_r \frac{\Gamma_{n,r}(E) \Gamma_{f,r}}{\Gamma_r^2} \psi(\theta, x), \quad (2.3.36)$$

$$\sigma_\gamma(E) = \frac{4\pi}{k^2} \sum_J g_J \sum_r \frac{\Gamma_{n,r}(E) \Gamma_{\gamma,r}}{\Gamma_r^2} \psi(\theta, x), \quad (2.3.37)$$

where

$$\psi(\theta, x) = \frac{\sqrt{\pi}}{2} \theta \times \text{Re} \left[W \left(\frac{\theta x}{2}, \frac{\theta}{2} \right) \right], \quad (2.3.38)$$

$$\chi(\theta, x) = \frac{\sqrt{\pi}}{2} \theta \times \text{Im} \left[W \left(\frac{\theta x}{2}, \frac{\theta}{2} \right) \right], \quad (2.3.39)$$

$$\theta = \frac{\Gamma}{\sqrt{\frac{4k_B T E}{A}}} \quad (2.3.40)$$

The symbol $W(x, y)$ is the complex error function. The complex error function is defined by

$$W(x, y) = W(z) = e^{-z^2} \text{erfc}(-iz) = \frac{2e^{-z^2}}{\sqrt{\pi}} \int_{-iz}^{\infty} e^{-t^2} dt = \frac{i}{\pi} \int_{-\infty}^{\infty} \frac{e^{-t^2}}{z-t} dt, \quad (2.3.41)$$

$$z = x + iy, \quad (2.3.42)$$

where $\text{erfc}(z)$ is the complementary error function.

2.3.2 Multi-Level Breit-Wigner Resonance Formula

The Multi-Level Breit-Wigner (MLBW) resonance formula is the same as the SLBW resonance formula, except for the elastic scattering cross-section. The elastic scattering cross-section is as follows:

$$\sigma_{n,n}(E) = \frac{4\pi}{k^2} \sum_l \sum_J g_J \left\{ \left(1 - \cos 2\phi_l - \sum_r \frac{\Gamma_{n,r}(E)}{\Gamma_r} \frac{2}{1+x_r^2} \right)^2 \right. \\ \left. + \left(\sin 2\phi_l + \sum_r \frac{\Gamma_{n,r}(E)}{\Gamma_r} \frac{2x_r}{1+x_r^2} \right)^2 + 2D_l(1 - \cos 2\phi_l) \right\}, \quad (2.3.43)$$

where

$$D_l = (2l+1) - \sum_{J=\left|l-l-\frac{1}{2}\right|}^{l+l+\frac{1}{2}} g_J. \quad (2.3.44)$$

2.3.3 Adler-Adler Resonance Formula

The Adler-Adler resonance formula is as follows:

$$\sigma_t(E) = \sigma_p + \frac{\pi\sqrt{E}}{k^2} \left\{ \sum_r \frac{1}{v_{t,r}} \left[(G_{t,r} \cos 2\phi_0 + H_{t,r} \sin 2\phi_0) \times \psi(x_{t,r}) \right] \right\}, \quad (2.3.45)$$

$$\text{where } G_{t,r} = \frac{A_{t,1}}{E} + \frac{A_{t,2}}{E^2} + \frac{A_{t,3}}{E^3} + \frac{A_{t,4}}{E^4}, \quad H_{t,r} = +A_{t,1} + \frac{A_{t,2}}{E} + \frac{A_{t,3}}{E^2} + \frac{A_{t,4}}{E^3} + B_{t,1}E + B_{t,2}E^2.$$

$$\sigma_f(E) = \frac{\pi\sqrt{E}}{k^2} \sum_r \left\{ \sum_r \frac{1}{v_r} (G_{f,r} \psi(x_{f,r}) + H_{f,r} \chi(x_{f,r})) \right\}, \quad (2.3.46)$$

$$\text{where } G_{f,r} = \frac{A_{f,1}}{E} + \frac{A_{f,2}}{E^2} + \frac{A_{f,3}}{E^3} + \frac{A_{f,4}}{E^4}, \quad H_{f,r} = +A_{f,1} + \frac{A_{f,2}}{E} + \frac{A_{f,3}}{E^2} + \frac{A_{f,4}}{E^3} + B_{f,1}E + B_{f,2}E^2.$$

$$\sigma_\gamma(E) = \frac{\pi\sqrt{E}}{k^2} \sum_r \left\{ \sum_r \frac{1}{v_r} (G_{\gamma,r} \psi(x_{\gamma,r}) + H_{\gamma,r} \chi(x_{\gamma,r})) \right\}, \quad (2.3.47)$$

$$\text{where } G_{\gamma,r} = \frac{A_{\gamma,1}}{E} + \frac{A_{\gamma,2}}{E^2} + \frac{A_{\gamma,3}}{E^3} + \frac{A_{\gamma,4}}{E^4}, \quad H_{\gamma,r} = +A_{\gamma,1} + \frac{A_{\gamma,2}}{E} + \frac{A_{\gamma,3}}{E^2} + \frac{A_{\gamma,4}}{E^3} + B_{\gamma,1}E + B_{\gamma,2}E^2.$$

$$\sigma_{n,n}(E) = \sigma_t(E) - \sigma_f(E) - \sigma_\gamma(E), \quad (2.3.48)$$

$$\sigma_p = \frac{4\pi}{k^2} \sin^2 \phi_0, \quad (2.3.49)$$

where

$$\psi(x_{c,r}) = \frac{1}{x_{c,r}^2 + 1}, \quad (2.3.50)$$

$$\chi(x_{c,r}) = \frac{x_{c,r}}{x_{c,r}^2 + 1}, \quad (2.3.51)$$

$$x_{c,r} = \frac{\mu_{c,r} - E}{v_{c,r}}. \quad (2.3.52)$$

Here $v_{c,r}$ is the resonance half-width $\Gamma_{c,r}/2$ for the reaction type c , $G_{c,r}$ the symmetrical parameter for the reaction type c , $H_{c,r}$ the asymmetrical parameter for reaction type c , and $A_{c,i}$ and $B_{c,j}$ the background constants for the reaction type c , and $\mu_{c,r}$ the resonance energy for the reaction type c . These values are obtained from the evaluated nuclear data file.

2.3.4 Reich-Moore Resonance Formula

The Reich-Moore resonance formula is as follows:

$$\sigma_t(E) = \frac{2\pi}{k^2} \sum_l \sum_J g_J \{(1 - \text{Re}[U_{n,n}^{l,J}]) + 2d_{l,J}(1 - \cos 2\phi_l)\}, \quad (2.3.53)$$

$$\sigma_{n,n}(E) = \frac{\pi}{k^2} \sum_l \sum_J g_J \{|1 - U_{n,n}^{l,J}|^2 + 2d_{l,J}(1 - \cos 2\phi_l)\}, \quad (2.3.54)$$

$$\sigma_f(E) = \frac{4\pi}{k^2} \sum_l \sum_J g_J \sum_c |L_{n,c}^{l,J}|^2, \quad (2.3.55)$$

$$\sigma_\gamma(E) = \sigma_t(E) - \sigma_{n,n}(E) - \sigma_f(E). \quad (2.3.56)$$

Here $U_{n,n}^{l,J}$ is an element of the collision matrix and $L_{n,c}^{l,J}$ is an element of the R-matrix $\mathbf{R}^{l,J}$ which are given by

$$U_{n,n}^{l,J} = e^{2i\phi_l} (2L_{n,n}^{l,J} - 1), \quad (2.3.57)$$

$$L_{n,c}^{l,J} = (\mathbf{R}^{l,J})_{n,c}^{-1}, \quad (2.3.58)$$

$$R_{n,c}^{l,J} = \delta_{n,c} - \frac{i}{2} \sum_r \frac{\Gamma_{n,r}^{\frac{1}{2}} \Gamma_{c,r}^{\frac{1}{2}}}{E_r - E - \frac{i}{2} \Gamma_{r,r}}. \quad (2.3.59)$$

The term d_{lJ} is used to account for the possibility of an additional contribution to the potential scattering cross-section from the second channel spin. It is unity when there is a second J value equal to J , and zero otherwise^{8,13)}.

It is difficult to calculate the inverse matrix $(\mathbf{R}^{l,J})_{n,c}^{-1}$ directly since the R-matrix is the complex matrix. In the ENDF-6 format, the maximum number of channels is 3, *i.e.*, 1 channel for elastic scattering and 2 channels for fission. Therefore, the maximum matrix size of the R-matrix $\mathbf{R}^{l,J}$ in Eq. (2.3.59) is 3×3 . The inverse of 3×3 complex matrix can be analytically calculated without using the iteration method. FRENDY directly calculates the inverse of 3×3 complex matrix as follows:

$$\mathbf{R}^{-1} = \frac{1}{\det \mathbf{R}} \begin{pmatrix} R_{2,2}R_{3,3} - R_{2,3}R_{3,2} & R_{1,3}R_{3,2} - R_{1,2}R_{3,3} & R_{1,2}R_{2,3} - R_{1,3}R_{2,2} \\ R_{2,3}R_{3,1} - R_{2,1}R_{3,3} & R_{1,1}R_{3,3} - R_{1,3}R_{3,1} & R_{1,3}R_{2,1} - R_{1,1}R_{2,3} \\ R_{2,1}R_{3,2} - R_{2,2}R_{3,1} & R_{1,2}R_{3,1} - R_{1,1}R_{3,2} & R_{1,1}R_{2,2} - R_{1,2}R_{2,1} \end{pmatrix}, \quad (2.3.60)$$

where

$$\mathbf{R} = \begin{pmatrix} R_{1,1} & R_{1,2} & R_{1,3} \\ R_{2,1} & R_{2,2} & R_{2,3} \\ R_{3,1} & R_{3,2} & R_{3,3} \end{pmatrix}, \quad (2.3.61)$$

$$\det \mathbf{R} = \frac{R_{1,1}R_{2,2}R_{3,3} + R_{2,1}R_{3,2}R_{1,3} + R_{3,1}R_{1,2}R_{2,3}}{-R_{1,1}R_{3,2}R_{2,3} - R_{3,1}R_{2,2}R_{1,3} - R_{2,1}R_{1,2}R_{3,3}}. \quad (2.3.62)$$

2.4 Cross-Section Formulae in Unresolved Resonance Region

In the ENDF-6 format, only the Single-Level Breit-Wigner representation is available for the unresolved resonance region¹³⁾.

Each resonance parameter cannot be determined in the unresolved resonance region. The average value and the distribution are used to represent the unresolved resonance cross-sections. Porter and Thomas revealed that the reaction width distribution is described by the chi-square distribution³¹⁾:

$$P_\mu(x) = \frac{\mu}{2} \frac{1}{\Gamma(\frac{\mu}{2})} \left(\frac{\mu x}{2} \right)^{\frac{\mu}{2}-1} e^{-\frac{\mu x}{2}}, \quad (2.4.1)$$

where $P_\mu(x)$ is the chi-square distribution for μ degrees of freedom, x the ratio of $\Gamma(E)$ to $\bar{\Gamma}$:

$$x = \frac{\Gamma(E)}{\bar{\Gamma}}. \quad (2.4.2)$$

$\Gamma(E)$ is the reaction width at energy E , and $\bar{\Gamma}$ the average reaction width. It should be noted that $\Gamma(\mu/2)$ in Eq. (2.4.1) is the gamma function. The unresolved resonance cross-sections are obtained using the chi-square distribution and the average reaction width which are obtained from the evaluated nuclear data file.

Infinitely dilute cross-sections in the unresolved resonance region are defined based on the SLBW approximation as follows^{8,13)}:

$$\sigma_t = \sigma_{n,n} + \sigma_\gamma + \sigma_f, \quad (2.4.3)$$

$$\sigma_\gamma = \frac{2\pi^2}{k^2} \sum_l \frac{g_J}{\bar{D}} \langle \frac{\Gamma_n \Gamma_\gamma}{\Gamma} \rangle, \quad (2.4.4)$$

$$\sigma_f = \frac{2\pi^2}{k^2} \sum_l \frac{g_J}{\bar{D}} \langle \frac{\Gamma_n \Gamma_f}{\Gamma} \rangle, \quad (2.4.5)$$

$$\sigma_{n,n} = \sigma_p + \frac{2\pi^2}{k^2} \sum_l \frac{g_J}{\bar{D}} \left(\langle \frac{\Gamma_n \Gamma_n}{\Gamma} \rangle - 2\bar{\Gamma}_n \sin^2 \varphi_l \right), \quad (2.4.6)$$

where

$$\begin{aligned} \langle \frac{\Gamma_{n,l} \Gamma_{f,l}}{\Gamma} \rangle &= \int_0^\infty P_\mu(x_{n,l}) dx_{n,l} \int_0^\infty P_\nu(x_{f,l}) dx_f \int_0^\infty P_\lambda(x_{c,l}) dx_c \frac{\Gamma_{n,l} \Gamma_{f,l}}{\Gamma_{n,l} + \Gamma_{f,l} + \Gamma_{\gamma,l} + \Gamma_{c,l}} \\ &= \int_0^\infty P_\mu(x_{n,l}) dx_n \int_0^\infty P_\nu(x_{f,l}) dx_f \int_0^\infty P_\lambda(x_{c,l}) dx_c \frac{\bar{\Gamma}_{n,l} x_{n,l} \bar{\Gamma}_{f,l} x_{f,l}}{\bar{\Gamma}_{n,l} x_{n,l} + \bar{\Gamma}_{f,l} x_{f,l} + \bar{\Gamma}_{\gamma,l} + \bar{\Gamma}_{c,l} x_{c,l}}, \end{aligned} \quad (2.4.7)$$

\bar{D} is the average level spacing, $\bar{\Gamma}_{n,l}$ average neutron width, $\bar{\Gamma}_{f,l}$ average fission width, $\bar{\Gamma}_{\gamma,l}$ average radiation width, and $\bar{\Gamma}_{c,l}$ average competitive reaction width. It should be noted that Eq. (2.4.7) assumes that the radiation width is constant.

In the ENDF-6 format, the average reduced neutron width at the angular momentum quantum number l is given instead of the average neutron width. The average neutron width is written by the average reduced neutron width as

$$\bar{\Gamma}_{n,l} = \bar{\Gamma}_{n,l}^0 \sqrt{E} \mu_{n,l} V_l(E), \quad (2.4.8)$$

where $\bar{\Gamma}_{n,l}^0$ is the average reduced neutron width, $\mu_{n,l}$ the number of degrees of freedom in the neutron width, and $V_l(E)$ penetrabilities for the unresolved region. Penetrabilities $V_l(E)$ are given by^{8,13)}

$$V_0 = 1, \quad (2.4.9)$$

$$V_1 = \frac{\rho^2}{\rho^2 + 1}, \quad (2.4.10)$$

$$V_2 = \frac{\rho^4}{\rho^4 + 3\rho^2 + \rho}. \quad (2.4.11)$$

As shown in Eq. (2.4.7), integrals of the form

$$\langle f(x, y) \rangle = \int_0^\infty P_\mu(x) dx \int_0^\infty P_\nu(y) f(x, y) dy, \quad (2.4.12)$$

are required³⁰⁾ to calculate the unresolved resonance cross-sections. Equation (2.4.12) is evaluated using the method proposed by Hwang³²⁾ as

$$\langle f(x, y) \rangle = \sum_{j=1}^{10} \sum_{k=1}^{10} A_j^\mu A_k^\nu \times f(x_j^\mu, y_k^\nu), \quad (2.4.13)$$

where A_j^μ is the quadrature weight and x_j^μ is the abscissa. The A_j^μ and x_j^μ have been calculated for $\mu=1, 2, 3$, and 4 . The ten-point quadrature is used for both the neutron and the fission width distributions. For odd μ

$$A_j^\mu = \frac{2w_j^S z_j^{\mu-1}}{\Gamma(\frac{\mu}{2})}, \quad (2.4.14)$$

$$x_j^\mu = \frac{2z_j^2}{\mu}, \quad (2.4.15)$$

while for even μ

$$A_j^\mu = \frac{\mu w_j^L \left(\frac{\mu x_j}{2}\right)^{\frac{\mu}{2}-1} e\left(-\frac{\mu x_j}{2}\right)}{\Gamma\left(\frac{\mu}{2}\right)(1+s_j)}, \quad (2.4.16)$$

$$x_j^\mu = \frac{(1-s_j)}{(1+s_j)}. \quad (2.4.17)$$

w_j^S and z_j in Eqs. (2.4.14) and (2.4.15) are respectively the ordinates and the weights of the half-range Gauss-Hermite quadrature derived by Steen, et al³³⁾. On the other hand, w_j^L and s_j in Eqs. (2.4.16) and (2.4.17) are the usual Gauss-Legendre ordinates and the weights, respectively. The same relationship holds for A_k^ν and y_k^ν . The A_j^μ and x_j^μ for $\mu=1, 2, 3$, and 4 and $j=1, 2, \dots, 10$ are shown in Tables 2.4.1 and 2.4.2^{29,32)}.

Substituting Eq. (2.4.13) into Eq. (2.4.7), the latter equation is

$$\begin{aligned} \langle \frac{\Gamma_{n,l} \Gamma_{f,l}}{\Gamma} \rangle &= \sum_i^{10} A_i^{\mu_{n,l}} \sum_j^{10} A_j^{\nu_{f,l}} \sum_k^{10} A_k^{\lambda_{c,l}} \frac{\overline{\Gamma_{n,l}} x_i^{\mu_{n,l}} \overline{\Gamma_{f,l}} x_j^{\nu_{f,l}}}{\overline{\Gamma_{n,l}} x_i^{\mu_{n,l}} + \overline{\Gamma_{f,l}} x_j^{\nu_{f,l}} + \overline{\Gamma_{\gamma,l}} + \overline{\Gamma_{c,l}} x_k^{\lambda_{c,l}}} \\ &= \overline{\Gamma_{n,l} \Gamma_{f,l}} R_{f,l}, \end{aligned} \quad (2.4.18)$$

where

$$R_{f,l} = \sum_i^{10} A_i^{\mu_{n,l}} \sum_j^{10} A_j^{\nu_{f,l}} \sum_k^{10} A_k^{\lambda_{c,l}} \frac{x_i^{\mu_{n,l}} x_j^{\nu_{f,l}}}{\bar{\Gamma}_{n,l} x_i^{\mu_{n,l}} + \bar{\Gamma}_{f,l} x_j^{\nu_{f,l}} + \bar{\Gamma}_{\gamma,l} + \bar{\Gamma}_{c,l} x_k^{\lambda_{c,l}}}. \quad (2.4.19)$$

$\nu_{f,l}$ is the number of degrees of freedom in the fission width, and $\lambda_{c,l}$ the number of degrees of freedom in the competitive reaction width. Using Eq. (2.4.19), Eqs. (2.4.3) - (2.4.6) are rearranged as

$$\sigma_t = \sigma_{n,n} + \sigma_\gamma + \sigma_f, \quad (2.4.20)$$

$$\sigma_\gamma = \frac{2\pi^2}{k^2} \sum_l \frac{g_J}{\bar{D}} \Gamma_{n,l} \Gamma_{\gamma,l} R_{\gamma,l}, \quad (2.4.21)$$

$$\sigma_f = \frac{2\pi^2}{k^2} \sum_l \frac{g_J}{\bar{D}} \Gamma_{n,l} \Gamma_{f,l} R_{f,l}, \quad (2.4.22)$$

$$\sigma_{n,n} = \sigma_p + \frac{2\pi^2}{k^2} \sum_l \frac{g_J}{\bar{D}} (\Gamma_{n,l}^2 R_{n,l} - 2\bar{\Gamma}_n \sin^2 \varphi_l), \quad (2.4.23)$$

where

$$R_{\gamma,l} = \sum_i^{10} A_i^{\mu_{n,l}} \sum_j^{10} A_j^{\nu_{f,l}} \sum_k^{10} A_k^{\lambda_{c,l}} \frac{x_i^{\mu_{n,l}}}{\bar{\Gamma}_{n,l} x_i^{\mu_{n,l}} + \bar{\Gamma}_{f,l} x_j^{\nu_{f,l}} + \bar{\Gamma}_{\gamma,l} + \bar{\Gamma}_{c,l} x_k^{\lambda_{c,l}}}, \quad (2.4.24)$$

$$R_{n,l} = \sum_i^{10} A_i^{\mu_{n,l}} \sum_j^{10} A_j^{\nu_{f,l}} \sum_k^{10} A_k^{\lambda_{c,l}} \frac{(x_i^{\mu_{n,l}})^2}{\bar{\Gamma}_{n,l} x_i^{\mu_{n,l}} + \bar{\Gamma}_{f,l} x_j^{\nu_{f,l}} + \bar{\Gamma}_{\gamma,l} + \bar{\Gamma}_{c,l} x_k^{\lambda_{c,l}}}. \quad (2.4.25)$$

Infinitely dilute cross-sections in the unresolved resonance region are calculated using Eqs. (2.4.20) - (2.4.23).

Table 2.4.1 Ten Point Quadrature Weights and Abscissa for Statistical Integration ($\mu=1, 2$)

	One Degree of Freedom ($\mu=1$)		Two Degree of Freedom ($\mu=2$)	
	Abscissa x_j	Weight A_j	Abscissa x_j	Weight A_j
j	1	3.0013465E-03	1.1120413E-01	1.3219203E-02
	2	7.8592886E-02	2.3546798E-01	7.2349624E-02
	3	4.3282415E-01	2.8440987E-01	1.9089473E-01
	4	1.3345267E+00	2.2419127E-01	3.9528842E-01
	5	3.0481846E+00	1.0967668E-01	7.4083443E-01
	6	5.8263198E+00	3.0493789E-02	1.3498293E+00
	7	9.9452656E+00	4.2930874E-03	2.5297983E+00
	8	1.5782128E+01	2.5827047E-04	5.2384894E+00
	9	2.3996824E+01	4.9031965E-06	1.3821772E+01
	10	3.6216208E+01	1.4079206E-08	7.5647525E+01

Table 2.4.2 Ten Point Quadrature Weights and Abscissa for Statistical Integration ($\mu=3, 4$)

	Three Degree of Freedom ($\mu=3$)		Four Degree of Freedom ($\mu=4$)	
	Abscissa x_j	Weight A_j	Abscissa x_j	Weight A_j
j	1	1.0004488E-03	3.3376214E-04	1.3219203E-02
	2	2.6197629E-02	1.8506108E-02	7.2349624E-02
	3	1.4427472E-01	1.2309946E-01	1.9089473E-01
	4	4.4484223E-01	2.9918923E-01	3.9528842E-01
	5	1.0160615E+00	3.3431475E-01	7.4083443E-01
	6	1.9421066E+00	1.7766657E-01	1.3498293E+00
	7	3.3150885E+00	4.2695894E-02	2.5297983E+00
	8	5.2607092E+00	4.0760575E-03	5.2384894E+00
	9	7.9989414E+00	1.1766115E-04	1.3821772E+01
	10	1.2072069E+01	5.0989546E-07	7.5647525E+01

3 Doppler Broadening

3.1 Task of Doppler Broadening

The task of the Doppler broadening is to calculate the cross sections at T_B K when cross sections are given at T_A K (where $T_A < T_B$)³⁴⁾. Most of the evaluated nuclear data files contain the cross sections at 0 K. The Doppler broadening is required when the cross sections at T K are required.

At 0 K, a target nucleus is at rest in the laboratory system and the relative velocity between an incident particle and the nucleus is uniquely determined. At an arbitrary temperature of T K, the nucleus vibrates with an average energy $3k_B T/2$, where k_B is the Boltzmann constant. In a such case, the relative velocity between the incident particle and nucleus varies with the velocity of the nucleus, v , in the laboratory system. For example, when the velocity of the incident particle is v_n , the energy range of the incident channel E is

$$\frac{1}{2} \underbrace{(mv_n^2 - Mv^2)}_{E_{\text{particula}}} \leq E \leq \frac{1}{2} \underbrace{(mv_n^2 + Mv^2)}_{E_{\text{nucleo}}}, \quad (3.1.1)$$

where m and M are the masses of the incident particle and nucleus, respectively.

An example of Doppler broadened cross-sections is shown in Fig. 3.1.1. The resonance width becomes wider as the temperature increases, whereas a peak value of the Doppler broadened cross-section becomes lower as the nuclear temperature increases. It should be noted that the integral value of the cross section remains unchanged even if the temperature is changed.

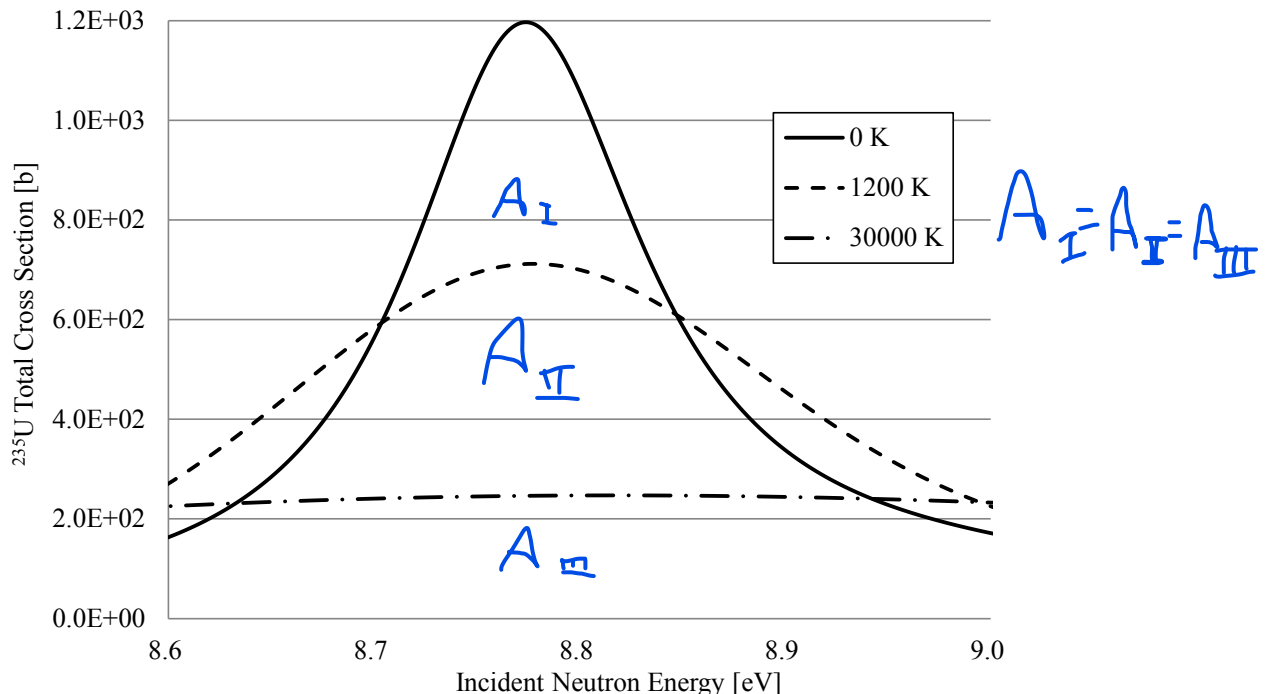


Figure 3.1.1 Example of Doppler broadened cross-sections

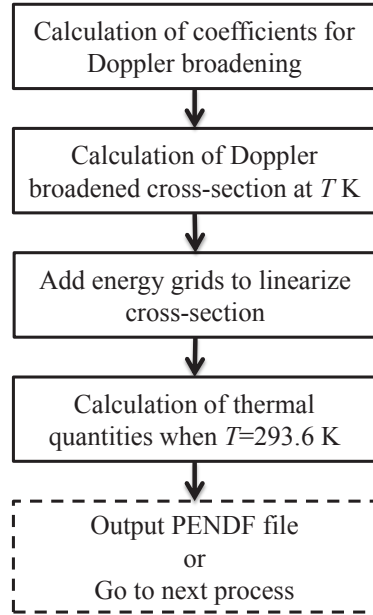
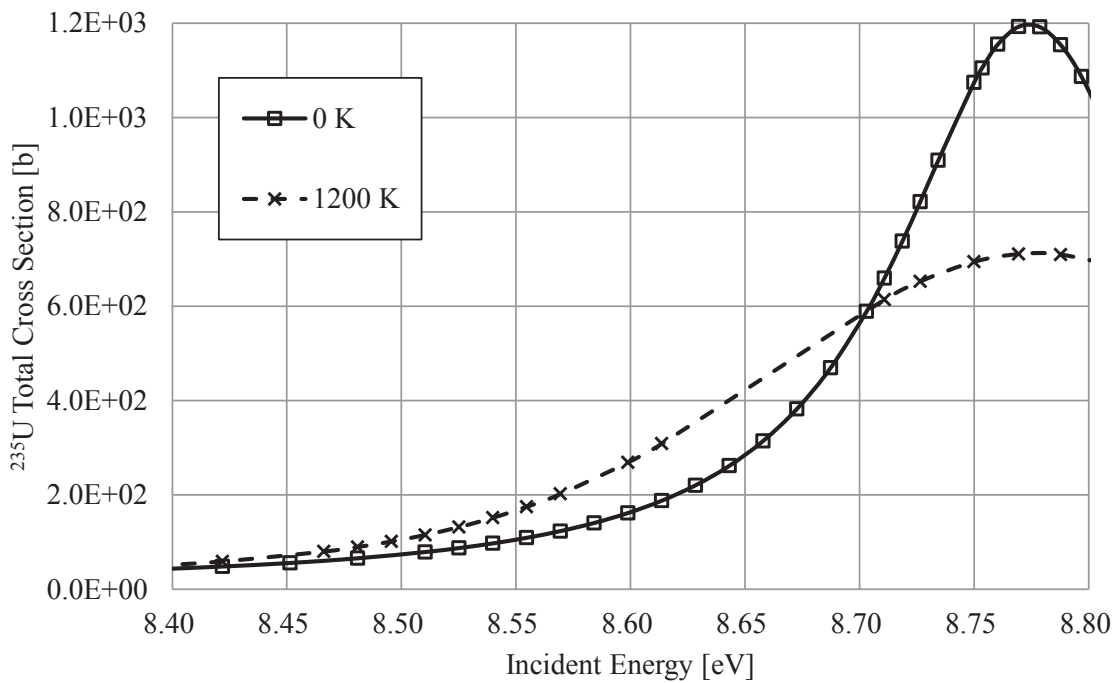
3.2 Calculation Flow of Doppler Broadening

A calculation flow of the Doppler broadening is shown in Fig. 3.2.1. First, coefficients used for the Doppler broadening are calculated to reduce the calculation time since these coefficients are independent of the incident particle energies. Next, FRENDY calculates the Doppler broadened cross-sections. Figure 3.2.2 shows an example of the difference of energy grid points at each temperature. Additional energy grid points are required from 8.40 to 8.50 eV to reduce the linearization error. The linearization flow of the Doppler broadening is similar to that of the resonance reconstruction described in Sec. 2.2.1. It should be noted that FRENDY sets an upper limit of the Doppler broadening as the upper limit of the resolved resonance region or 10^6 eV.

As the temperature becomes higher, the cross sections may be linearized with less number of energy grid points as shown in Fig. 3.2.2. In such a case, NJOY eliminates redundant energy grid points. However, FRENDY does not eliminate the redundant energy grid points. The current computational platform accepts a large memory size and a large data size. The elimination of the energy grid points is not necessary from the view point of utilizing the computational resources. Keeping the unionized base energy grid *i.e.*, keeping the original energy grid at 0 K, will be useful for the generation of the cross-section data library and the comparison of the cross sections.

NJOY outputs thermal quantities when the temperature is equal to 293.6 K, *i.e.*, the most probable nucleus energy $k_B T$ is equal to 0.0253 eV^{7,8)}. Though these quantities may not be used in the current reactor analysis, users might know them for their applications. FRENDY calculates the thermal quantities for the users. The thermal quantities consist of the fission and radiative capture cross-sections at the standard thermal value of 0.0253 eV, the integrals of these cross sections against a Maxwellian distribution at 0.0253 eV, the g-factors, η , α , and K_1 . Here the g-factor is the ratio between a Maxwellian integral and a corresponding thermal cross-section, η Maxwellian-weighted average of $(\bar{v}\sigma_f)/(\sigma_f + \sigma_c)$, α average of σ_f/σ_c , and K_1 average of $(\bar{v} - 1)\sigma_f - \sigma_c$, where \bar{v} , σ_f , and σ_c are the average number of neutrons per fission, fission cross-section, radiation capture cross-section, respectively.

The diagram illustrates the components of the g-factor. A blue bracket underlines the expression $(\bar{v}\sigma_f)/(\sigma_f + \sigma_c)$. Above the bracket, the symbol v is written in red. To the right of the bracket, the symbol σ_f is written in red. Further to the right, the symbol σ_c is written in red.

**Figure 3.2.1 Calculation flow of the Doppler broadening****Figure 3.2.2 Example of the difference of energy grids in each temperature
($^{235}\text{U}(n, \text{total})$ cross-section in JENDL-4.0)**

It should be noted that the actual FRENDY calculation does not delete the energy grid points and keeps the original energy grid points.



3.3 Doppler Broadening Formula

3.3.1 Doppler Broadening Theory

3.3.1.1 Derivation of Doppler Broadening Formula

The neutron flux ϕ is written with the velocity vector of a neutron in the laboratory system \mathbf{v}_n and the neutron density n as

$$\phi = n |\mathbf{v}_n|. \quad (3.3.1)$$

Considering the velocity distribution of the target nucleus at temperature T K in the laboratory system as $P(\mathbf{v}_t, T)$, the number of reactions between the neutron and target nucleus is

probab. ?



$$\int_0^\infty n |\mathbf{v}_r| \sigma(|\mathbf{v}_r|) N P(\mathbf{v}_t, T) d\mathbf{v}_t. \quad (3.3.2)$$

Here \mathbf{v}_t is the velocity vector of the target nucleus, N the number density of the target nucleus and \mathbf{v}_r the relative velocity vector between the neutron and target nucleus

$$\mathbf{v}_r = \mathbf{v}_n - \mathbf{v}_t. \quad (3.3.3)$$

Here the effective cross-section $\sigma(|\mathbf{v}_n|, T)$ at T K is defined as follows:

$$\phi N \sigma(|\mathbf{v}_n|, T) = \int_{-\infty}^{\infty} n |\mathbf{v}_r| \sigma(|\mathbf{v}_r|) N P(\mathbf{v}_t, T) d\mathbf{v}_t, \quad (3.3.4)$$

$$\sigma(|\mathbf{v}_n|, T) \equiv \frac{1}{|\mathbf{v}_n|} \int_{-\infty}^{\infty} |\mathbf{v}_r| \sigma(|\mathbf{v}_r|) P(\mathbf{v}_t, T) d\mathbf{v}_t. \quad (3.3.5)$$

Let us approximate the velocity distribution of the target nucleus $P(\mathbf{v}_t, T)$ as the Maxwell-Boltzmann distribution as follows:

$$P(\mathbf{v}_t, T) = \left(\frac{M}{2\pi k_B T} \right)^{\frac{3}{2}} e^{-\frac{M}{2k_B T} |\mathbf{v}_t|^2}. \quad (3.3.6)$$

Substituting Eq. (3.3.6) into Eq. (3.3.5), the effective cross-section is expressed by

$$\sigma(v_n, T) = \frac{1}{v_n} \int_{-\infty}^{\infty} v_r \sigma(v_r) \left(\frac{M}{2\pi k_B T} \right)^{\frac{3}{2}} e^{-\frac{M}{2k_B T} |\mathbf{v}_t|^2} d\mathbf{v}_t, \quad (3.3.7)$$

where

$$v_n = |\mathbf{v}_n|, \quad (3.3.8)$$

$$v_r = |\mathbf{v}_r|. \quad (3.3.9)$$

The relation between the velocity vector of the neutron \mathbf{v}_n and that of the target nucleus \mathbf{v}_t is shown in Fig. 3.3.1. \mathbf{v}_t is written by xy - and z -components of the target nucleus velocity vectors $\mathbf{v}_{t,xy}$ and $\mathbf{v}_{t,z}$ as

$$\mathbf{v}_t = \mathbf{v}_{t,xy} + \mathbf{v}_{t,z} = (v_{t,xy} \cos \varphi, v_{t,xy} \sin \varphi, v_{t,z}), \quad (3.3.10)$$

where $v_{t,xy} \cos \varphi$ and $v_{t,xy} \sin \varphi$ are the x - and y -components of the target nucleus velocity. Using Eq. (3.3.10), Eq. (3.3.7) becomes

$$\sigma(v_n, T) = \frac{1}{v_n} \int_{-\infty}^{\infty} v_r \sigma(v_r) \left(\frac{M}{2\pi k_B T} \right)^{\frac{3}{2}} e^{-\frac{M}{2k_B T} (v_r^2 - v_n^2 + 2v_n v_{t,z})} d\mathbf{v}_t \quad (3.3.11)$$

$$\begin{aligned}
&= \left(\frac{\beta}{\pi}\right)^{\frac{3}{2}} \frac{1}{v_n} \int_{-\infty}^{\infty} \int_0^{\infty} v_{t,xy} v_r \sigma(v_r) e^{-\beta(v_r^2 - v_n^2 + 2v_n v_{t,z})} dv_{t,xy} dv_{t,z} \int_0^{2\pi} d\varphi \\
&= \frac{2\beta^{\frac{3}{2}}}{\pi^{\frac{1}{2}} v_n} \int_0^{\infty} v_{t,xy} v_r \sigma(v_r) e^{-\beta(v_r^2 - v_n^2)} \int_{-\infty}^{\infty} e^{-2\beta v_n v_{t,z}} dv_{t,z} dv_{t,xy}.
\end{aligned}$$

Here the following relations are used:

$$\beta = \frac{M}{2k_B T}, \quad (3.3.12)$$

$$v_{t,z} = |\mathbf{v}_{t,z}|, \quad (3.3.13)$$

$$v_{t,xy} = |\mathbf{v}_{t,xy}|, \quad (3.3.14)$$

$$\begin{aligned}
v_r^2 &= |\mathbf{v}_n - \mathbf{v}_t|^2 = |\mathbf{v}_n - \mathbf{v}_{t,z}|^2 + |\mathbf{v}_{t,xy}|^2 = v_n^2 - 2v_n v_{t,z} + v_{t,z}^2 + v_{t,xy}^2 \\
&= v_n^2 + v_t^2 - 2v_n v_{t,z},
\end{aligned} \quad (3.3.15)$$

$$\int_{-\infty}^{\infty} dv = \int_0^{\infty} v_{t,xy} dv_{t,xy} \int_{-\infty}^{\infty} dv_{t,z} \int_0^{2\pi} d\varphi. \quad (3.3.16)$$

Using Eq. (3.3.15), the following relation is obtained:

$$\begin{aligned}
\frac{dv_r}{dv_{t,xy}} &= \frac{d}{dv_{t,xy}} \sqrt{v_n^2 - 2v_n v_{t,z} + v_{t,z}^2 + v_{t,xy}^2} \\
&= \frac{1}{2} (v_n^2 - 2v_n v_{t,z} + v_{t,z}^2 + v_{t,xy}^2)^{-\frac{1}{2}} \times 2v_{t,xy} = \frac{v_{t,xy}}{v_r}.
\end{aligned} \quad (3.3.17)$$

Substituting Eq. (3.3.17) into Eq. (3.3.11), the effective cross-section is calculated from

$$\sigma(v_n, T) = \frac{2\beta^{\frac{3}{2}}}{\pi^{\frac{1}{2}} v_n} \int_0^{\infty} v_r^2 \sigma(v_r) e^{-\beta(v_r^2 - v_n^2)} \int_{-\infty}^{\infty} e^{-2\beta v_n v_{t,z}} dv_{t,z} dv_r. \quad (3.3.18)$$

As shown in Fig. 3.3.1, the range of v_z is

$$v_n - v_r \leq v_z \leq v_n + v_r. \quad (3.3.19)$$

Using the range of v_z , the integral range in Eq. (3.3.18) is

$$\begin{aligned}
\sigma(v_n, T) &= \frac{2\beta^{\frac{3}{2}}}{\pi^{\frac{1}{2}} v_n} \int_0^{\infty} v_r^2 \sigma(v_r) e^{-\beta(v_r^2 - v_n^2)} \int_{v_n - v_r}^{v_n + v_r} e^{-2\beta v_n v_{t,z}} dv_{t,z} dv_r \\
&= \frac{\beta^{\frac{1}{2}}}{\pi^{\frac{1}{2}} v_n^2} \int_0^{\infty} v_r^2 \sigma(v_r) e^{-\beta(v_r^2 - v_n^2)} \{e^{-2\beta v_n (v_n - v_r)} - e^{-2\beta v_n (v_n + v_r)}\} dv_r \quad (3.3.20) \\
&= \frac{\beta^{\frac{1}{2}}}{\pi^{\frac{1}{2}} v_n^2} \int_0^{\infty} v_r^2 \sigma(v_r) \{e^{-\beta(v_r - v_n)^2} - e^{-\beta(v_r + v_n)^2}\} dv_r
\end{aligned}$$

$$= \sqrt{\frac{\beta}{\pi}} \frac{1}{v_n^2} \int_0^\infty v_r^2 \sigma(v_r) \left\{ e^{-(\sqrt{\beta}v_r - \sqrt{\beta}v_n)^2} - e^{-(\sqrt{\beta}v_r + \sqrt{\beta}v_n)^2} \right\} dv_r.$$

The Doppler broadened cross-section is finally expressed by Eq. (3.3.20). Eq. (3.3.20) is given by a simple form as follows:

$$\sigma(v_n, T) = \sigma^*(v_n, T) - \sigma^*(-v_n, T), \quad (3.3.21)$$

where

$$\sigma^*(v_n, T) = \sqrt{\frac{\beta}{\pi}} \frac{1}{v_n^2} \int_0^\infty v_r^2 \sigma(v_r) e^{-(\sqrt{\beta}v_r - \sqrt{\beta}v_n)^2} dv_r. \quad (3.3.22)$$

Though the integral range in Eq. (3.3.22) is from zero to infinity, it is practically limited from v_{min} to v_{max} . Using v_{min} and v_{max} , Eq. (3.3.22) is

$$\sigma^*(v_n, T) = \sqrt{\frac{\beta}{\pi}} \frac{1}{v_n^2} \int_{v_{min}}^{v_{max}} v_r^2 \sigma(v_r) e^{-(\sqrt{\beta}v_r - \sqrt{\beta}v_n)^2} dv_r. \quad (3.3.23)$$

The number of energy grid points from v_{min} to v_{max} is very large. For example, ^{238}U has more than one million energy grid points. In such a case, a long computing time is required to calculate Eq. (3.3.23).

In the equations described above, the distribution of the relative speed v_r is considered. As shown in Eqs. (3.3.3) and (3.3.15), the relative speed is given by the sum of the target nucleus and incident particle velocities. Because the neutron speed in Eq. (3.3.23) is constant, only the target nucleus speed distribution affects the relative speed distribution. As shown in Eq. (3.3.6), the target nucleus speed distribution is approximated by the Maxwell-Boltzmann distribution. The relation of $\sqrt{\beta}v_t$ and the Maxwell-Boltzmann distribution $P(v_t, T)$ is shown in Fig. 3.3.2 and Table 3.3.1. It should be noted that $P(v_t, T)$ in Fig. 3.3.2 and Table 3.3.1 is normalized by a maximal value of $P(v_t, T)$. As shown in Fig. 3.3.2 and Table 3.3.1, $P(v_t, T)$ is extremely reduced with increasing $\sqrt{\beta}v_t$.

The target nucleus speed range of FRENDY is set as follows^{7,8)}:

$$\sqrt{\beta}v_t \leq 4.0. \quad (3.3.24)$$

As shown in Table 3.3.1, $P(v_t, T)$ is 1.1×10^{-7} when $\sqrt{\beta}v_t = 4.0$. This speed range would not cause any problems practically. Using Eq. (3.3.24), the integral range in Eq. (3.3.23) is

$$v_n - \frac{4}{\sqrt{\beta}} \leq v_r \leq v_n + \frac{4}{\sqrt{\beta}}. \quad (3.3.25)$$

The integral range for $\sigma^*(-v_n, T)$ is also given by Eq. (3.3.24)

$$0 \leq v_r \leq \frac{4}{\sqrt{\beta}}. \quad (3.3.26)$$

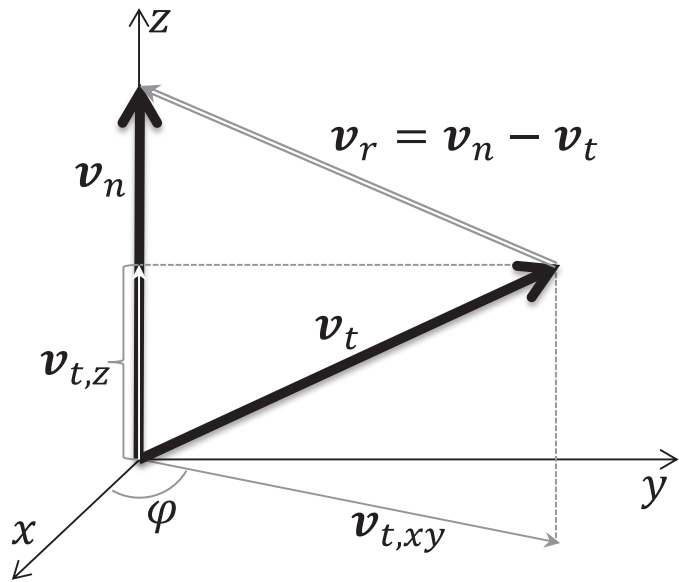


Figure 3.3.1 The relation between the neutron velocity vector v_n and the target nucleus velocity vector v_t

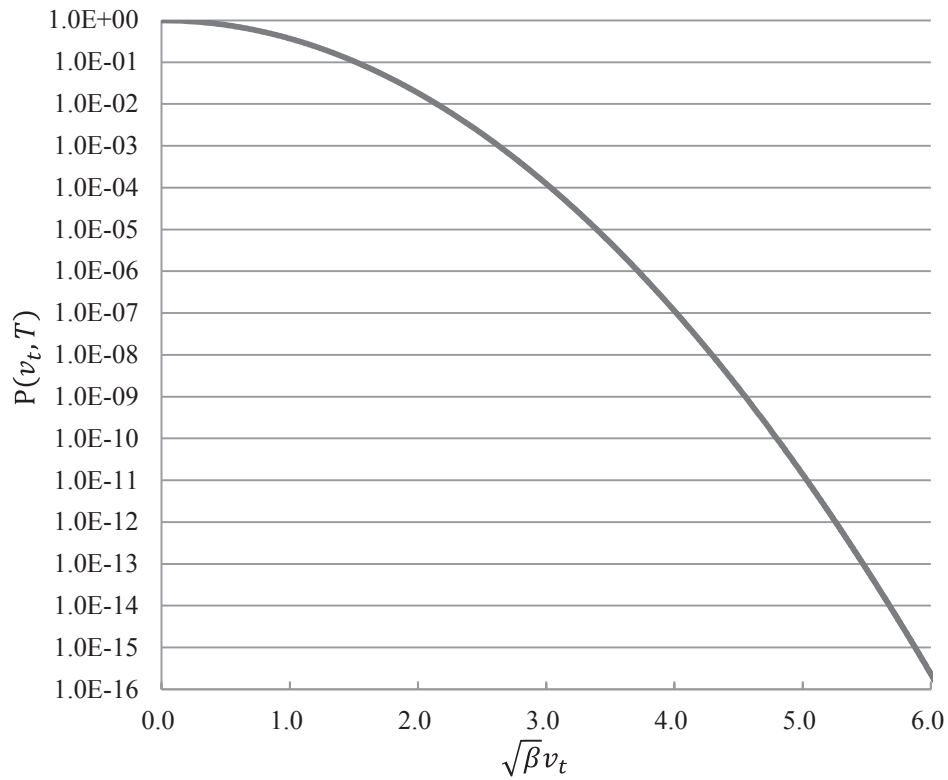


Figure 3.3.2 The relation of $\sqrt{\beta} v_t$ and the Maxwell-Boltzmann distribution $P(v_t, T)$
($P(v_t, T)$ is normalized by a maximal value of $P(v_t, T)$)

Table 3.3.1 The relation of $\sqrt{\beta}v_t$ and the Maxwell-Boltzmann distribution $P(v_t, T)$
($P(v_t, T)$ is normalized by a maximal value of $P(v_t, T)$)

$\sqrt{\beta}v_t$	$P(v_t, T)$	$\sqrt{\beta}v_t$	$P(v_t, T)$
0.0	1.00E+00	4.0	1.12E-07
0.5	7.79E-01	4.5	1.61E-09
1.0	3.68E-01	5.0	1.38E-11
1.5	1.05E-01	5.5	7.29E-14
2.0	1.83E-02	6.0	2.31E-16
2.5	1.93E-03	6.5	4.46E-19
3.0	1.23E-04	7.0	5.24E-22
3.5	4.79E-06	7.5	3.72E-25

To rewrite Eq. (3.3.23) with a simpler form, x and y are defined as follows:

$$x = \sqrt{\beta}v_r = \sqrt{\frac{M}{2k_B T}} \sqrt{\frac{2E_r}{m}} = \sqrt{\frac{A}{k_B T}} E_r = \sqrt{\alpha E_r}, \quad (3.3.27)$$

$$y = \sqrt{\beta}v_n = \sqrt{\frac{M}{2k_B T}} \sqrt{\frac{2E_n}{m}} = \sqrt{\frac{A}{k_B T}} E_n = \sqrt{\alpha E_n}. \quad (3.3.28)$$

Here E_r is the relative energy of the neutron given by $\frac{1}{2}mv_r^2$, E_n the neutron energy in the laboratory system, A the ratio of the mass of the nucleus to that of a neutron and

$$\alpha = \frac{A}{k_B T} = \frac{2}{m}\beta. \quad (3.3.29)$$

Substituting Eqs. (3.3.25) - (3.3.29) into Eq. (3.3.23), the latter equation leads to

$$\sigma^*(y, T) = \frac{1}{\sqrt{\pi}} \frac{1}{y^2} \int_{y-4}^{y+4} x^2 \sigma(x) e^{-(x-y)^2} dx. \quad (3.3.30)$$

where

$$dv_r = \frac{1}{\sqrt{\beta}} dx. \quad (3.3.31)$$

To calculate Eq. (3.3.30), $\sigma(x)$ is linearized as³⁵⁾ \rightarrow Elementos finitos?

$$\begin{aligned} \sigma(x) &= \frac{E - E_i}{E_{i+1} - E_i} \sigma(E_{i+1}) + \frac{E_{i+1} - E}{E_{i+1} - E_i} \sigma(E_i) \\ &= \frac{x^2 - x_i^2}{x_{i+1}^2 - x_i^2} \sigma(x_{i+1}^2) + \frac{x_{i+1}^2 - x^2}{x_{i+1}^2 - x_i^2} \sigma(x_i^2) \\ &= A_i + B_i x^2, \end{aligned} \quad (3.3.32)$$

where

$$A_i = \frac{x_{i+1}^2 \sigma(x_i^2) - E_i \sigma(x_{i+1}^2)}{x_{i+1}^2 - x_i^2} \quad (3.3.33)$$

$$B_i = \frac{\sigma(x_{i+1}^2) - \sigma(x_i^2)}{x_{i+1}^2 - x_i^2}. \quad (3.3.34)$$

Substituting Eq. (3.3.32) into Eq. (3.3.30), the latter equation turns out to be

$$\sigma^*(y, T) = \frac{1}{\sqrt{\pi}} \frac{1}{y^2} \sum_{i=0}^N \int_{x_i}^{x_{i+1}} \{A_i x^2 + B_i x^4\} e^{-(x-y)^2} dx. \quad (3.3.35)$$

To calculate Eq. (3.3.35), z is defined as

$$z = x - y. \quad (3.3.36)$$

Using Eq. (3.3.36), Eq. (3.3.35) is given by

$$\sigma^*(y, T) = \frac{1}{\sqrt{\pi}} \frac{1}{y^2} \sum_{i=0}^N \int_{x_i-y}^{x_{i+1}-y} C_i(z) e^{-z^2} dz, \quad (3.3.37)$$

where

$$C_i(z) = B_i z^4 + 4B_i y z^3 + (A_i + 6B_i y^2) z^2 + (2A_i y + 4B_i y^3) z + (A_i y^2 + B_i y^4). \quad (3.3.38)$$

To calculate Eq. (3.3.37), $G_n(a, b)$ is introduced as

$$G_n(a, b) = \frac{1}{\sqrt{\pi}} \int_a^b z^n e^{-z^2} dz. \quad (3.3.39)$$

Here, Eq. (3.3.39) is rewritten as

$$G_n(a, b) = \frac{1}{2} (D_n(b) - D_n(a)), \quad (3.3.40)$$

where

$$D_n(a) = \frac{2}{\sqrt{\pi}} \int_0^a z^n e^{-z^2} dz. \quad (3.3.41)$$

Equation (3.3.41) satisfies the following recursive relations³⁶⁾:

$$D_0(a) = \text{erf}(a), \quad (3.3.42)$$

$$D_1(a) = \frac{1}{\sqrt{\pi}} (1 - e^{-a^2}), \quad (3.3.43)$$

$$D_n(a) = \frac{n-1}{2} F_{n-2}(a) - \frac{1}{\sqrt{\pi}} a^{n-1} e^{-a^2} + \frac{1}{\sqrt{\pi}} \delta_{n,1}. \quad (3.3.44)$$

Here $\delta_{n,1}$ is the Kronecker delta and $\text{erf}(a)$ the error function. The error function is defined by

$$\text{erf}(a) = \frac{1}{\sqrt{\pi}} \int_0^a e^{-z^2} dz. \quad (3.3.45)$$

Using Eq. (3.3.39), Eq. (3.3.35) is written by

$$\sigma^*(y, T) = \frac{1}{\pi^{\frac{1}{2}} y^2} \sum_{i=0}^N C_i, \quad (3.3.46)$$

where

$$C_i = B_i G_4 + 4B_i y G_3 + (A_i + 6B_i y^2) G_2 + (2A_i y + 4B_i y^3) G_1 + (A_i y^2 + B_i y^4) G_0, \quad (3.3.47)$$

$$G_n = G_n(x_i - y, x_{i+1} - y). \quad (3.3.48)$$

3.3.1.2 Treatment of cross section at 0 eV

- Treatment of cross section is required from 0 eV to the lowest energy (E_L) given in an evaluated nuclear data file. Normally, a cross section at 0 eV is not included in the evaluated nuclear data file. The cross section at 0 eV is required to calculate the Doppler broadened cross-section in low energy region.

NJOY and SIGMA1 approximate that the cross section obeys the 1/v law. Eq. (3.3.30) is given by

$$\begin{aligned} \sigma^*(v) &= \frac{1}{\sqrt{\pi} y^2} \int_0^{x_1} \frac{\sigma_1 x_1}{x} x^2 e^{-(x-y)^2} dx = \frac{\sigma_1 x_1}{\sqrt{\pi} y^2} \int_0^{x_1-y} (z-y) e^{-z^2} dz \\ &= -\frac{\sigma_1 x_1}{\sqrt{\pi}} \left(\frac{H_1(0, x_1 - y)}{y^2} + \frac{H_0(0, x_1 - y)}{y^2} \right). \end{aligned} \quad (3.3.49)$$

$$H_n(a, b) = \frac{1}{\sqrt{\pi}} \int_a^b z^n e^{-z^2} dz \quad (3.3.50)$$

Here σ_1 and x_1 are the cross section and the x value at E_L , respectively. Equation (3.3.49) is valid below E_L as far as since the cross section obeys the 1/v law. However, the cross sections which do not exhibit the 1/v behavior, *e.g.*, the elastic scattering cross-section, are not expressed, appropriately.

FRENDDY determines the cross sections at 0 eV by the linear extrapolation with the cross sections at the lowest and next-to-the-lowest energy grid points. Our study³⁷⁾ has revealed that the difference of the cross sections of the linear extrapolation is so small, even if the capture cross-section, which obeys the 1/v law, is concerned. Therefore, the linear extrapolation is appropriate for the treatment of the cross section at 0 eV.

3.3.2 Speed-Up of Doppler Broadening

The Doppler broadening process requires a relatively long computational time for the calculation of the error function of Eq. (3.3.45). As shown in Eq. (3.3.46), $G_n(a, b)$ is dependent only on the x value, *i.e.*, the relative neutron energy E_r . The $G_n(a, b)$ values for each cross section at energy grid point E are identical since the energy grids of many cross sections are unionized by the previous process. FRENDDY calculates all cross-sections at energy grid point E simultaneously to reduce the number of the error function calculation.

Consequently, the actual calculation formula is as follows:

$$\sigma_c^*(y, T) = \frac{1}{\pi^2 y^2} \sum_{i=0}^N C_{i,c}, \quad (3.3.51)$$

where

$$C_{i,c} = \frac{B_{i,c}G_4 + 4B_{i,c}yG_3 + (A_{i,c} + 6B_{i,c}y^2)G_2}{+(2A_{i,c}y + 4B_{i,c}y^3)G_1 + (A_{i,c}y^2 + B_{i,c}y^4)G_0}, \quad (3.3.52)$$

$$A_{i,c} = \frac{E_{i+1}\sigma_c(E_i) - E_i\sigma_c(E_{i+1})}{x_{i+1}^2 - x_i^2}, \quad (3.3.53)$$

$$B_{i,c} = \frac{\sigma_c(E_{i+1}) - \sigma_c(E_i)}{x_{i+1}^2 - x_i^2}. \quad (3.3.54)$$

Many reactions have a threshold and their cross sections are zero below the **threshold**. FRENDY eliminates the energy grid points below the threshold because these energy grid points are not used in the nuclear data processing and the nuclear calculations. Therefore, the number of energy grid becomes lower when the reaction has a higher threshold energy. The Doppler broadening below the threshold is not required since the Doppler broadened cross-sections are also zero below the threshold. To skip the Doppler broadening below the threshold, FRENDY divides all reactions into six groups, *i.e.*, the number of energy grid points is less than 100, 500, 1000, 5000, 10000, and more than 10000, and the Doppler broadening is carried out in each group.

3.4 Calculation of Thermal Quantities

The evaluated thermal quantities are as follows:

- Fission cross-section at 0.0253 eV $\sigma_{f,th}$
- Average neutron production at 0.0253 eV \bar{v}_{th}
- Capture cross-section at 0.0253 eV $\sigma_{c,th}$
- Integral of fission cross-section against a Maxwell-Boltzmann distribution in thermal region $I_{f,th}$
- Integral of **radiative capture cross-section** against a Maxwell-Boltzmann distribution in thermal region $I_{c,th}$
- g -factor of fission reaction g_f
- g -factor of **radiative capture reaction** g_c
- Average value of α at thermal region α
- Average value of η at thermal region η
- Average value of K_1 at thermal region K_1
- Integral of fission cross-section against a Maxwell-Boltzmann

- distribution in resonance region $I_{f,reso}$
- Integral of radiative capture cross-section against a Maxwell-Boltzmann distribution in resonance region $I_{c,reso}$

$\sigma_{f,th}$, \bar{v}_{th} and $\sigma_{c,th}$ are values at 0.0253 eV. Other values are defined as follows^{8,38)}:

$$I_{r,th} = \int_{E \in th} \sigma_r(E) \frac{E}{(k_B T)^2} e^{-\frac{E}{k_B T}} dE, \quad (3.4.1)$$

$$g_r = \frac{2}{\sqrt{\pi}} \frac{1}{\sqrt{k_B T} \sigma_{r,th}} \int_{E \in th} \sqrt{E} \sigma_r(E) \sqrt{\frac{E}{(k_B T)^3}} e^{-\frac{E}{k_B T}} dE = \frac{2}{\sqrt{\pi}} \frac{I_{r,th}}{\sigma_{r,th}}, \quad (3.4.2)$$

$$\alpha = \int_{E \in th} \frac{\sigma_c(E)}{\sigma_f(E)} \frac{E}{(k_B T)^2} e^{-\frac{E}{k_B T}} dE, \quad (3.4.3)$$

$$\eta = \int_{E \in th} \frac{\sigma_f(E)}{\sigma_f(E) + \sigma_c(E)} \frac{E}{(k_B T)^2} e^{-\frac{E}{k_B T}} dE, \quad (3.4.4)$$

$$K_1 = \int_{E \in th} \{(v(E) - 1)\sigma_f(E) - \sigma_c(E)\} \frac{E}{(k_B T)^2} e^{-\frac{E}{k_B T}} dE, \quad (3.4.5)$$

$$I_{r,reso} = \int_{E \in reso} \sigma_r(E) \frac{E}{(k_B T)^2} e^{-\frac{E}{k_B T}} dE, \quad (3.4.6)$$

where r indicates the reaction, *i.e.*, $r=f$ for the fission reaction and $r=c$ for the radiative capture reaction. The integral range in Eqs. (3.4.1) - (3.4.6) is from the lowest energy grid point to 1.0 eV for the thermal region and from 0.5 eV to the highest energy grid point for the resonance region, respectively. The trapezoidal integration is used to calculate the integration in Eqs. (3.4.1) - (3.4.6)

$$I_{r,th} = \sum_{E_{min}}^{E_i < 1.0} \frac{E_i - E_{i-1}}{2(k_B T)^2} \left(\sigma_r(E_i) E_i e^{-\frac{E_i}{k_B T}} - \sigma_r(E_{i-1}) E_{i-1} e^{-\frac{E_{i-1}}{k_B T}} \right), \quad (3.4.7)$$

$$\alpha = \sum_{E_{min}}^{E_i < 1.0} \frac{E_i - E_{i-1}}{2(k_B T)^2} \left(\frac{\sigma_c(E_i)}{\sigma_f(E_i)} E_i e^{-\frac{E_i}{k_B T}} - \frac{\sigma_c(E_{i-1})}{\sigma_f(E_{i-1})} E_{i-1} e^{-\frac{E_{i-1}}{k_B T}} \right), \quad (3.4.8)$$

$$\eta = \sum_{E_{min}}^{E_i < 1.0} \frac{E_i - E_{i-1}}{2(k_B T)^2} \left(\frac{\sigma_c(E_i)}{\sigma_f(E_i) + \sigma_c(E_i)} E_i e^{-\frac{E_i}{k_B T}} - \frac{\sigma_c(E_{i-1})}{\sigma_f(E_{i-1}) + \sigma_c(E_{i-1})} E_{i-1} e^{-\frac{E_{i-1}}{k_B T}} \right), \quad (3.4.9)$$

$$K_1 = \sum_{E_{min}}^{E_i < 1.0} \frac{E_i - E_{i-1}}{2(k_B T)^2} \left(\begin{aligned} &\{(v(E_i) - 1)\sigma_f(E_i) + \sigma_c(E_i)\} E_i e^{-\frac{E_i}{k_B T}} \\ &- \{(v(E_{i-1}) - 1)\sigma_f(E_{i-1}) + \sigma_c(E_{i-1})\} E_{i-1} e^{-\frac{E_{i-1}}{k_B T}} \end{aligned} \right), \quad (3.4.10)$$

$$I_{r,reso} = \sum_{E_i=0.5}^{E_{max}} \frac{E_i - E_{i-1}}{2(k_B T)^2} \left(\sigma_r(E_i) E_i e^{-\frac{E_i}{k_B T}} - \sigma_r(E_{i-1}) E_{i-1} e^{-\frac{E_{i-1}}{k_B T}} \right). \quad (3.4.11)$$

4 Thermal Scattering Cross-section Calculation

4.1 Thermal Scattering Law Data

At high energies, the wavelengths of neutrons are small, and it is reasonable to treat scattering as classical collisions between particles. At thermal energies, the wavelengths of neutrons are similar to the size of molecules and the spacing of crystalline lattice and the theory of classical collisions cannot be adopted, directly³⁴⁾. In such energy regions, consideration of thermal scattering caused by crystalline and chemical binding is important for many materials, *e.g.*, H₂O, ZrH, and graphite, to improve the prediction accuracy of neutron calculations. The evaluated nuclear data file gives the Thermal Scattering Law (TSL) data to consider the scattering by crystalline and chemical binding. In the ENDF-6 format¹³⁾, the following scattering cross-sections are defined:

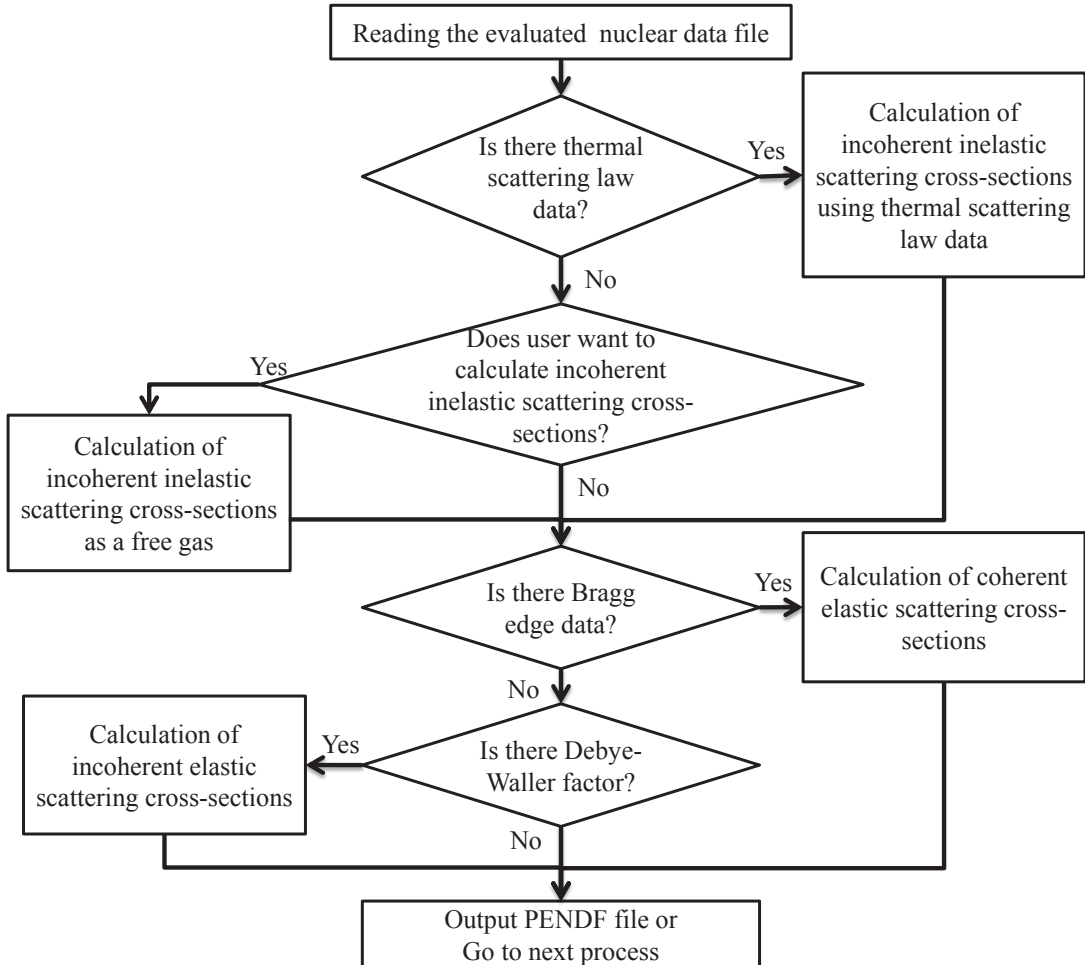
- coherent elastic scattering for crystalline materials,
- incoherent elastic scattering for partially ordered materials,
- incoherent inelastic scattering for non-crystalline materials.

The evaluated nuclear data file contains only parameters to calculate the thermal scattering cross-sections. Reconstruction and linearization of the thermal scattering cross-sections, secondary neutron energy, and scattering angle are required.

4.2 Calculation Flow of Thermal Scattering Cross-Sections

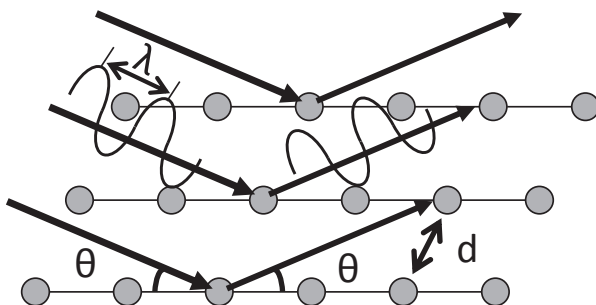
A calculation flow of the thermal scattering cross-sections is shown in Fig. 4.2.1. The thermal scattering cross-sections, secondary neutron energy, and scattering angle are calculated when the evaluated nuclear data file contains the parameters of these cross-sections. FRENDY also calculates the incoherent inelastic thermal scattering cross-sections with the free monatomic gas model⁸⁾ when the evaluated nuclear data file does not contain the parameters or users want to calculate them.

As shown in Fig. 4.2.1, FRENDY skips the calculation of the incoherent elastic scattering cross-section using the Debye-Waller factor when the Bragg edge data is included in the evaluated nuclear data file. The ENDF-6 format cannot contain the parameters of both the coherent and incoherent elastic scattering cross-sections in the evaluated nuclear data file. If a new nuclear data format contains both parameters, the calculation flow can be changed and FRENDY will be able to calculate both the coherent and incoherent elastic scattering cross-sections.

**Figure 4.2.1 Calculation flow of the thermal scattering cross-sections**

4.2.1 Coherent Elastic Scattering

The coherent elastic scattering is observed in crystalline materials such as graphite. As shown in Fig. 4.2.2, the crystalline atoms cause neutrons to scatter into many specific directions and it is called “Bragg diffraction”.

**Figure 4.2.2 Example of Bragg diffraction**

The Bragg diffraction is observed in the specified energy. In the Bragg's law, the interference is strongest when the wavelength λ is satisfied with Eq. (4.2.1)³⁹⁾

$$2d \sin \theta = n\lambda = \frac{h}{\sqrt{2mE_i}}, \quad (4.2.1)$$

where d is the distance between atomic layers in a crystal, θ the scattering angle, n a positive integer, h Planck's constant, and E_i the energy of the i -th Bragg edge.

Figure 4.2.3 shows the coherent elastic scattering cross-section for graphite at 296 K taken from JENDL-4.0¹⁾. As shown in Fig. 4.2.3, the very strong peaks which are known as Bragg edges are observed in the coherent elastic scattering cross-section. It should be noted that the cross section is zero below the first Bragg edge.

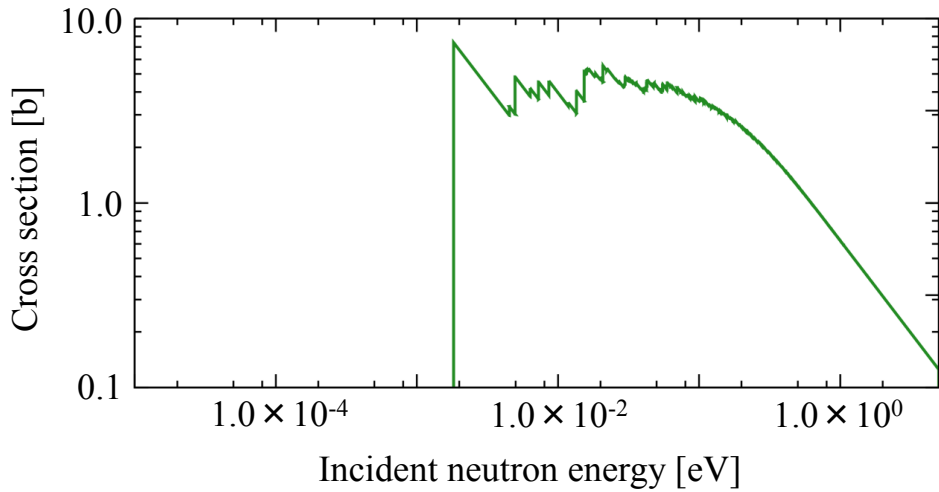


**Figure 4.2.3 Example of coherent elastic scattering cross-section for a crystalline material
(Graphite, 296 K, JENDL-4.0)**

The evaluated nuclear data file provides the number of the Bragg edges, the energy of the Bragg edges, and the crystallographic structure factor. The coherent elastic scattering cross-section σ^{coh} is represented as follows⁴⁰⁾:

$$\sigma^{coh}(E, E', \mu) = \frac{1}{E} \sum_i^{E_i < E} \sigma_c f_i e^{-2WE_i} \delta(\mu - \mu_i) \delta(E - E'), \quad (4.2.2)$$

where

$$\mu_i = 1 - \frac{2E_i}{E}, \quad (4.2.3)$$

$$E_i = \frac{\hbar^2 \tau_i^2}{8m}, \quad (4.2.4)$$

$$f_i = \frac{\pi^2 \hbar^2}{2mNV} \sum_{\tau_i} |F(\tau_i)|, \quad (4.2.5)$$

$$\hbar = \frac{h}{2\pi}. \quad (4.2.6)$$

In the above equations, E is the incident neutron energy, E' the secondary neutron energy, μ the scattering cosine in the laboratory system, σ_c the characteristics coherent scattering cross-section, W the Debye-Waller factor, E_i the energy of the Bragg edge, $\delta(x)$ the delta function, τ_i the vectors of one particular “shell” of the reciprocal lattice, m the neutron mass, N the number of atoms in the unit shell, V the volume in the unit shell, and $F(\tau_i)$ the crystallographic structure factors. The evaluated nuclear data file contains s_i which is the proportional to the structure factor. Using s_i , Eq. (4.2.2) is

$$\sigma^{coh}(E, E', \mu) = \frac{1}{E} \sum_i^{E_i < E} s_i \delta(\mu - \mu_i) \delta(E - E'). \quad (4.2.7)$$

The coherent elastic scattering cross-section is linearized in this module using the similar method which is used in the resonance reconstruction. As described in Eq. (4.2.7), the secondary neutron energy is equal to the incident neutron energy and the scattering cosine is fixed. The linearization of the secondary energy and scattering angle is not required for the coherent elastic scattering.

For the incident neutron energy, FRENDY adds a middle energy grid point when the following conditions are satisfied:

$$\sigma^{inc}\left(E_{i+\frac{1}{2}}, E', \mu\right) - \frac{\sigma^{inc}(E_{i+1}, E', \mu) + \sigma^{inc}(E_i, E', \mu)}{2} \geq err \times \sigma^{inc}\left(E_{i+\frac{1}{2}}, E', \mu\right), \quad (4.2.8)$$

$$\sigma^{inc}\left(E_{i+\frac{1}{2}}, E', \mu\right) - \frac{\sigma^{inc}(E_{i+1}, E', \mu) + \sigma^{inc}(E_i, E', \mu)}{2} \geq 1.0 \times 10^{-6}, \quad (4.2.9)$$

where err is the tolerance value for the linearization. FRENDY terminates the linearization when energy interval satisfies the following criterion:

$$E_{i+1} - E_i \geq E_{i+\frac{1}{2}} \times 3.0 \times 10^{-5}. \quad (4.2.10)$$

4.2.2 Incoherent Elastic Scattering

The incoherent elastic scattering is observed in partially ordered materials such as ZrH and polyethylene. The incoherent elastic scattering is isotropic and contains no structural information since the intensity of this type of scattering is independent of the scattering angle.⁴¹⁾ The incoherent inelastic scattering cross-section $\sigma^{iel}(E, E', \mu)$ is given by

$$\sigma^{iel}(E, E', \mu) = \frac{\sigma_b}{2} e^{-2WE(1-\mu)} \delta(E - E'), \quad (4.2.11)$$

where σ_b is the characteristic bound scattering cross-section⁴⁰⁾.

The angle-integrated cross-section $\sigma^{iel}(E)$, which is divided into equally probable cosine bins, and the cumulative distribution are output in the PENDF file. Because the incoherent elastic scattering is isotropic, the integrated cross-section $\sigma^{iel}(E)$ is calculated by

$$\sigma^{iel}(E) = \int_{-1}^1 \frac{\sigma_b}{2} e^{-2WE(1-\mu)} d\mu = \frac{\sigma_b}{2} \left\{ \frac{1 - e^{-4WE}}{2WE} \right\}. \quad (4.2.12)$$

The equally probable angle $\bar{\mu}_i$ is also calculated by

$$\bar{\mu}_i = \frac{n_{bin}}{2WE} \frac{e^{-2WE(1-\mu_i)}(2WE\mu_i - 1) - e^{-2WE(1-\mu_{i-1})}(2WE\mu_{i-1} - 1)}{1 - e^{-4WE}}, \quad (4.2.13)$$

where n_{bin} is the number of cosine bins and μ_i is the upper limit of cosine bin which is given by

$$\mu_i = 1 + \frac{1}{2WE} \ln \left(\frac{1 - e^{-4WE}}{n_{bin}} + e^{-2WE(1-\mu_{i-1})} \right), \quad (4.2.14)$$

$$\mu_0 = -1. \quad (4.2.15)$$

Figure 4.2.4 shows the incoherent elastic scattering cross-section for H in ZrH at 296 K taken from JENDL-4.0. Comparing to the other reactions, the incoherent elastic scattering cross-section can be represented with a slowly varying function. Therefore, the linearization of the incoherent elastic scattering cross-section is not performed and the energy grid of the total cross-section is used for the incident neutron energy grid.

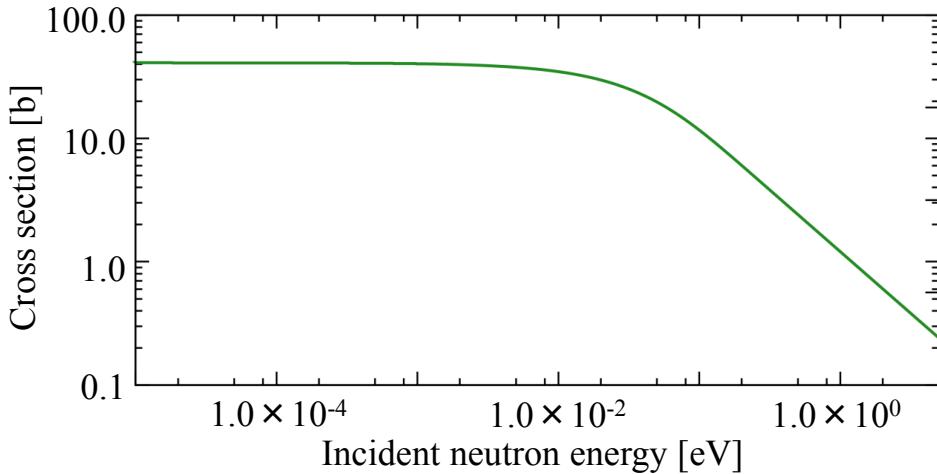


**Figure 4.2.4 Example of incoherent elastic scattering cross-section
(H in ZrH, 296 K, JENDL-4.0)**

4.2.3 Incoherent Inelastic Scattering

The incoherent inelastic scattering is observed in non-crystalline materials such as H₂O and ZrH³⁴⁾. The thermal scattering law data is used to consider the effect of chemical binding of a molecule on neutron scattering. Using the thermal scattering law data $S(\alpha, \beta)$, the double differential scattering

cross-section $\frac{d^2\sigma^{inc}(E,E',\mu)}{dEd\Omega}$ is written as follows⁴²⁾:

$$\frac{d^2\sigma^{inc}(E,E',\mu)}{dEd\Omega} = \frac{\sigma_b}{4\pi k_B T} \sqrt{\frac{E'}{E}} S(\alpha, \beta), \quad (4.2.16)$$

where

$$\alpha = \frac{E' + E - 2\mu\sqrt{EE'}}{Ak_B T}, \quad (4.2.17)$$

$$\beta = \frac{E' - E}{k_B T}, \quad (4.2.18)$$

α the dimensionless momentum transfer, β the dimensionless energy transfer, A the ratio of the target mass to the neutron mass, and k_B the Boltzmann constant.

The evaluated nuclear data file provides the thermal scattering law data of n -th type atom because molecule consists of many elements. FRENDY uses the following equations to calculate the inelastic incoherent scattering cross-section at T K in each energy grid point¹³⁾:

$$\sigma^{inc}(E, E', \mu) = \sum_{n=0}^{N_s} \frac{M_n \sigma_{bn}}{2k_B T} \sqrt{\frac{E'}{E}} e^{-\frac{\beta}{2}} S_n(\alpha_n, \beta), \quad (4.2.19)$$

$$\sigma_{bn} = \sigma_{fn} \left(\frac{A_n + 1}{A_n} \right)^2, \quad (4.2.20)$$

$$\sigma_{fn} = 4\pi \alpha_n^2, \quad (4.2.21)$$

$$\alpha_n = \frac{E' + E - 2\mu\sqrt{EE'}}{A_n k_B T}, \quad (4.2.22)$$

where N_s is the number of non-principal scattering atom types, M_n the number of n -th type atoms in the molecule or unit cell, σ_{bn} the characteristic bound incoherent scattering cross-section, and σ_{fn} the characteristic free atom scattering cross-section.

The thermal scattering law data describes the thermal neutron scattering cross section of the atom for which the chemical binding is considered⁴⁰⁾. For a free gas of scatterers with no internal structure, the thermal scattering law data $S_n(\alpha_n, \beta)$ is

$$S_n(\alpha_n, \beta) = \frac{1}{\sqrt{4\pi \alpha_n}} \exp \left\{ -\frac{\alpha_n^2 + \beta^2}{4\alpha_n} \right\}. \quad (4.2.23)$$

When the evaluated nuclear data file does not include the thermal scattering law data or users want to calculate the incoherent inelastic scattering cross-section as a free gas, FRENDY assumes that the nucleus is a free particle with no internal structure and the thermal scattering law data is calculated using Eq. (4.2.23).

When α or β value is outside the range of the table, the differential scattering cross-section can

be computed using the short collision time (SCT) approximation⁴⁰⁾:

$$\sigma^{inc,SCT}(E, E', \mu) = \sum_{n=0}^{N_s} \frac{\sigma_{bn}}{2k_B T} \sqrt{\frac{E'}{E} \frac{T}{T_{eff}}} \frac{1}{\sqrt{4\pi\alpha_n}} \exp \left\{ -\frac{(\alpha_n - |\beta|)^2}{4\alpha_n} \frac{T}{T_{eff}} - \frac{\beta + |\beta|}{2} \right\}, \quad (4.2.24)$$

where T_{eff} is the effective temperature for the SCT approximation which is given in the evaluated nuclear data file.

Figures 4.2.5 and 4.2.6 show the incoherent inelastic scattering cross-section for H in H₂O and H in ZrH at 296 K taken from JENDL-4.0. The THERMR module of NJOY^{7,8)} uses the fixed incident neutron energy grid, which consists of 117 energy grid points from 1.0×10^{-5} to 10 eV, to calculate the incoherent inelastic scattering cross section and secondary energy and angular distributions. The incoherent inelastic scattering cross section at the other energy grid points are interpolated using the fifth order Lagrange interpolation and secondary energy and angular distributions are not calculated to reduce calculation time and data size. As shown in Fig. 4.2.5, the incoherent inelastic scattering cross-section for many materials can be represented with a slowly varying function. In such a case, the fixed incident neutron energy grid is appropriate. However, the fixed incident neutron energy grid is inappropriate for some materials, *e.g.*, H in ZrH for which the incoherent inelastic scattering cross-section is oscillated as shown in Fig. 4.2.6. The adoption of the finer energy grid is required to adequately reproduce the incoherent inelastic scattering cross-section distribution in such materials⁴³⁾.

FRENDDY calculates the incoherent inelastic scattering cross-section in all energy grid points of the total cross-section to appropriately treat such materials when the thermal scattering law data is given. FRENDDY uses the fixed energy grid points to calculate the incoherent inelastic scattering cross-section when the thermal scattering law data is not given. Similar to NJOY, the fixed incident neutron energy grid, which consists of 117 energy grid points from 1.0×10^{-5} to 10 eV, is used to calculate the incoherent inelastic scattering and other energy grid points are interpolated using the fifth order Lagrange interpolation. This is because the number of energy grid points of heavy nuclides is very large. The incoherent inelastic scattering cross-section for a free gas is not so important for neutronics calculation and it can be represented with a slowly varying function of the incident neutron energy. A large amount of data size is required to show the secondary energy and angular distributions. The secondary energy and angular distributions are output only in the fixed incident neutron energy grid points to reduce calculation time and data size.

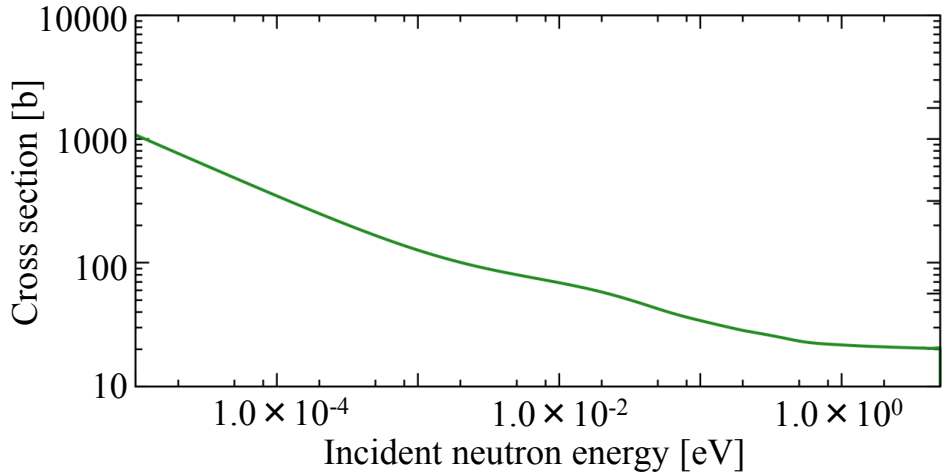


**Figure 4.2.5 Example of incoherent inelastic scattering cross-section
(H in H₂O, 296 K, JENDL-4.0)**

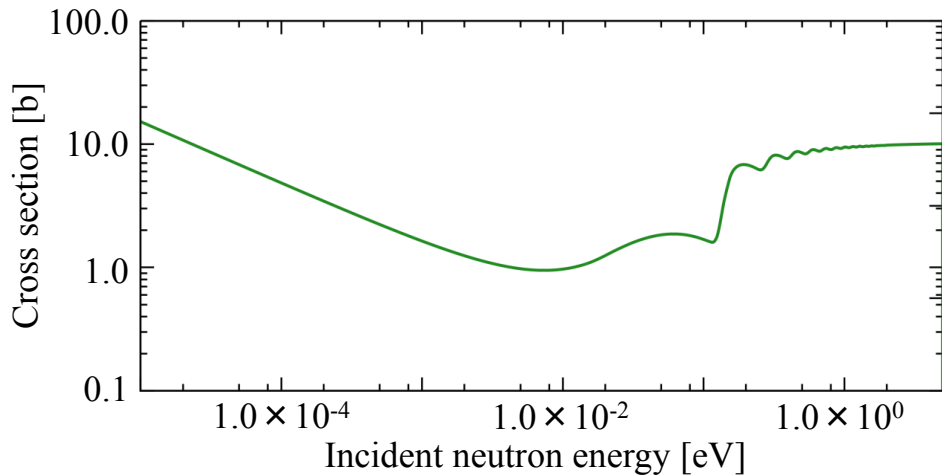


**Figure 4.2.6 Example of incoherent inelastic scattering cross-section
(H in ZrH, 296 K, JENDL-4.0)**

Linearization of the secondary energy and angular distributions for the incoherent inelastic scattering is required. For the secondary energy, FRENDY adds a middle energy grid point when the following condition is satisfied:

$$\begin{aligned} & \left| \sigma^{inc} \left(E, E'_{i+\frac{1}{2}} \right) - \frac{\sigma^{inc}(E, E'_{i+1}) + \sigma^{inc}(E, E'_i)}{2} \right| \\ & \geq err \times \left| \sigma^{inc} \left(E, E'_{i+\frac{1}{2}} \right) + 1.0 \times 10^{-3} \right|, \end{aligned} \quad (4.2.25)$$

where *err* is the tolerance value for the linearization and

$$\sigma^{inc}(E, E') = \int_{-1}^1 \sigma^{inc}(E, E', \mu) d\mu. \quad (4.2.26)$$

When the integrated incoherent inelastic scattering cross-section satisfies the following equation, the linearization at this energy grid point is finished and moves to the next energy grid point

$$\frac{1}{2}(E'_{i+1} - E'_i) \left(\sigma^{inc}(E, E'_{i+1}) + \sigma^{inc}(E, E'_i) \right) < 1.0 \times 10^{-6}. \quad (4.2.27)$$

For the angular distribution, FRENDY adds a middle angular point when either of the following conditions is satisfied:

$$\begin{aligned} & \left| \sigma^{inc}(E, E', \mu_{i+\frac{1}{2}}) - \frac{\sigma^{inc}(E, E', \mu_i) + \sigma^{inc}(E, E', \mu_{i+1})}{2} \right| \\ & > err \times \left| \sigma^{inc}(E, E', \mu_{i+\frac{1}{2}}) \right|, \end{aligned} \quad (4.2.28)$$

$$|\sigma^{inc}(E, E', \mu_i) - \sigma^{inc}(E, E', \mu_{i+1})| \geq \left| \frac{\sigma^{inc}(E, E', \mu_i) + \sigma^{inc}(E, E', \mu_{i+1})}{2} \right|. \quad (4.2.29)$$

The linearization is finished and moves to the next angular point when the distance of the angular points is so small, *i.e.*, it satisfies following equation:

$$\mu_i - \mu_{i+1} < 1.0 \times 10^{-5}. \quad (4.2.30)$$

The integrated cross-section $\sigma^{inc}(E)$, which is divided into equally probable cosine bins, and the cumulative distribution are written in the PENDF file. Because the incoherent inelastic scattering cross-sections are linearized, $\sigma^{inc}(E)$ is easily calculated with the trapezoidal integration as follows:

$$\begin{aligned} \sigma^{inc}(E) &= \int_0^\infty \sigma^{inc}(E, E') dE' \\ &= \sum_i \frac{\sigma^{inc}(E, E'_i) + \sigma^{inc}(E, E'_{i-1})}{2} \times (E'_i - E'_{i-1}), \end{aligned} \quad (4.2.31)$$

where

$$\begin{aligned} \sigma^{inc}(E, E') &= \int_{-1}^1 \sigma^{inc}(E, E', \mu) d\mu \\ &= \sum_j \frac{\sigma^{inc}(E, E' \mu_j) + \sigma^{inc}(E, E' \mu_{j-1})}{2} \times (\mu_j - \mu_{j-1}). \end{aligned} \quad (4.2.32)$$

To calculate the cumulative distribution, FRENDY searches for the j -th cosine bin μ_j that satisfies the following equation:

$$\int_{\mu_{j-1}}^{\mu_j} \sigma^{inc}(E, E', \mu) d\mu = \frac{\sigma^{inc}(E, E')}{n_{bin}}, \quad (4.2.33)$$

where n_{bin} is the number of bins. The cumulative $\sigma_{PENDF}^{inc}(E, E', \mu_j)$ value, which is calculated by the following equation, is written in the PENDF file

$$\begin{aligned}
\sigma_{PENDF}^{inc}(E, E', \mu_j) &= \int_1^{\mu_j} \mu \times \sigma^{inc}(E, E', \mu) d\mu \\
&= \sum_i \frac{1}{3} (\sigma^{inc}(E, E', \mu_{i+1}) - \sigma^{inc}(E, E', \mu_i)) (\mu_{i+1}^2 + \mu_{i+1}\mu_i + \mu_i^2) \\
&\quad + \frac{1}{2} (\mu_{i+1}\sigma^{inc}(E, E', \mu_i) - \mu_i\sigma^{inc}(E, E', \mu_{i+1})) (\mu_{i+1} + \mu_i) \\
&= \sum_i \int_{\mu_i}^{\mu_{i+1}} \mu(a\mu + b) d\mu,
\end{aligned} \tag{4.2.34}$$

where

$$a = \frac{\sigma^{inc}(E, E', \mu_{i+1}) - \sigma^{inc}(E, E', \mu_i)}{\mu_{i+1} - \mu_i}, \tag{4.2.35}$$

$$b = \frac{\mu_i\sigma^{inc}(E, E', \mu_{i+1}) - \mu_{i+1}\sigma^{inc}(E, E', \mu_i)}{\mu_{i+1} - \mu_i}. \tag{4.2.36}$$

5 Probability Table Generation

5.1 Treatment of Self-Shielding Effect in Unresolved Resonance Region

In the unresolved resonance region, each resonance cannot be separated and the evaluated nuclear data file provides mean values of resonance spacing and resonance partial width¹³⁾. The self-shielding effect in the unresolved resonance region also has a large impact on the fast reactor⁴⁴⁾. The probability table method is widely used in order to appropriately treat the self-shielding effect in the unresolved resonance region for continuous energy Monte Carlo codes^{40,45)}. In this method, a table provides the probability distribution of the cross section in a given energy grid point which corresponds to the resonance structure. Consideration of the self-shielding effect in the unresolved resonance region is also used for the multi-group transport calculation. The Bondarenko-style self-shielded cross-section⁴⁶⁾ is used to treat this effect and it is generated using the probability table. Though some nuclear data processing codes generate the Bondarenko-style self-shielded cross-section by the deterministic method, *e.g.*, the UNRESR module in NJOY^{7,8)}. According to the manual of NJOY, the Bondarenko-style self-shielded cross-section generated by the probability table is more appropriate than that by the deterministic method⁴⁰⁾. Actually, the self-shielding factor generated by the deterministic method sometimes shows inappropriate values, *e.g.*, negative or larger than 1.0. Therefore, FRENDY uses only the probability method to calculate it.

5.2 Calculation Flow of Probability Table Generation

The evaluated nuclear data file provides only mean values of the resonance parameters in the unresolved resonance region. In the unresolved resonance region, the ladder method⁴⁰⁾ is used to generate a lot of pseudo resonance structures using random numbers based on the averaged resonance parameters. A resonance structure generated by random numbers is called “ladder” and an example is shown in Fig. 5.2.1. The pseudo resonance structure is generated as follows:

- (1) Determination of the i -th resonance energy $E_{r,i}$ by multiplying the average level spacing \bar{D} by the random number R_W conforming to the Wigner distribution function,
- (2) Determination of the resonance width $\Gamma_{r,i}$ by multiplying the average resonance width $\bar{\Gamma}_r$ by the chi-squared random numbers with k degrees of freedom $R_{\chi^2}(k)$,
- (3) Determination of the energy grid point E_j at which the cross section is calculated using the uniform random number R_u ,
- (4) Calculation of the cross-section $\sigma_{r,j}(E_j, T)$ of the energy grid point E_j at T K with the $\psi\text{-}\chi$ method⁴⁷⁾, and
- (5) Calculation of the probability $P_n(T)$ of $\sigma_{n-1} \leq \sigma_{t,j}(E_j, T) < \sigma_n$,

where r is a reaction type, σ_n the upper limit cross-section of the n -th probability bin, and $\sigma_{t,j}(E_j, T)$ the total cross-section of the energy grid point E_j at T K.

To calculate probability table $P_n(T)$, we generate a lot of ladders. The evaluated nuclear data library contains the energy-dependent average resonance parameters. Therefore, the probability table is calculated in each energy point which corresponds to the energy-dependent parameters. Generally, the number of sampling energy grid point E_j is 10,000 and the number of ladders is 20-100. When the number of energy points is 30, the cross section should be calculated 6-30 million times. Since the number of the energy grid points of the linearized cross section is less than a few million, the calculation of probability tables in all energy points requires a long calculation time.

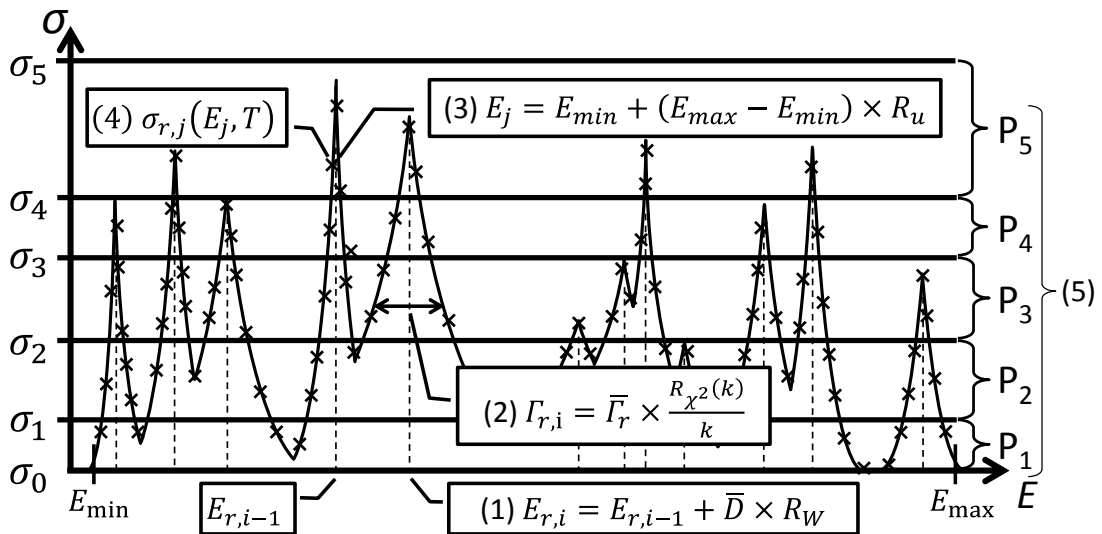


Figure 5.2.1 Example of pseudo resonance structure generation for the ladder method

5.2.1 Determination of resonance energy

The average level spacing \bar{D} is the mean value of the distribution of resonance spacing and it obeys the Wigner distribution. The resonance spacing is determined by multiplying the average level spacing \bar{D} by the random number R_W conforming to the Wigner distribution function. R_W is calculated using the inverse transform sampling. The Wigner distribution function $P_w(y)$ is given as follows:

$$P_w(y) = \frac{\pi}{2} y e^{-\frac{\pi}{4} y^2}. \quad (5.2.1)$$

The cumulative distribution function $F_w(\zeta)$ of the Wigner distribution is

$$F_w(\zeta) = \int_0^\zeta P_w(y) dy = 1 - e^{-\frac{\pi}{4} \zeta^2}. \quad (5.2.2)$$

The inverse function of $F_w(\zeta)$ is

$$\zeta = \pm \sqrt{\frac{4}{\pi} \ln \left(\frac{1}{1 - F_W(\zeta)} \right)}. \quad (5.2.3)$$

Using Eq. (5.2.3), R_W is calculated using the uniform random number R_u as follows:

$$R_W = \frac{2}{\sqrt{\pi}} \sqrt{\ln \left(\frac{1}{1 - R_u} \right)} = \frac{2}{\sqrt{\pi}} \sqrt{\ln \left(\frac{1}{R_u} \right)}. \quad (5.2.4)$$

5.2.2 Determination of resonance width

The resonance width Γ_r distributes according to the chi-squared distribution with a certain number of degrees of freedom¹³⁾. The resonance width is determined by multiplying the average resonance width $\bar{\Gamma}_r$ by the chi-squared random numbers with k degrees of freedom $R_{\chi^2}(k)$. To calculate $R_{\chi^2}(k)$, the PURR module in NJOY and the U3R code⁴⁸⁾ use discrete random numbers. Table 5.2.1 shows the chi-squared random numbers $R_{\chi^2}(k)$ in PURR. For example, if R_u is 0.03 and the number of degrees of freedom is 1, the chi-squared random number is 0.0013100 from Table 5.2.1. The discrete random numbers are inappropriate because the resonance structure depends on the chi-squared random numbers.

To appropriately calculate the chi-squared random numbers, FRENDY uses⁴⁹⁾

$$R_{\chi^2}(k) = \begin{cases} R_{\Gamma}\left(\frac{k}{2}, 2\right) & (k > 1) \\ (R_u)^2 R_{\Gamma}\left(\frac{3}{2}, 2\right) & (k = 1) \end{cases}, \quad (5.2.5)$$

where $R_{\Gamma}(\alpha, \beta)$ is the gamma random number, α a shape parameter, and β a scale parameter. Marsaglina's method⁵⁰⁾ is used to calculate the gamma random number.

Table 5.2.1 Chi-squared random numbers $R_{\chi^2}(k)$ in PURR

R_u	$R_{\chi^2}(1)$	$R_{\chi^2}(2)$	$R_{\chi^2}(3)$	$R_{\chi^2}(4)$
0.00~0.05	0.0013100	0.0508548	0.2068320	0.4594620
0.05~0.10	0.0091950	0.1561670	0.4707190	0.8937350
0.10~0.15	0.0250905	0.2673350	0.6919330	1.2175300
0.15~0.20	0.0492540	0.3850500	0.9016740	1.5087200
0.20~0.25	0.0820892	0.5101310	1.1086800	1.7860500
0.25~0.30	0.1241690	0.6435640	1.3176500	2.0585400
0.30~0.35	0.1762680	0.7865430	1.5319300	2.3319400
0.35~0.40	0.2394170	0.9405410	1.7544400	2.6106900
0.40~0.45	0.3149770	1.1074000	1.9881200	2.8987800
0.45~0.50	0.4047490	1.2894700	2.2362100	3.2003200
0.50~0.55	0.5111450	1.4898100	2.5025700	3.5199500
0.55~0.60	0.6374610	1.7124900	2.7921300	3.8633100
0.60~0.65	0.7883150	1.9631400	3.1114300	4.2377600
0.65~0.70	0.9704190	2.2498400	3.4696700	4.6534500
0.70~0.75	1.1940000	2.5847300	3.8805300	5.1253300
0.75~0.80	1.4757300	2.9874400	4.3658600	5.6771200
0.80~0.85	1.8454700	3.4927800	4.9641700	6.3504400
0.85~0.90	2.3652200	4.1723800	5.7542300	7.2299600
0.90~0.95	3.2037100	5.2188800	6.9464600	8.5410000
0.95~1.00	5.5820100	7.9914600	10.0048000	11.8359000

5.2.3 Determination of Energy Grid Points

To calculate the probability $P_n(T)$ of $\sigma_{n-1} \leq \sigma_r(E, T) \leq \sigma_n$, FRENDY sets 10,000 energy grid points in each ladder and calculates only the Doppler broadened cross-section on these energy grid points. The energy grid point is determined by the uniform random number R_u as follows:

$$E_j = E_{min} + (E_{max} - E_{min}) \times R_u, \quad (5.2.6)$$

where E_j is j -th energy grid point, E_{min} the lower energy limit of a resonance range in the unresolved resonance region, and E_{max} the upper energy limit of the resonance range in the unresolved resonance region.

5.2.4 Calculation of Cross Sections

In general, the kernel broadening method³⁵⁾, which is adopted in Doppler broadening of FRENDY,

the BROADR module in NJOY, and SIGMA1 module in PREPRO⁹⁾, is used to more accurately calculate the Doppler broadened cross-sections in the resolved resonance region than the other calculation methods. This method requires a long calculation time to calculate the Doppler broadened cross-sections. The ladder method generates a lot of resonance structures and calculates the Doppler broadened cross-sections. Thus, the kernel broadening method for the ladder method is not accepted in the unresolved resonance region from the view point of calculation time.

In the ENDF-6 format, only the Single-Level Breit-Wigner (SLBW) representation is available for the unresolved resonance region¹³⁾. The SLBW approximation allows the use of the $\psi\text{-}\chi$ method⁴⁷⁾ which approximately calculates the Doppler broadened cross-sections in short calculation time.

In the $\psi\text{-}\chi$ method, the cross sections at T K are calculated as follows⁴⁰⁾:

$$\sigma_\gamma(E, T) \cong \frac{\sigma_1 \Gamma_{\gamma r}}{\Gamma_r} \psi(\zeta, x), \quad (5.2.7)$$

$$\sigma_f(E, T) \cong \frac{\sigma_1 \Gamma_{fr}}{\Gamma_r} \psi(\zeta, x), \quad (5.2.8)$$

$$\sigma_s(E, T) = \sigma_1 \left(\psi(\zeta, x) \left(\cos 2\phi_l - 1 + \frac{\Gamma_{nr}}{\Gamma_r} \right) + \chi(\zeta, x) \sin 2\phi_l \right) + \sigma_p, \quad (5.2.9)$$

where

$$\sigma_1 = \frac{4\pi}{k_r^2} g_J \frac{\Gamma_{nr}}{\Gamma_r}, \quad (5.2.10)$$

$$\psi(\zeta, x) = \frac{\zeta}{2\sqrt{\pi}} \int_{-\infty}^{\infty} \frac{1}{1+y^2} e^{-\frac{\zeta^2}{4}(x-y)^2} dy, \quad (5.2.11)$$

$$\chi(\zeta, x) = \frac{\zeta}{2\sqrt{\pi}} \int_{-\infty}^{\infty} \frac{y}{1+y^2} e^{-\frac{\zeta^2}{4}(x-y)^2} dy, \quad (5.2.12)$$

$$x = \frac{2}{\Gamma_r} (E - E_1), \quad (5.2.13)$$

$$y = \frac{2}{\Gamma_r} (E_r - E_1), \quad (5.2.14)$$

$$\zeta = \frac{\Gamma_r}{\sqrt{4E k_B T \frac{m}{M}}} \quad (5.2.15)$$

$$E_1 = E_r + \frac{S_l(|E_r|) - S_l(E)}{2(P_l(|E_r|))} \frac{P_l(E)}{P_l(|E_r|)} \Gamma_{nr}, \quad (5.2.16)$$

σ_γ the radiative capture cross-section, σ_f the fission cross-section, σ_s the elastic scattering cross-section, σ_p the potential scattering cross-section, Γ_r the total width, $\Gamma_{\gamma r}$ the radiative capture width, Γ_{fr} the fission width, Γ_{nr} the neutron widths, k_r a wave number, g_J a spin statistical factor, E an incident neutron energy, E_r a relative kinetic energy, ϕ_l a hard sphere

phase shift, S_l a shift factor, P_l a penetration factor, m the mass of neutron, M the mass of target nucleus, and k_B the Boltzmann constant.

Equations (5.2.11) and (5.2.12) are rewritten as

$$\begin{aligned}\psi(s, x) &= \frac{1}{\sqrt{\pi}} \int_{-\infty}^{\infty} \frac{1}{1 + \left(x - \frac{2}{\zeta}s\right)^2} e^{-s^2} ds \\ &= \frac{\zeta}{2\sqrt{\pi}} \int_{-\infty}^{\infty} \frac{\frac{\zeta}{2}}{s^2 - \zeta s x + \frac{\zeta^2}{4}x^2 + \frac{\zeta^2}{4}} e^{-s^2} ds,\end{aligned}\tag{5.2.17}$$

$$\begin{aligned}\chi(s, x) &= \frac{1}{\sqrt{\pi}} \int_{-\infty}^{\infty} \frac{x - \frac{2}{\zeta}s}{1 + \left(x - \frac{2}{\zeta}s\right)^2} e^{-s^2} ds \\ &= \frac{\zeta}{2\sqrt{\pi}} \int_{-\infty}^{\infty} \frac{\frac{\zeta}{2}x - s}{s^2 - \zeta s x + \frac{\zeta^2}{4}x^2 + \frac{\zeta^2}{4}} e^{-s^2} ds,\end{aligned}\tag{5.2.18}$$

where

$$s = \frac{\zeta}{2}(x - y),\tag{5.2.19}$$

$$y = x - \frac{2}{\zeta}s,\tag{5.2.20}$$

$$\frac{dy}{ds} = -\frac{2}{\zeta}.\tag{5.2.21}$$

We re-introduce the complex error function $w(z)$ mentioned in Eq. (2.3.41) as follows:

$$w(z) = e^{-z^2} \operatorname{erfc}(-iz) = e^{-z^2} (1 - \operatorname{erf}(-iz)) = \frac{i}{\pi} \int_{-\infty}^{\infty} \frac{e^{-s^2}}{z - s} ds.\tag{5.2.22}$$

Here $\operatorname{erfc}(\alpha)$ is the complimentary error function of complex argument α , $\operatorname{erf}(\alpha)$ the error function of complex argument α , and

$$z = (x + i)\frac{\zeta}{2} = u + ih,\tag{5.2.23}$$

where

$$u = \frac{\zeta}{2}x,\tag{5.2.24}$$

$$h = \frac{\zeta}{2}.\tag{5.2.25}$$

Substituting Eq. (5.2.23) into Eq. (5.2.22), the latter equation is rearranged as

$$\begin{aligned}
w(z) &= \frac{i}{\pi} \int_{-\infty}^{\infty} \frac{1}{s - (x + i)\frac{\zeta}{2}} e^{-s^2} ds \\
&= \frac{i}{\pi} \int_{-\infty}^{\infty} \left(s - \frac{\zeta}{2}x + i\frac{\zeta}{2} \right) \frac{1}{s^2 - \zeta sx + \frac{\zeta^2}{4}x^2 + \frac{\zeta^2}{4}} e^{-s^2} ds.
\end{aligned} \tag{5.2.26}$$

From the above equation, we obtain

$$\operatorname{Re}[w(z)] = \frac{1}{\pi} \int_{-\infty}^{\infty} \frac{\frac{\zeta}{2}}{s^2 - \zeta sx + \frac{\zeta^2}{4}x^2 + \frac{\zeta^2}{4}} e^{-s^2} ds, \tag{5.2.27}$$

and

$$\operatorname{Im}[w(z)] = \frac{1}{\pi} \int_{-\infty}^{\infty} \frac{\frac{\zeta}{2}x - s}{s^2 - \zeta sx + \frac{\zeta^2}{4}x^2 + \frac{\zeta^2}{4}} e^{-s^2} ds. \tag{5.2.28}$$

Using Eqs. (5.2.27) and (5.2.28), Eqs. (5.2.17) and (5.2.18) are expressed as

$$\psi(s, x) = \frac{\zeta\sqrt{\pi}}{2} \operatorname{Re}[w(z)], \tag{5.2.29}$$

$$\chi(s, x) = \frac{\zeta\sqrt{\pi}}{2} \operatorname{Im}[w(z)]. \tag{5.2.30}$$

As shown in Eqs. (5.2.29) and (5.2.30), $\psi(s, x)$ and $\chi(s, x)$ are calculated using the real and imaginary parts of the complex error function $w(z)$.

To estimate the complex error function, some calculation methods are proposed^{51,52)}. We adopted the 4-pole Padé approximation⁵³⁻⁵⁵⁾ to reduce the calculation time while keeping the enough accuracy. This is one of the most efficient methods to reduce the calculation time with the ψ - χ method.

The complex error function using the 4-pole Padé approximation is written as

$$\begin{aligned}
w(u + ih) &\approx \frac{i}{\sqrt{\pi}} \frac{p_0 + p_1(u + ih) + p_2(u + ih)^2 + p_3(u + ih)^3}{1 + q_1(u + ih) + q_2(u + ih)^2 + q_3(u + ih)^3 + q_4(u + ih)^4} \\
&= \frac{i}{\sqrt{\pi}} \frac{A_1 u + A_2 u^3 + i(A_3 + A_4 u^2)}{B_1 + B_2 u^2 + B_3 u^4 + i(B_4 u + B_5 u^3)}
\end{aligned} \tag{5.2.31}$$

where

$$A_1 = p_1 - 2p_2 h - 3p_3 h^2, \tag{5.2.32}$$

$$A_2 = p_3, \tag{5.2.33}$$

$$A_3 = p_0 + p_1 h - p_2 h^2 - p_3 h^3, \tag{5.2.34}$$

$$A_4 = p_2 + 3p_3 h, \tag{5.2.35}$$

$$B_1 = 1 - q_1 h - q_2 h^2 + q_3 h^3 + q_4 h^4, \tag{5.2.36}$$

$$B_2 = q_2 - 3q_3 h - 6q_4 h^2, \tag{5.2.37}$$

$$B_3 = q_4, \tag{5.2.38}$$

$$B_4 = q_1 + 2q_2 h - 3q_3 h^2 - 4q_4 h^3, \tag{5.2.39}$$

$$B_5 = q_3 + 4q_4 h, \quad (5.2.40)$$

$$p_0 = i\sqrt{\pi}, \quad (5.2.41)$$

$$p_1 = \frac{-15\pi^2 + 88\pi - 128}{2(6\pi^2 - 29\pi + 32)}, \quad (5.2.42)$$

$$p_2 = -i \frac{-33\pi + 104}{6(6\pi^2 - 29\pi + 32)} \sqrt{\pi}, \quad (5.2.43)$$

$$p_3 = - \frac{9\pi^2 - 69\pi + 128}{3(6\pi^2 - 29\pi + 32)}, \quad (5.2.44)$$

$$q_1 = -i \frac{9\pi - 28}{2(6\pi^2 - 29\pi + 32)} \sqrt{\pi}, \quad (5.2.45)$$

$$q_2 = - \frac{-36\pi^2 + 195\pi - 256}{6(6\pi^2 - 29\pi + 32)}, \quad (5.2.46)$$

$$q_3 = i \frac{-33\pi + 104}{6(6\pi^2 - 29\pi + 32)} \sqrt{\pi}, \quad (5.2.47)$$

$$q_4 = \frac{9\pi^2 - 69\pi + 128}{3(6\pi^2 - 29\pi + 32)}. \quad (5.2.48)$$

5.2.5 Calculation of the probability

To calculate the probability of the n -th bin $P_n(T)$, we count the number of energy grid points that the total cross-section $\sigma_{t,j}(E_j, T)$ satisfies the following equation

$$\sigma_{n-1} \leq \sigma_{t,j}(E_j, T) \leq \sigma_n. \quad (5.2.49)$$

The PENDF file contains $P_n(T)$, average cross-section $\bar{\sigma}_r(T)$, and cross section of the n -th bin $\sigma_{r,n}(T)$. $\bar{\sigma}_r(T)$ and $\sigma_{r,n}(T)$ are obtained by

$$\bar{\sigma}_r(T) = \frac{\sum_j \sigma_{r,j}(E_j, T)}{N_{ladder} \times N_{sample}}, \quad (5.2.50)$$

$$\sigma_{r,n}(T) = \frac{\bar{\sigma}_{r,n}(T)}{\bar{\sigma}_r(T)}, \quad (5.2.51)$$

where, $\bar{\sigma}_{x,n}$ is an average cross-section of $\sigma_{n-1} \leq \sigma_{t,j}(E_j, T) < \sigma_n$, N_{ladder} the number of ladders, and N_{sample} the number of sampling energy grid points.

The Bondarenko-style self-shielded cross-section $\sigma_{b,r}(T)$ is also calculated using $\sigma_{r,n}(T)$ and $\bar{\sigma}_{t,n}(T)$ as follows:

$$\sigma_{b,r}(T) = \frac{\sum_n \frac{\sigma_0 \bar{\sigma}_{r,n}(T)}{\sigma_0 + \bar{\sigma}_{t,n}(T)}}{\sum_n \frac{\sigma_0}{\sigma_0 + \bar{\sigma}_{t,n}(T)}}, \quad (5.2.52)$$

where r is the reaction type, *i.e.*, the total, elastic scattering, fission, and radiative capture.

5.3 Investigation of Appropriate Number of Ladders

The ladder method generates a lot of pseudo resonance structures to produce a probability table. Investigation of the appropriate number of ladders, *i.e.*, the number of pseudo resonance structures, is important to reduce nuclear data processing time while keeping the accuracy of neutronics calculations⁵⁵⁾.

To determine the appropriate number of ladders, we address major heavy nuclides, *i.e.*, ^{232}Th , ^{233}U , ^{234}U , ^{235}U , ^{238}U , ^{237}Np , ^{238}Pu , ^{239}Pu , ^{240}Pu , ^{241}Pu , ^{242}Pu , ^{241}Am , and ^{242}Cm , from JENDL-4.0¹⁾ as target nuclides. The number of probability bins is 20 and the number of ladders is 10, 50, 100, 200, 300, and 500. The number of ladders for the reference case is 1,000. The calculation time of ^{235}U and ^{238}U are 10 hours and 4 hours, respectively, using Intel Core i7-3960X processor (3.30GHz) without parallel computation when the number of ladders is 1,000. From the view point of calculation time, the larger number of ladders is not acceptable.

As described in Sec. 5.2, the probability table is calculated in each energy point which corresponds to the energy-dependent average resonance parameter. In this study, we compared the RMS value of the all energy points and probability bins. The RMS value $RMS_{l,r}(T)$ is calculated as follows:

$$RMS_{l,r}(T) = \sqrt{\frac{\sum_g^G \sum_n^B \left\{ P_{l_{ref},g,n}(T) \times \sigma_{l_{ref},r,g,n}(T) - P_{l,g,n}(T) \times \sigma_{l,r,g,n}(T) \right\}^2}{G \times B}}, \quad (5.3.1)$$

where l is an index of the ladder number, x a reaction type, G the number of energy points, B the number of probability bin, and l_{ref} a reference ladder number. Tables 5.3.1 - 5.3.3 show the RMS value of each ladder number. As shown in Tables 5.3.1 - 5.3.3, the RMS values are enough small when the number of ladders is 100. The generation time of the probability table for each nuclide (number of ladders: 100, number of temperatures: 1) was usually 1-2 hours. This generation time is acceptable from the view point of the current computational performance.

Table 5.3.1 RMS value of probability table difference in each number of ladders (293.6 K) (1/3)

Nuclide	Ladder No.	Total	Scatter	Fission	Radiation
^{232}Th	10	0.20%	0.20%	0.18%	0.22%
	20	0.15%	0.15%	0.14%	0.16%
	30	0.12%	0.12%	0.11%	0.12%
	50	0.08%	0.08%	0.08%	0.09%
	100	0.06%	0.06%	0.06%	0.07%
	200	0.05%	0.05%	0.04%	0.05%
	300	0.04%	0.04%	0.03%	0.04%
	500	0.03%	0.03%	0.03%	0.03%
^{233}U	10	0.31%	0.31%	0.33%	0.35%
	20	0.24%	0.23%	0.26%	0.27%
	30	0.18%	0.18%	0.20%	0.22%
	50	0.16%	0.16%	0.17%	0.19%
	100	0.11%	0.10%	0.12%	0.12%
	200	0.08%	0.08%	0.08%	0.09%
	300	0.06%	0.06%	0.06%	0.07%
	500	0.05%	0.05%	0.05%	0.05%
^{234}U	10	0.23%	0.23%	0.33%	0.26%
	20	0.15%	0.15%	0.23%	0.17%
	30	0.14%	0.14%	0.21%	0.16%
	50	0.09%	0.09%	0.13%	0.11%
	100	0.07%	0.07%	0.09%	0.08%
	200	0.05%	0.05%	0.06%	0.05%
	300	0.04%	0.04%	0.05%	0.05%
	500	0.03%	0.03%	0.05%	0.04%
^{235}U	10	0.31%	0.30%	0.33%	0.34%
	20	0.23%	0.22%	0.24%	0.25%
	30	0.18%	0.18%	0.19%	0.20%
	50	0.14%	0.13%	0.15%	0.15%
	100	0.10%	0.10%	0.11%	0.11%
	200	0.07%	0.07%	0.08%	0.08%
	300	0.06%	0.06%	0.07%	0.07%
	500	0.05%	0.05%	0.05%	0.05%
^{236}U	10	0.22%	0.22%	0.20%	0.23%
	20	0.14%	0.14%	0.13%	0.15%
	30	0.11%	0.12%	0.11%	0.12%
	50	0.09%	0.09%	0.08%	0.09%
	100	0.07%	0.07%	0.06%	0.08%
	200	0.05%	0.05%	0.05%	0.05%
	300	0.04%	0.04%	0.04%	0.04%
	500	0.03%	0.03%	0.03%	0.03%

Table 5.3.1 RMS value of probability table difference in each number of ladders (293.6 K) (2/3)

Nuclide	Ladder No.	Total	Scatter	Fission	Radiation
^{238}U	10	0.23%	0.23%	0.22%	0.23%
	20	0.15%	0.15%	0.15%	0.17%
	30	0.12%	0.12%	0.12%	0.13%
	50	0.10%	0.10%	0.10%	0.11%
	100	0.08%	0.08%	0.07%	0.08%
	200	0.06%	0.06%	0.06%	0.06%
	300	0.04%	0.04%	0.04%	0.05%
	500	0.03%	0.03%	0.03%	0.03%
^{237}Np	10	0.31%	0.30%	0.36%	0.32%
	20	0.22%	0.22%	0.25%	0.24%
	30	0.18%	0.18%	0.20%	0.19%
	50	0.15%	0.14%	0.17%	0.15%
	100	0.11%	0.11%	0.11%	0.11%
	200	0.07%	0.07%	0.08%	0.07%
	300	0.07%	0.07%	0.07%	0.07%
	500	0.05%	0.05%	0.05%	0.05%
^{238}Pu	10	0.24%	0.24%	0.34%	0.27%
	20	0.16%	0.16%	0.25%	0.18%
	30	0.13%	0.13%	0.20%	0.15%
	50	0.11%	0.11%	0.16%	0.12%
	100	0.09%	0.09%	0.12%	0.10%
	200	0.05%	0.05%	0.07%	0.06%
	300	0.04%	0.05%	0.06%	0.05%
	500	0.04%	0.04%	0.05%	0.04%
^{239}Pu	10	0.26%	0.26%	0.30%	0.30%
	20	0.19%	0.18%	0.22%	0.22%
	30	0.14%	0.14%	0.16%	0.16%
	50	0.12%	0.12%	0.15%	0.14%
	100	0.08%	0.08%	0.09%	0.10%
	200	0.06%	0.06%	0.06%	0.07%
	300	0.05%	0.05%	0.05%	0.06%
	500	0.04%	0.04%	0.05%	0.05%
^{240}Pu	10	0.23%	0.23%	0.28%	0.24%
	20	0.16%	0.16%	0.22%	0.18%
	30	0.12%	0.12%	0.18%	0.14%
	50	0.10%	0.10%	0.13%	0.11%
	100	0.06%	0.06%	0.08%	0.07%
	200	0.05%	0.05%	0.06%	0.05%
	300	0.04%	0.04%	0.05%	0.04%
	500	0.03%	0.03%	0.04%	0.04%

Table 5.3.1 RMS value of probability table difference in each number of ladders (293.6 K) (3/3)

Nuclide	Ladder No.	Total	Scatter	Fission	Radiation
^{241}Pu	10	0.19%	0.18%	0.23%	0.24%
	20	0.14%	0.13%	0.16%	0.17%
	30	0.11%	0.10%	0.12%	0.13%
	50	0.09%	0.08%	0.10%	0.11%
	100	0.06%	0.06%	0.07%	0.08%
	200	0.05%	0.05%	0.05%	0.06%
	300	0.04%	0.04%	0.04%	0.05%
	500	0.03%	0.03%	0.04%	0.04%
^{242}Pu	10	0.21%	0.21%	0.33%	0.23%
	20	0.14%	0.14%	0.22%	0.15%
	30	0.12%	0.12%	0.19%	0.13%
	50	0.09%	0.09%	0.14%	0.11%
	100	0.06%	0.06%	0.10%	0.07%
	200	0.05%	0.05%	0.07%	0.05%
	300	0.04%	0.04%	0.05%	0.04%
	500	0.03%	0.03%	0.05%	0.04%
^{241}Am	10	0.30%	0.29%	0.36%	0.31%
	20	0.22%	0.21%	0.26%	0.23%
	30	0.17%	0.16%	0.20%	0.18%
	50	0.14%	0.14%	0.17%	0.15%
	100	0.10%	0.10%	0.11%	0.10%
	200	0.07%	0.07%	0.08%	0.08%
	300	0.06%	0.06%	0.07%	0.07%
	500	0.04%	0.04%	0.05%	0.05%
^{242}Cm	10	0.25%	0.25%	0.39%	0.28%
	20	0.19%	0.18%	0.28%	0.21%
	30	0.14%	0.14%	0.20%	0.16%
	50	0.11%	0.10%	0.17%	0.13%
	100	0.08%	0.08%	0.12%	0.09%
	200	0.06%	0.06%	0.07%	0.06%
	300	0.05%	0.05%	0.07%	0.05%
	500	0.04%	0.04%	0.05%	0.04%

Table 5.3.2 RMS value of probability table difference in each number of ladders (1000 K) (1/3)

Nuclide	Ladder No.	Total	Scatter	Fission	Radiation
^{232}Th	10	0.25%	0.25%	0.23%	0.26%
	20	0.15%	0.15%	0.14%	0.16%
	30	0.14%	0.14%	0.13%	0.15%
	50	0.10%	0.10%	0.10%	0.11%
	100	0.08%	0.08%	0.08%	0.08%
	200	0.06%	0.06%	0.05%	0.06%
	300	0.04%	0.04%	0.04%	0.05%
	500	0.03%	0.03%	0.03%	0.04%
^{233}U	10	0.41%	0.40%	0.42%	0.44%
	20	0.31%	0.31%	0.33%	0.34%
	30	0.23%	0.23%	0.25%	0.25%
	50	0.19%	0.19%	0.21%	0.22%
	100	0.14%	0.14%	0.15%	0.16%
	200	0.09%	0.09%	0.10%	0.11%
	300	0.08%	0.08%	0.09%	0.09%
	500	0.06%	0.06%	0.07%	0.07%
^{234}U	10	0.27%	0.27%	0.34%	0.28%
	20	0.18%	0.18%	0.24%	0.19%
	30	0.16%	0.16%	0.21%	0.18%
	50	0.11%	0.11%	0.15%	0.12%
	100	0.08%	0.08%	0.10%	0.09%
	200	0.05%	0.05%	0.06%	0.06%
	300	0.05%	0.05%	0.06%	0.05%
	500	0.04%	0.04%	0.05%	0.04%
^{235}U	10	0.42%	0.42%	0.44%	0.45%
	20	0.30%	0.30%	0.31%	0.32%
	30	0.25%	0.25%	0.27%	0.27%
	50	0.18%	0.18%	0.19%	0.19%
	100	0.13%	0.13%	0.14%	0.13%
	200	0.09%	0.09%	0.10%	0.09%
	300	0.08%	0.08%	0.08%	0.08%
	500	0.07%	0.06%	0.07%	0.07%
^{236}U	10	0.28%	0.28%	0.26%	0.30%
	20	0.17%	0.17%	0.16%	0.18%
	30	0.14%	0.14%	0.13%	0.14%
	50	0.10%	0.10%	0.10%	0.11%
	100	0.09%	0.09%	0.08%	0.09%
	200	0.06%	0.06%	0.06%	0.06%
	300	0.05%	0.05%	0.05%	0.05%
	500	0.04%	0.04%	0.03%	0.04%

Table 5.3.2 RMS value of probability table difference in each number of ladders (1000 K) (2/3)

Nuclide	Ladder No.	Total	Scatter	Fission	Radiation
^{238}U	10	0.28%	0.28%	0.27%	0.29%
	20	0.20%	0.20%	0.19%	0.20%
	30	0.15%	0.15%	0.15%	0.16%
	50	0.13%	0.13%	0.13%	0.14%
	100	0.09%	0.09%	0.09%	0.09%
	200	0.07%	0.07%	0.07%	0.07%
	300	0.05%	0.05%	0.05%	0.06%
	500	0.04%	0.04%	0.04%	0.04%
^{237}Np	10	0.40%	0.40%	0.43%	0.41%
	20	0.32%	0.32%	0.34%	0.33%
	30	0.25%	0.25%	0.26%	0.26%
	50	0.19%	0.18%	0.20%	0.19%
	100	0.14%	0.14%	0.14%	0.14%
	200	0.10%	0.10%	0.10%	0.10%
	300	0.08%	0.08%	0.09%	0.09%
	500	0.07%	0.07%	0.07%	0.07%
^{238}Pu	10	0.29%	0.29%	0.36%	0.31%
	20	0.19%	0.19%	0.26%	0.21%
	30	0.14%	0.14%	0.19%	0.16%
	50	0.13%	0.13%	0.16%	0.14%
	100	0.09%	0.09%	0.11%	0.10%
	200	0.06%	0.06%	0.07%	0.06%
	300	0.05%	0.05%	0.06%	0.05%
	500	0.04%	0.04%	0.05%	0.04%
^{239}Pu	10	0.32%	0.31%	0.36%	0.35%
	20	0.24%	0.24%	0.26%	0.27%
	30	0.19%	0.19%	0.20%	0.20%
	50	0.15%	0.15%	0.17%	0.16%
	100	0.10%	0.10%	0.11%	0.11%
	200	0.08%	0.07%	0.08%	0.08%
	300	0.06%	0.06%	0.07%	0.07%
	500	0.05%	0.05%	0.06%	0.06%
^{240}Pu	10	0.27%	0.27%	0.32%	0.27%
	20	0.18%	0.18%	0.23%	0.19%
	30	0.15%	0.15%	0.18%	0.16%
	50	0.12%	0.12%	0.14%	0.12%
	100	0.07%	0.07%	0.09%	0.08%
	200	0.06%	0.06%	0.07%	0.06%
	300	0.05%	0.05%	0.06%	0.05%
	500	0.04%	0.04%	0.05%	0.04%

Table 5.3.2 RMS value of probability table difference in each number of ladders (1000 K) (3/3)

Nuclide	Ladder No.	Total	Scatter	Fission	Radiation
^{241}Pu	10	0.22%	0.21%	0.25%	0.24%
	20	0.16%	0.15%	0.18%	0.18%
	30	0.13%	0.13%	0.14%	0.14%
	50	0.11%	0.11%	0.12%	0.13%
	100	0.07%	0.07%	0.08%	0.08%
	200	0.06%	0.06%	0.06%	0.06%
	300	0.05%	0.04%	0.05%	0.05%
	500	0.04%	0.04%	0.04%	0.04%
^{242}Pu	10	0.26%	0.26%	0.33%	0.26%
	20	0.17%	0.17%	0.24%	0.19%
	30	0.13%	0.13%	0.17%	0.15%
	50	0.10%	0.10%	0.14%	0.12%
	100	0.08%	0.08%	0.09%	0.09%
	200	0.05%	0.05%	0.07%	0.06%
	300	0.04%	0.04%	0.06%	0.05%
	500	0.04%	0.04%	0.05%	0.04%
^{241}Am	10	0.43%	0.42%	0.46%	0.43%
	20	0.29%	0.29%	0.32%	0.30%
	30	0.24%	0.24%	0.26%	0.24%
	50	0.18%	0.18%	0.21%	0.19%
	100	0.13%	0.13%	0.14%	0.13%
	200	0.10%	0.09%	0.10%	0.10%
	300	0.08%	0.08%	0.09%	0.08%
	500	0.07%	0.07%	0.07%	0.07%
^{242}Cm	10	0.30%	0.30%	0.40%	0.32%
	20	0.22%	0.21%	0.30%	0.24%
	30	0.17%	0.17%	0.23%	0.19%
	50	0.13%	0.12%	0.16%	0.14%
	100	0.09%	0.09%	0.12%	0.10%
	200	0.06%	0.06%	0.08%	0.07%
	300	0.06%	0.06%	0.07%	0.06%
	500	0.05%	0.04%	0.06%	0.05%

Table 5.3.3 RMS value of probability table difference in each number of ladders (2000 K) (1/3)

Nuclide	Ladder No.	Total	Scatter	Fission	Radiation
^{232}Th	10	0.28%	0.28%	0.26%	0.30%
	20	0.17%	0.18%	0.16%	0.18%
	30	0.16%	0.16%	0.15%	0.16%
	50	0.11%	0.11%	0.10%	0.11%
	100	0.09%	0.09%	0.09%	0.09%
	200	0.06%	0.06%	0.06%	0.07%
	300	0.05%	0.05%	0.05%	0.05%
	500	0.04%	0.04%	0.04%	0.04%
^{233}U	10	0.45%	0.44%	0.46%	0.48%
	20	0.36%	0.36%	0.37%	0.38%
	30	0.28%	0.28%	0.28%	0.29%
	50	0.23%	0.23%	0.24%	0.25%
	100	0.17%	0.16%	0.17%	0.18%
	200	0.11%	0.11%	0.11%	0.12%
	300	0.10%	0.09%	0.10%	0.10%
	500	0.08%	0.08%	0.08%	0.08%
^{234}U	10	0.32%	0.32%	0.37%	0.33%
	20	0.22%	0.22%	0.28%	0.23%
	30	0.17%	0.17%	0.22%	0.18%
	50	0.12%	0.12%	0.15%	0.13%
	100	0.09%	0.09%	0.10%	0.09%
	200	0.07%	0.07%	0.08%	0.07%
	300	0.05%	0.05%	0.06%	0.06%
	500	0.04%	0.04%	0.05%	0.05%
^{235}U	10	0.48%	0.48%	0.49%	0.51%
	20	0.36%	0.36%	0.37%	0.37%
	30	0.30%	0.30%	0.31%	0.31%
	50	0.24%	0.24%	0.24%	0.25%
	100	0.15%	0.15%	0.16%	0.16%
	200	0.12%	0.12%	0.12%	0.11%
	300	0.09%	0.09%	0.09%	0.10%
	500	0.08%	0.08%	0.08%	0.08%
^{236}U	10	0.32%	0.32%	0.31%	0.33%
	20	0.20%	0.20%	0.19%	0.21%
	30	0.16%	0.16%	0.15%	0.16%
	50	0.13%	0.13%	0.12%	0.13%
	100	0.10%	0.10%	0.10%	0.10%
	200	0.07%	0.07%	0.07%	0.07%
	300	0.06%	0.06%	0.05%	0.06%
	500	0.04%	0.04%	0.04%	0.04%

Table 5.3.3 RMS value of probability table difference in each number of ladders (2000 K) (2/3)

Nuclide	Ladder No.	Total	Scatter	Fission	Radiation
^{238}U	10	0.31%	0.31%	0.30%	0.32%
	20	0.22%	0.22%	0.22%	0.23%
	30	0.17%	0.17%	0.17%	0.18%
	50	0.15%	0.15%	0.15%	0.16%
	100	0.10%	0.10%	0.10%	0.10%
	200	0.09%	0.09%	0.08%	0.09%
	300	0.06%	0.06%	0.06%	0.06%
	500	0.05%	0.05%	0.05%	0.05%
^{237}Np	10	0.48%	0.48%	0.51%	0.49%
	20	0.38%	0.38%	0.40%	0.39%
	30	0.29%	0.29%	0.30%	0.29%
	50	0.23%	0.23%	0.24%	0.23%
	100	0.15%	0.15%	0.15%	0.15%
	200	0.12%	0.12%	0.13%	0.12%
	300	0.10%	0.10%	0.11%	0.10%
	500	0.08%	0.08%	0.08%	0.08%
^{238}Pu	10	0.32%	0.32%	0.38%	0.34%
	20	0.22%	0.22%	0.28%	0.23%
	30	0.15%	0.15%	0.20%	0.17%
	50	0.13%	0.13%	0.16%	0.14%
	100	0.10%	0.10%	0.12%	0.11%
	200	0.06%	0.06%	0.07%	0.07%
	300	0.06%	0.06%	0.06%	0.06%
	500	0.04%	0.04%	0.05%	0.05%
^{239}Pu	10	0.36%	0.36%	0.39%	0.39%
	20	0.27%	0.27%	0.30%	0.29%
	30	0.20%	0.20%	0.22%	0.22%
	50	0.18%	0.17%	0.20%	0.19%
	100	0.13%	0.13%	0.13%	0.14%
	200	0.08%	0.08%	0.09%	0.09%
	300	0.08%	0.08%	0.08%	0.08%
	500	0.06%	0.06%	0.07%	0.07%
^{240}Pu	10	0.31%	0.31%	0.35%	0.31%
	20	0.21%	0.21%	0.25%	0.22%
	30	0.17%	0.18%	0.20%	0.18%
	50	0.13%	0.13%	0.15%	0.13%
	100	0.08%	0.08%	0.09%	0.08%
	200	0.06%	0.06%	0.07%	0.07%
	300	0.06%	0.06%	0.06%	0.06%
	500	0.05%	0.05%	0.05%	0.05%

Table 5.3.3 RMS value of probability table difference in each number of ladders (2000 K) (3/3)

Nuclide	Ladder No.	Total	Scatter	Fission	Radiation
^{241}Pu	10	0.25%	0.25%	0.28%	0.27%
	20	0.18%	0.17%	0.20%	0.19%
	30	0.15%	0.14%	0.16%	0.16%
	50	0.12%	0.12%	0.13%	0.14%
	100	0.08%	0.08%	0.09%	0.09%
	200	0.06%	0.06%	0.06%	0.07%
	300	0.05%	0.05%	0.06%	0.06%
	500	0.04%	0.04%	0.04%	0.04%
^{242}Pu	10	0.29%	0.30%	0.35%	0.29%
	20	0.20%	0.20%	0.25%	0.21%
	30	0.15%	0.15%	0.20%	0.16%
	50	0.11%	0.11%	0.14%	0.12%
	100	0.09%	0.09%	0.11%	0.10%
	200	0.06%	0.06%	0.07%	0.06%
	300	0.05%	0.05%	0.06%	0.05%
	500	0.04%	0.04%	0.05%	0.04%
^{241}Am	10	0.50%	0.49%	0.52%	0.50%
	20	0.37%	0.36%	0.39%	0.37%
	30	0.29%	0.29%	0.31%	0.30%
	50	0.21%	0.21%	0.23%	0.22%
	100	0.16%	0.16%	0.17%	0.17%
	200	0.11%	0.11%	0.11%	0.11%
	300	0.10%	0.10%	0.10%	0.10%
	500	0.08%	0.08%	0.09%	0.08%
^{242}Cm	10	0.34%	0.34%	0.44%	0.36%
	20	0.25%	0.25%	0.32%	0.26%
	30	0.19%	0.19%	0.24%	0.21%
	50	0.15%	0.14%	0.18%	0.15%
	100	0.11%	0.11%	0.13%	0.11%
	200	0.07%	0.07%	0.08%	0.07%
	300	0.06%	0.06%	0.08%	0.06%
	500	0.05%	0.05%	0.06%	0.05%

6 Gas Production Cross-Section Calculation

When the incident particle energy is large, the induced nuclear reactions yield such the light particles as proton (^1H), deuteron (^2H), triton (^3H), ^3He , and alpha particle (^4He). These light particles accumulate as gases in a nuclear system. The estimation of the gas generation is important since the gas generation affects the embrittlement of material and the internal gas pressure in a fuel pin.

Though the ENDF-6 format defines the total gas production cross-sections, *i.e.*, (z, Xp) , (z, Xd) , (z, Xt) , $(z, \text{X}^3\text{He})$, and $(z, \text{X}\alpha)$ in MT 203-207 sections of File 3, these production cross-sections are mainly used for derived libraries¹³⁾. Here, z is the incident particle and X is the number of emitted light particles. FRENDY sums all the gas production reactions to calculate the total gas production cross-sections. For example, when a nucleus has only (n, p) and $(n, 2p)$ reactions for gas production cross-section, the total proton production cross-section $\sigma_{(n,Xp)}(E)$ is calculated as follows:

$$\sigma_{(n,Xp)}(E) = \sigma_{(n,p)}(E) + 2 \times \sigma_{(n,2p)}(E), \quad (6.1)$$

where E is the incident particle energy.

FRENDY also considers the residual nucleus for the calculation of the total gas production cross-section. For example, $^2\text{H}(n, \gamma)^3\text{H}$ or $^6\text{Li}(n, \alpha)^3\text{H}$ reactions yield tritium as the residual nucleus. In such cases, FRENDY adds tritium to the total gas production cross-section.

FRENDY overwrites the total gas production cross-sections even if the total gas production cross-sections are already defined in the evaluated nuclear data file.

7 ACE File Generation

Continuous-energy Monte Carlo calculation codes do not use either the evaluated nuclear data file or the PENDF file which is the intermediate file of NJOY^{7,8)}, directly. The ACE (A Compact ENDF) file is one of the cross-section data library formats and it is employed in many continuous-energy Monte Carlo calculation codes including PHITS⁴⁾, MCNP¹⁵⁾, and Serpent¹⁶⁾. Users can consult the MCNP manual¹⁵⁾ for the ACE format. The ACE format is designed to include all the details of the ENDF-6 representations for neutron and photon data⁴⁰⁾. The ACE format adopts the unionized energy grid and the cumulative probability distribution for the Monte Carlo calculation codes to handle the data conveniently. The unit of energy is changed from eV to MeV. The detail of the transformation is explained in Reference 40.

The ACE file generation module transforms the original nuclear data format, *e.g.*, the ENDF-6 format¹³⁾, to the ACE format. The ACE file generation module transforms the original angular and energy distributions to the specific representation suitable for Monte Carlo sampling procedures.

The ACE format provides for several different “data classes⁸⁾” as shown in Table 7.1. Each class is distinguished by the suffix. For example, “92235.50c” represents the continuous-energy neutron data. It should be noted that the current version of FRENDY does not generate the photo-atomic and the photo-nuclear data. Though the processing modules for the continuous-energy neutron data, the thermal scattering law data, and the dosimetry data are well verified, those for the other data, *i.e.*, the continuous-energy photon, deuteron, triton, ^3He , and alpha data, are not verified. Users must carefully check the processing results when they process these incident particles data.

As described in Sec. 1.2, FRENDY prepares the ACE data parser and writer modules to easily handle the ACE file. There are some cases where users want to modify the cross-section data library to estimate the impact of the modification of cross-section data library on the nuclear calculation results. The modification of the ACE file is so difficult for the users who do not know well about the ACE format. The ACE file uses random access with pointers to the various parts of the data. If the users want to modify the parameters of the ACE files, they also have to modify the pointers. The users can easily modify the ACE file using the ACE data parser and writer modules of FRENDY since FRENDY automatically adjust the pointers in the writer module.

Table 7.1 ACE data classes and suffixes

Suffix	ACE data class	Implementation of FRENDY
c	continuous-energy neutron data	Yes
t	thermal scattering law data	Yes
y	dosimetry data	Yes
p	photo-atomic data	No
u	photonuclear data	No
h	continuous-energy proton data	Yes but not verified
o	continuous-energy deuteron data	Yes but not verified
r	continuous-energy triton data	Yes but not verified
s	continuous-energy ^3He data	Yes but not verified
a	continuous-energy alpha data	Yes but not verified

8 Input Instructions

8.1 Input Format

FRENDDY accepts two types of input formats:

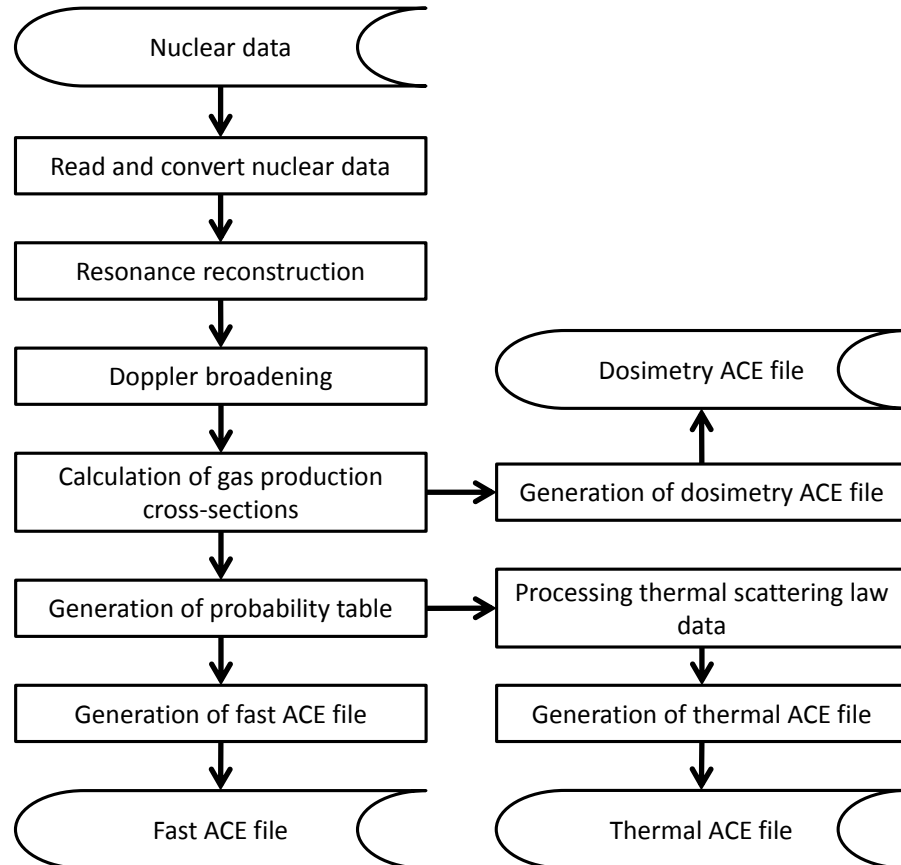
- FRENDDY original input format,
- NJOY99⁷⁾ compatible format.

The original input format requires only the processing mode name and evaluated nuclear data file name at minimum. FRENDDY has default values in the source code for the processing. Users can give the parameters in the input file if they want to change the parameters. The original input format is simple and it does not require the expertise of the nuclear data processing.

FRENDDY can also treat the NJOY99 input files. Many users process the evaluated nuclear data file with NJOY. They can easily use FRENDDY without changing the input files for NJOY. They can therefore replace NJOY modules with FRENDDY ones as they need. In addition, the modules of FRENDDY and NJOY can be used in combination. For example, users can generate the multi-group cross-section data library using the GROUPR module of NJOY with the PENDF file generated by FRENDDY.

8.2 FRENDDY Original Input Format

In the conventional processing code including NJOY and PREPRO⁹⁾, users have to select the running modules and prepare the input parameters for these modules to generate the cross-section data library. FRENDDY automatically generates the cross-section data library with the recommended processing flow as shown in Fig. 8.2.1 when users select an appropriate processing mode at least. They do not need to worry about what modules are required to generate the cross-section data library when they use FRENDDY original input format. FRENDDY also prepares the skip option to manually select the modules to be executed. Using this option, users can skip some modules in the recommended processing flow.

**Figure 8.2.1 Processing flow to generate ACE files**

8.2.1 Processing Mode

The order of the input data is free except the first parameter. Users have to set the processing mode as the first parameter. The available processing modes are listed in Table 8.2.1. The notation of the ACE file processing mode is identical to NJOY. The first parameter is also used to check the input file format. When the first parameter is the NJOY module name, *e.g.*, MODER, RECONR, BROADR, THERMR, PURR, and ACER, FRENDY interprets the input as the NJOY99 compatible format.

Table 8.2.1 Available processing mode

Processing mode name	Description
ace_file_generation_fast_mode or ace_fast_mode or ace_fast or ace_file_generation_normal_mode or ace_normal_mode or ace_normal	Generation of the particle incident ACE file
ace_file_generation_thermal_scattering_mode or ace_file_generation_thermal_scatter_mode or ace_therm_mode or ace_therm or ace_file_generation_tsl_mode or ace tsl mode or ace_tsl	Generation of ACE file of the thermal scattering law data
ace_file_generation_dosimetry_mode or ace_dosi_mode or ace_dosi	Generation of ACE file of the dosimetry data

8.2.2 Input Parameters

The input data except the processing mode consists of “parameter name” and “parameter value”. Users need to set the parameters if they want to modify the default values. FRENDY original input format accepts comment lines. The C++ style comments are available, *i.e.*, “//” for a single line comment and “/* ... */” for multi-line comments. FRENDY can read four types of data, *i.e.*, integer, real, string, and text, and the vector data of integer and real. The available types are as follows:

integer : integer number, *e.g.*, -2, -1, 0, 1, 2,
 real : real number, *e.g.*, -1.0, 0.0, 1.0, 1.0E-1, 1.0E+1, 1.0D-1, 1.0D+1, 1.0-1, 1.0+1,
 string : character data without space, *e.g.*, nuclide_name, calculation-type,
 text : multiple lines character data.

Users have to set the vector data in a bracket when they want to set the vector data of integer and real value. If users want to set three values, *i.e.*, 1.0, 2.0, and 3.0, users write as follows:

(1.0 2.0 3.0).

Since FRENDY can read data specified in multiple lines, the following input style is also acceptable

**(1.0
2.0
3.0),**

or

**(
1.0
2.0
3.0
).**

If users want to set the text data, they need to enclose single or double quotation marks. The text data allows multiple lines as follows:

**“92-U-238 from JENDL-4.0
Processed with FRENDY**

Processed day: 2017/10/13"

or

'92-U-238 from JENDL-4.0

Processed with FRENDY

Processed day: 2017/10/13'

If users want to use double quotation marks in the comment line, single quotation marks are used to enclose the text data as follows:

'This is the comment line for the PENDF file.

Users can use the “double quotation marks” when the comment line is enclosed by the single quotation marks.'

If users want to use single quotation marks in the comment line, double quotation marks are used to enclose the text data as follows:

"This is the comment line for the PENDF file.

Users can use the ‘single quotation marks’ when the comment line is enclosed by the double quotation marks."

The input parameter name and its recommended value for the FRENDY original input format are listed in Tables 8.2.2 - 8.2.9. The parameters shaded in Tables 8.2.2 - 8.2.9 always need input. In the default option, FRENDY does not output the PENDF file and users do not need to select the modules to be executed. Users have to set the print and process flags as listed in Tables 8.2.4 - 8.2.9 when they want to write the PENDF file or skip the modules. FRENDY can recognize synonymous words. For example, FRENDY prepares "ene_grid_no_per_ladder", "ene_grid_per_ladder", and "ene_no_per_ladder" as the parameter name to change the number of ladders to generate the probability table and "on", "yes", "print", "write", and "output" to write the PENDF file.

The examples of the input files for the FRENDY original input format are shown in Figs. 8.2.2 - 8.2.4. As shown in Fig. 8.2.3, the “parameter name” and “parameter value” do not need to be placed in the same line. Comment lines can be put among the “parameter name” and the “parameter value”. As shown in Fig. 8.2.4, the minimum input parameters are the processing mode and the evaluated nuclear data file name. FRENDY prepares the recommended values for the other parameters as listed in Tables 8.2.2 - 8.2.9.

Table 8.2.2 Input parameter name and recommended value for common parameter (1/3)

Parameter name	Type	Default value	Description
nucl_file_name	string	-	Evaluated nuclear data file name
pendf_label_data	string	none	Label for a new PENDF file (Maximum 66 words)
			Descriptive comments for the PENDF file (MT 451 section of File 1)
			FRENODY recognizes the comment line that is enclosed by double or single quotation marks.
			If users want to use double or single quotation marks in the comment line, they have to use single or double quotation marks to enclose the comment line.
			Ex)
			"This is the comment line for the PENDF file.
			Users can use the 'single quotation marks' when the comment line is enclosed by the double quotation marks."
error	real	1.00×10^{-3}	Tolerance value for linearization
error_max	real	$\text{error} \times 10.0$	Maximum tolerance value for linearization
error_integral	real	$\text{error}/20000.0$	Maximum integral error for linearization
add_grid_data	vector(real)	none	Additional energy grid point [eV]

Table 8.2.2 Input parameter name and recommended value for common parameter (2/3)

Parameter name	Type	Default value	Description
temp	real	293.6	Temperature [K]
max_broadening_ene	real	1.00×10 ⁶	Maximum energy for Doppler broadening [eV]
probability_bin_no	integer	20	Number of probability table bins
ladder_no	integer	200	Number of resonance ladders for generating the probability table
sigma_zero_data	vector(real)	1.0×10 ¹⁰ , 1.0×10 ⁶ , 1.0×10 ⁵ , 10000.0, 1000.0, 100.0, 35.0, 10.0, 1.0, 0.1	σ_0 values for the Bondarenko-type self-shielded cross-section in the unresolved resonance region [b] Maximum σ_0 is considered as the infinite dilution cross section (σ_{inf})
ene_grid_no_per_ladder or ene_grid_per_ladder or ene_no_per_ladder	integer	10000	Number of sampling energy grid points for each ladder
random_seed	integer	12345	Random number seed for probability table generation

Table 8.2.2 Input parameter name and recommended value for common parameter (3/3)

Parameter name	Type	Default value	Description
ace_file_name	string	"nucl_file_name".ace or "nucl_file_name_tsl".ace	ACE file name If the processing mode is ace_therm_mode, the default value is "nucl_file_name_tsl".ace.
ace_dir_file_name or ace_dir	string	"nucl_file_name".ace.dir or "nucl_file_name_tsl".ace.dir. or "ace_file_name".ace.dir (If the ace_file_name is changed by users)	MCNP directory information for ACE file If the processing mode is ace_therm_mode, the default value is "nucl_file_name_tsl".ace.dir.
mcnp_dir_file_name or mcnp_dir	real	.00	Suffix ID for ACE file
suffix_id	string	none	Label for ACE file (Maximum 70 words)
ace_label_data	vector(real)	none	List of (iz, aw) pair iz=1000.0×Z+A, aw=mass
iz_aw_data	string or integer	string = yes, integer = 1	Calculation option whether new cumulative angle distributions for ACE file generation are used or not. Available value is use, yes, no, default or 0-1 (0=no, 1=use or yes)
cumulative_angle_distribution_format			

Table 8.2.3 Input parameter name and recommended value which are used only for thermal scattering law data

Parameter name	Type	Default value	Description
nucl_file_name_ts1	string	-	Evaluated nuclear data file name for thermal scattering law data
equi_probable_angle_no	integer	80	Number of equi-probable angles for thermal scattering law data
principal_atom_no	integer	-	Number of principal atoms for thermal scattering law data (If users do not set this parameter, FRENDY automatically set from the evaluated nuclear data file.)
inelastic_reaction_type_no	integer	221	Reaction type (MT) number for inelastic reaction. (MT=221-250 only)
max_thermal_ene	real	max(4.0, temp/300.0, E _{max} in nuclear data file)	Maximum energy for thermal treatment
thermal_za_id_name	string	ZA value of evaluated nuclear data file	ZA ID name for thermal ACE file (ZA=1000.0×Z+A, Maximum 6 words)
moderator_za_data	integer	none	Moderator component ZA value
atom_type_no	integer	-	Number of atom types in mixed moderator (If users do not set this parameter, FRENDY automatically set from evaluated nuclear data file name and so on.)
weight_option	string or integer	string = variable, integer = 0	Weighting option for thermal ACE file Available value is variable, constant, tabulated, default or 0-2 (0=variable, 1=constant, 2=tabulated)

Table 8.2.4 Input parameter name and recommended value for resonance reconstruction (1/2)

Parameter name	Type	Default value	Description
print_set_data_resonance_reconstruction or print_set_data_linearize	string	on	<Writing input case> on, yes, print, write, output, default, or def <Skip case> off, no, or skip
process_resonance_reconstruction or process_linearize	string	on	Processing option for resonance reconstruction <Running resonance reconstruction case> on, yes, process, run, default, or def <Skip resonance reconstruction case> off, no, or skip
write_pendf_resonance_reconstruction or write_pendf_linearize	string	off	Output the PENDF file option for resonance reconstruction <Writing PENDF case> on, yes, print, write, or output <Writing PENDF case with specific name> on, yes, print, write, or output + “PENDF file name” <Skip PENDF case> off, no, skip, default, or def

Table 8.2.4 Input parameter name and recommended value for resonance reconstruction (2/2)

Parameter name	Type	Default value	Description
pendf_file_name_resonance_reconstruction or pendf_file_name_linearize	string	none	PENDF file name for resonance reconstruction If this parameter is set, “write_pendf_linearize” parameter is automatically changed from off to on.

Table 8.2.5 Input parameter name and recommended value for Doppler broadening (1/2)

Parameter name	Type	Default value	Description
print_set_data_doppler_broadening or print_set_data_dop	string	on	<p>Output input information for Doppler broadening</p> <p><Writing input case> on, yes, print, write, output, default, or def</p> <p><Skip case> off, no, or skip</p>
process_doppler_broadening or process_dop	string	on	<p>Processing option for Doppler broadening</p> <p><Running Doppler broadening case> on, yes, process, run, default, or def</p> <p><Skip Doppler broadening case> off, no, or skip</p>
write_pendf_doppler_broadening or write_pendf_dop	string	off	<p>Output the PENDF file option for Doppler broadening</p> <p><Writing PENDF case> on, yes, print, write, or output</p> <p><Writing PENDF case with specific name> on, yes, print, write, or output + “PENDF file name”</p> <p><Skip PENDF case> off, no, skip, default, or def</p>

Table 8.2.5 Input parameter name and recommended value for Doppler broadening (2/2)

Parameter name	Type	Default value	Description
pendf_file_name_doppler_broadening or pendf_file_name_dop	string	none	PENDF file name for Doppler broadening If this parameter is set, “write_pendf_dop” parameter is automatically changed from off to on.

Table 8.2.6 Input parameter name and recommended value for gas production cross-section calculation (1/2)

Parameter name	Type	Default value	Description
print_set_data_gas_production_cross_section, print_set_data_gas_production_xs, print_set_data_gas_production, print_set_data_gas_prod_xs, print_set_data_gas_xs, or print_set_data_gas	string	on	<Writing input case> on, yes, print, write, output, default, or def <Skip case> off, no, or skip
process_gas_production_cross_section, process_gas_production_xs, process_gas_production, process_gas_prod_xs, process_gas_xs, or process_gas	string	on	Processing option for gas production cross-section generation <Running gas production cross-section generation case> on, yes, process, run, default, or def <Skip gas production cross-section generation case> off, no, or skip

Table 8.2.6 Input parameter name and recommended value for gas production cross-section calculation (2/2)

Parameter name	Type	Default value	Description
write_pendf_gas_production_cross_section, write_pendf_gas_production_xs, write_pendf_gas_production, write_pendf_gas_prod_xs, write_pendf_gas_xs, or write_pendf_gas	string off		Output the PENDF file option for gas production cross-section generation <Writing PENDF case> on, yes, print, write, or output <Writing PENDF case with specific name> on, yes, print, write, or output + “PENDF file name” <Skip PENDF case> off, no, skip, default, or def
pendf_file_name_gas_production_cross_section, pendf_file_name_gas_production_xs, pendf_file_name_gas_production, pendf_file_name_gas_production_xs, pendf_file_name_gas_xs, or pendf_file_name_gas	string none		PENDF file name for gas production cross-section generation If this parameter is set, “write_pendf_gas” is automatically changed from off to on.

Table 8.2.7 Input parameter name and recommended value for probability table generation (1/2)

Parameter name	Type	Default value	Description
print_set_data_probability_table_generator, print_set_data_probability_table, print_set_data_prob_table_generator, print_set_data_prob_table, print_set_data_unreso_utils or	string	on	Output input information for probability table generation <Writing input case> on, yes, print, write, output, default, or def <Skip case> off, no, or skip
process_probability_table_generator, process_probability_table, process_prob_table_generator, process_prob_table, process_unreso_utils or	string	on	Processing option for probability table generation <Running probability table generation case> on, yes, process, run, default, or def <Skip probability table generation case> off, no, or skip

Table 8.2.7 Input parameter name and recommended value for probability table generation (2/2)

Parameter name	Type	Default value	Description
<code>write_pendf_probability_table_generator,</code> <code>write_pendf_probability_table,</code> <code>write_pendf_prob_table_generator,</code> <code>write_pendf_prob_table,</code> <code>or</code> <code>write_pendf_unreso_utils</code>	string off		Output the PENDF file option for probability table generation <Writing PENDF case> on, yes, print, write, or output <Writing PENDF case with specific name> on, yes, print, write, or output + “PENDF file name” <Skip PENDF case> off, no, skip, default, or def
<code>pendf_file_name_probability_table_generator,</code> <code>pendf_file_name_probability_table,</code> <code>pendf_file_name_prob_table_generator,</code> <code>pendf_file_name_prob_table,</code> <code>or</code> <code>pendf_file_name_unreso_utils</code>	string none		PENDF file name for probability table generation If this parameter is set, “wwrite_pendf_prob_table” parameter is automatically changed from off to on. - <code>pendf_file_name_probability_table_generator,</code> <code>pendf_file_name_probability_table,</code> <code>pendf_file_name_prob_table_generator,</code> <code>pendf_file_name_prob_table,</code> <code>or</code> <code>pendf_file_name_unreso_utils</code>

Table 8.2.8 Input parameter name and recommended value for thermal scattering law data (1/2)

Parameter name	Type	Default value	Description
print_set_data_thermal_scattering_law, print_set_data_thermal_scattering or print_set_data_ts1	string	on	<Writing input case> on, yes, print, write, output, default, or def <Skip case> off, no, or skip
process_thermal_scattering_law, process_thermal_scattering or process_ts1	string	on	Processing option for thermal scattering law data <Processing thermal scattering law data case> on, yes, process, run, default, or def <Skip thermal scattering law data case> off, no, or skip

Table 8.2.8 Input parameter name and recommended value for thermal scattering law data (2/2)

Parameter name	Type	Default value	Description
write_pendf_thermal_scattering_law, write_pendf_thermal_scattering or write_pendf_ts1	string	off	<Writing PENDF case> on, yes, print, write, or output <Writing PENDF case with specific name> on, yes, print, write, or output + “PENDF file name” <Skip PENDF case> off, no, skip, default, or def
pendf_file_name_thermal_scattering_law, pendf_file_name_thermal_scattering or pendf_file_name_ts1	string	on	PENDF file name for thermal scattering law data If this parameter is set, “write_pendf_ts1” parameter is automatically changed from off to on.

Table 8.2.9 Input parameter name and recommended value for ACE file generation

Parameter name	Type	Default value	Description
print_set_data_ace_data_generator or print_set_data_ace	string	on	<p>Output input information for ACE file generation</p> <p><Writing input case> on, yes, print, write, output, default, or def</p> <p><Skip case> off, no, or skip</p>
process_ace_data_generator or process_ace	string	on	<p>Processing option for ACE file generation</p> <p><Running ACE file generation case> on, yes, process, run, default, or def</p> <p><Skip ACE file generation case> off, no, or skip</p>

```

//Input file of FRENDY for continuous-energy neutron data
ace_fast_mode //processing mode (generate fast ACE file)

//Nuclear data file name
nucl_file_name      U235.dat
/* ace file name */
ace_file_name        U235.ace
temp                 296.0 // temperature [K]
add_grid_data        (0.625 4.0) //Additional energy grid point
sigima_zero_data    //sigma-infinity is 1.0E10 [b]
(1.0E10 1.0E06 1.0E05 1.0E04 1.0E03 1.0E02
 3.5E02 1.0E02 1.0E01 1.0E-1)

```

Figure 8.2.2 Example of input file for continuous-energy neutron data

```

//Input file of FRENDY for thermal scattering law data
ace_therm_mode //process mode (generate thermal ACE file)

//Nuclear data file name
nucl_file_name
  H001.dat
//Nuclear data file name for TSL
nucl_file_name_tsl
  H_in_H2O.txt
/* ace file name */
ace_file_name
  H_in_H2O.ace
temp /* temperature */ 296.0 // [K]

```

Figure 8.2.3 Example of input file for thermal scattering law data

```

//Input file of FRENDY for continuous-energy neutron data
ace_dosi_mode //processing mode (generate dosimetry ACE file)

//Nuclear data file name
nucl_file_name      U235.dat

```

Figure 8.2.4 Example of input file for dosimetry data

8.3 NJOY99 Compatible Format

The input format of NJOY99 is explained in the source code and manuals of the NJOY code system^{7,8)}. Users can consult them for the details of the format. FRENDY can process the evaluated nuclear data file with the input file of the following modules:

RECONR, BROADR, GASPR, PURR, UNRESR, THERMR, ACER, and MODER.

Though FRENDY processes the evaluated nuclear data file using the NJOY99 compatible format, users should pay attention to the following points.

- FRENDY reads and writes the PENDF file only in the text format.
- FRENDY does not calculate the self-shielding factor in the unresolved resonance region using the deterministic method and the input file of UNRESR is automatically converted to that of PURR.
- The fast, thermal, and dosimetry ACE file generation functions are only implemented and other functions in ACER are not currently implemented.

NJOY reads and writes PENDF files in the binary format when the input tape number is negative. The PENDF file in the binary format is used to efficiently access the evaluated nuclear data file. It is difficult to perfectly treat the binary file produced by FORTRAN since FRENDY is written in C++. Furthermore, the PENDF file in the binary format is mainly used as the temporary file. FRENDY changes the negative tape number (binary file) to a positive one (text file) when users set a negative tape number.

FRENDY calculates probability tables to treat the self-shielding effect in the unresolved resonance region with the ladder method. NJOY implements the deterministic method to calculate it with UNRESR. According to the manual of NJOY, it is not recommended to use the deterministic method⁴⁰⁾. Actually, the self-shielding factor generated by the deterministic method sometimes shows inappropriate values, *e.g.*, negative or larger than 1.0. We believe that the calculation time of the ladder method is acceptable on the current computational platforms. Therefore, we do not implement the deterministic method and FRENDY calculates the self-shielding effect in the unresolved resonance region using the ladder method even if users select UNRESR. The input parameters for the ladder method, *e.g.*, the numbers of bins and ladders, are obtained from the recommended value of the FRENDY original input as shown in Table 8.2.2.

As described in Chapter 7, the ACE file generation for the photo-atomic and the photo-nuclear data is not currently implemented. FRENDY terminates with an error message if users select these calculation modes.

8.4 Sample Input Data

8.4.1 Simplest Input Data

8.4.1.1 *Fast ACE file generation*

The simplest input format to generate the neutron incident ACE file requires only the processing mode name and evaluated nuclear data file name.

```
ace_file_generation_fast_mode // Processing mode name
      nucl_file_name          U235.fast.dat // Nuclear data file name
```

The above input data generates the ACE file at a temperature of 293.6 K named “U235.fast.dat.ace” and directory information file named “U235.fast.dat.ace.dir”. For the other calculation conditions, the default input parameters listed in Tables 8.2.4 - 8.2.9 are used.

8.4.1.2 *Thermal ACE file generation*

The simplest input format to generate the ACE file of the thermal scattering law data requires only the processing mode name, evaluated nuclear data file name, and thermal scattering law data file name.

```
ace_file_generation_thermal_scatter_mode // Processing mode name
      nucl_file_name          H001.dat // Nuclear data file name
      nucl_file_name_tsl       HinH2O.dat // Thermal scattering law data
                                    // file name
```

The above input data generates the ACE file at a temperature of 293.6 K named “HinH2O.dat.ace”, and directory information file named “HinH2O.dat.ace.dir”. For the other calculation conditions, the default input parameters listed in Tables 8.2.4 - 8.2.9 are used.

8.4.1.3 *Dosimetry ACE file generation*

The simplest input format to generate the ACE file for the dosimetry data requires only the processing mode name and evaluated nuclear data file name.

```
ace_file_generation_dosimetry_mode // Processing mode name
      nucl_file_name          U235.dosi.dat // Nuclear data file name
```

The above input data generates the ACE file at a temperature of 293.6 K named “U235.dosi.dat.ace”, and directory information file named “U235.dosi.dat.ace.dir”. For the other calculation conditions, the default input parameters listed in Tables 8.2.4 - 8.2.9 are used.

8.4.2 Input Data to Modify Default Input Parameters

As shown in Tables 8.2.4 - 8.2.9, many input parameters are prepared in the FRENDY original format. However, in conventional applications users usually change only 5 parameters, *i.e.*, the temperature, the number of equi-probable angle bins for thermal scattering law data, ACE file name, directory information for the ACE file, and a suffix ID for the ACE file. This section illustrates examples of the input files to change these input parameters.

8.4.2.1 Fast ACE file generation

ace_file_generation_fast_mode	// Processing mode name	
nucl_file_name	U235.fast.dat	// Nuclear data file name
temp	600.0	// Temperature [K]
suffix_id	.50	// Suffix ID for ACE file
ace_file_name	U235.fast.ace	// ACE file name
ace_dir_file_name	U235.fast.ace.dir// MCNP directory information	

The above input data generates the ACE file at a temperature of 600.0 K named “U235.fast.ace”, and directory information file named “U235.fast.ace.dir”. In this input file, the suffix ID of the ACE file is changed from 0.00 to 0.50.

8.4.2.2 Thermal ACE file generation

ace_file_generation_thermal_scatter_mode	// Processing mode name	
nucl_file_name	H001.dat	// Nuclear data file name
nucl_file_name_tsl	HinH2O.dat	// TSL data name
temp	600.0	// Temperature [K]
equi_probable_angle_no	30	// Number of equi-probable angles
suffix_id	.50	// Suffix ID for ACE file
ace_file_name	HinH2O.tsl.ace	// ACE file name
ace_dir_file_name	HinH2O.tsl.ace.dir	
	// MCNP directory information	

The above input data generates the ACE file at a temperature of 600.0 K named “HinH2O.tsl.ace”, and directory information file named “HinH2O.tsl.ace.dir”. In this input file, the number of

equi-probable angles is changed from 10 to 30 and the suffix ID of the ACE file is changed from 0.00 to 0.50.

8.4.2.3 Dosimetry ACE file generation

```
ace_file_generation_dosimetry_mode // Processing mode name
nucl_file_name U235.dosi.dat // Nuclear data file name
temp 600.0 // Temperature [K]
suffix_id .50 // Suffix ID for ACE file
ace_file_name U235.dosi.ace // ACE file name
ace_dir_file_name U235.dosi.ace.dir // MCNP directory information
```

The above input data generates the ACE file at a temperature of 600.0 K named “U235.dosi.ace”, and directory information file named “U235.dosi.ace.dir”. In this input file, the suffix ID of the ACE file is changed from 0.00 to 0.50.

8.4.3 Input Data to Reproduce NJOY99 Input

This section illustrates how to make FRENDY input files which is identical to NJOY input files. The details of the input parameters of the NJOY input files are explained in References 7 and 8. All the input parameters in the NJOY input files are explicitly set in the FRENDY input files. The processing conditions, PENDF file name, ACE file name, and so on of the FRENDY input files are identical to those of the NJOY input files.

8.4.3.1 Fast ACE file generation

The following input files are typical for the fast ACE file generation. These input files process the evaluated nuclear data file of ^{238}U at 300.0 K.

< NJOY99 compatible format >

```
reconr / command
20 21 / input(tape20), output(tape21)
'pendf tape for JENDL-4.0 U-238' / identifier for PENDF
9237 3 3 / mat, ncards, ngrid
1.00e-03 0.00 / err, temp
'92-U-238 from JENDL-4.0' / cards (1)
'Processed with FRENDY' / cards (2)
'Processed day: 2017/10/13' / cards (3)
0.625 4.0 100.0 / enode
```

```

0                                /
broadr                           / command
20 21 22                         / input(tape20), pendf(tape21), output(tape22)
9237 1 0 1 0                      / mat, temp_no, restart_opt, bootstrap, temp_initial
1.00E-03 100000                   / err, max_energy
300.0                            / temp
0                                /
gaspr                            / command
20 22 23                         / input(tape20), output(tape23)
0                                /
purr                             / command
20 23 25                         / input(tape20), pendf(tape23), output(tape25)
9237 1 7 20 100 1                / mat, temp_no, sig0_no, bin_no, ladder_no,
print_opt
300.0                            / temp
1.0E10 1.0E4 1.0E3 300.0 100.0 30.0 10.0 / sig0
0                                /
acer                             / command
20 25 0 30 31                   / nendif, npend, ngend, nace, ndir
1 1 1 0.30                       / iopt(fast), iprint(max), itype, suffix
'ACE file for JENDL-4 U238'     / descriptive character
9237 300.0                       / mat, temp
1 1                             / newfor(yes), iopp(yes)
1 1 1                           / thin(1), thin(2), thin(3)
stop                            /

```

< FRENDY original input format >

```

ace_file_generation_fast_mode // Processing mode name
    nucl_file_name          tape20

    pendf_label_data        "pendf tape for JENDL-4.0 U238"
    error                  1.0E-3
    temp                   300.0
    add_grid_data          (0.625 4.0 100.0)
    max_broadening_ene    100000 // 1 MeV

```

```

sigma_zero_data      (1.0E10  1.0E4  1.0E3  300.0  100.0  30.0  10.0)
probability_bin_no   20
ladder_no           100
ace_file_name        tape30
mcnp_dir_file_name   tape31
ace_label_data       "ACE file for JENDL-4 U238"
suffix_id            0.30
comment_data

“92-U-238 from JENDL-4.0
Processed with FRENDY
Processed day: 2017/10/13”

```

```

// Write PENDF file option for RECONR
    write_pendf_resonance_reconstruction  tape21
// Write PENDF file option for BROADR
    write_pendf_doppler_broadening        tape22
// Write PENDF file option for GASPR
    write_pendf_gas_prod_xs              tape23
// Write PENDF file option for PURR
    write_pendf_prob_table_generator     tape25

// Skip or running RECONR option
    process_resonance_reconstruction     on
// Skip or running BROADR option
    process_doppler_broadening          on
// Skip or running GASPR option
    process_gas_production_cross_section on
// Skip or running PURR option
    process_probability_table_generator  on
// Skip or running ACER option
    process_ace_data_generator          on

```

8.4.3.2 Thermal ACE file generation

The following input files are typical for the thermal ACE file generation. These input files process the evaluated nuclear data file of ^9Be in BeO at 300.0 K.

```
< NJOY99 compatible format >
reconr          / command
 20 21          / input(tape20), output(tape21)
'pendf tape for JENDL-4.0 Be-009' / identifier for PENDF
 425            / mat
 1.00e-03 0.00 / err, temp
 0              /
broadr          / command
 20 21 22       / input(tape20), pendf(tape21), output(tape22)
 425 1 0 1 0    / mat, temp_no, restart_opt, bootstrap, temp_initial
 1.00E-03 100000.0 / err, max_energy
 400.0          / temp
 0              /
gaspr           / command
 20 22 23       / input(tape20), pendf(tape22), output(tape23)
 0              /
thermr          / command
 60 23 25       / input(tape60), pendf(tape23), output(tape25)
 27 425 10 1 4 1 1 221 / natde, matdp, nbin, ntemp, iinc, icof
 400.0          / temp
 1.00E-2 4.0    / tolerance, max energy
purr            / command
 20 25 26       / input(tape20), pendf(tape25), output(tape26)
 425 1 7 20 200 1 / mat, temp_no, sig0_no, bin_no, lad_no, print_opt
 400.0          / temp
 1.0E10 1.0E4 1.0E3 300.0 100.0 30.0 10.0 / sig0
 0              /
acer            / command
 20 26 0 30 31 / nendif, npend, ngend, nace, ndir
 2 1 1 0.30     / iopt(fast), iprint(max), itype, suffix
'ACE file for JENDL-4 BeinBeO' / descriptive character
 425 400.0 'bebeo' / mat, temp
```

```

4009 8016           / iza01, iza02
221 10 222 0 2 4.0 0 / mti, nbint, mte, ielas, nmix, emax, iwt
stop                /

```

< FRENDY original input format >

```

ace_file_generation_thermal_scatter_mode      // Processing mode name
    nucl_file_name          tape20
    nucl_file_name_tsl       tape60

    pendf_label_data        "pendf tape for JENDL-4.0 Be-009"
    error                   1.0E-3
    temp                     400.0
    max_broadening_ene      100000.0      // 1 MeV
    sigma_zero_data         (1.0E10 1.0E4 1.0E3 300.0 100.0 30.0 10.0)
    probability_bin_no      20
    ladder_no               200
    ace_file_name           tape30_frendy
    mcnp_dir_file_name      tape31_frendy
    ace_label_data          "ACE file for JENDL-4 BeinBeO"
    thermal_za_id_name     "bebeo"
    suffix_id                0.30

//Thermal scattering law data only
    equi_probable_angle_no   10
    principal_atom_no        1 //Be
    inelastic_reaction_type_no 221
    max_thermal_ene          4.0
    thermal_za_id_name      "bebeo"
    moderator_za_data        4009
    atom_type_no              2 //Be and O
    weight_option             0 //0 = variable

// Write PENDF file option for RECONR
    write_pendf_resonance_reconstruction  tape21
// Write PENDF file option for BROADR

```

```

        write_pendf_doppler_broadening      tape22
// Write PENDF file option for GASPR
        write_pendf_gas_prod_xs           tape23
// Write PENDF file option for THERMR
        write_pendf_thermal_scattering    tape25
// Write PENDF file option for PURR
        write_pendf_prob_table_generator  tape26

// Skip or running RECONR option
        process_resonance_reconstruction  on
// Skip or running BROADR option
        process_doppler_broadening       on
// Skip or running GASPR option
        process_gas_production_cross_section on
// Skip or running THERMR option
        process_thermal_scattering_law   on
// Skip or running PURR option
        process_probability_table_generator on
// Skip or running ACER option
        process_ace_data_generator       on

```

8.4.3.3 Dosimetry ACE file generation

The following input files are typical for the dosimetry ACE file generation. These input files process the evaluated nuclear data file of ^{238}U at 300.0 K.

```

< NJOY99 compatible format >
reconr                  / command
20 21                   / input(tape20), output(tape21)
'pendf tape for JENDL-4 U238' / identifier for PENDF
9237                    / mat
1.00e-03  0.0            / err, temp
0                        /
broadr                  / command
20 21 22                / input(tape20), pendf(tape21), output(tape22)
9237 1 0 1 0             / mat, temp_no, restart_opt, bootstrap, temp_initial
1.00E-03  100000          / err, max_energy

```

```

300.0          / temp
0              /
gaspr         / command
20 22 23      / input(tape20), pendf(tape22), output(tape23)
acer          / command
20 23 0 30 31 / nendf, npend, ngend, nace, ndir
3 1 1 0.30    / iopt(fast), iprint(max), itype, suffix
'ACE file for JENDL-4 U238' / descriptive character
9237 300.0    / mat, temp
stop

```

< FRENDY original input format >

```

ace_file_generation_dosimetry_mode // Processing mode name
    nucl_file_name      tape20

    pendf_label_data   "pendf tape for JENDL-4.0 U-238"
    error             1.0E-3
    temp              300.0
    max_broadening_ene 100000 //1 MeV
    ace_file_name     tape30
    mcnp_dir_file_name tape31
    ace_label_data    "ACE file for JENDL-4 U238"
    suffix_id         0.30

// Write PENDF file option for RECONR
    write_pendf_resonance_reconstruction  tape21
// Write PENDF file option for BROADR
    write_pendf_doppler_broadening       tape22
// Write PENDF file option for GASPR
    write_pendf_gas_prod_xs            tape23

// Skip or running RECONR option
    process_resonance_reconstruction   on
// Skip or running BROADR option
    process_doppler_broadening        on
// Skip or running GASPR option

```

```
process_gas_production_cross_section on
// Skip or running ACER option
process_ace_data_generator          on
```

9 Installation of FRENDY

This chapter describes how to install FRENDY on Linux, UNIX, or MacOS platforms.

1. Disk space of about 1.2 Gbytes is required to make the executables from the program sources and run all test programs and sample files. Disk space of about 210 Mbytes is required if users make only the executables from the program sources.
2. A C++ compiler, the Boost library, and the LAPACK library are required to compile source programs. The compilation has been confirmed for an Intel compiler (icc) version 13.1.3 and a GNU compiler (gcc) version 4.4.7 with the Boost library version 1.60.0 and the LAPACK library⁵⁶⁾ version 3.8.0.
3. Since FRENDY stores all nuclear data on memory, the large memory size is required. More than 1 Gbytes is recommended to run FRENDY.

9.1 Directory Structure

The directory structure is shown in Fig. 9.1.1. The “frendy” directory contains the source files. The “sample” directory contains the input files for the test calculations to generate the fast and thermal ACE files. The “test” directory contains source files to run the Boost.Test library.

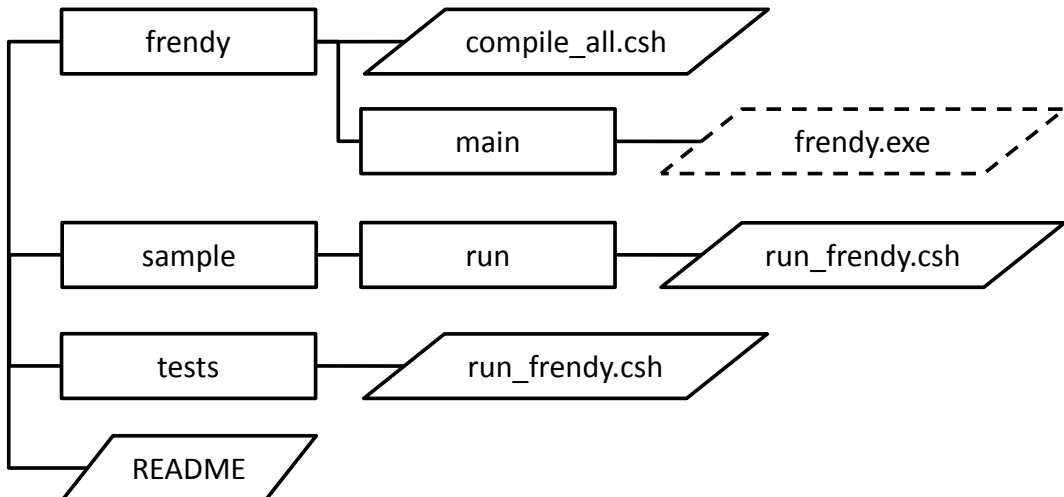


Figure 9.1.1 Directory structure

9.2 How to Install FRENDY on Linux, UNIX, or MacOS Platforms

A shell script of “compile_all.csh” is included in the “frendy” directory to compile FRENDY source codes. The users run only this shell script or issue the “make” command in “frendy/main” directory. If the compiler successfully builds the executable file of FRENDY, the following message

is written on the display.

Completed to make FRENDY

The executable file named “frendy.exe” is generated in “frendy/main” directory.

FRENDY has the NJOY mode which processes the evaluated nuclear data file with the NJOY calculation method. The differences between the NJOY mode and the original mode are as follows:

1. The NJOY mode calculates the unresolved resonance cross-section using cross-section formulae on the fixed energy grid points and other energy grid points are calculated by the interpolation method. The fixed energy grid points are 1.00×10^n , 1.25×10^n , 1.50×10^n , 1.70×10^n , 2.00×10^n , 2.50×10^n , 3.00×10^n , 3.50×10^n , 4.00×10^n , 5.00×10^n , 6.00×10^n , 7.20×10^n , and 8.50×10^n . This difference has an impact on the resonance reconstruction.
2. The calculation method of the complex error function which is defined in Eq. (2.3.41) is different. The complex error function is used to calculate the Doppler broadened cross-sections with the Single-Level Breit-Wigner representation. This difference has an impact on the resonance reconstruction and the probability table generation.
3. The calculation method of the cross sections at 0 eV is different. The cross section at 0 eV is required to calculate the Doppler broadened cross-sections at the low energy region. The NJOY mode assumes that the cross section obeys the 1/v law. This approximation is appropriate for many reactions. However, the elastic scattering cross-sections does not obey the 1/v law since the elastic scattering cross-section is constant due to the potential scattering cross-section at the low energy region. In such a case, the linear-linear interpolation is appropriate. The NJOY mode uses the 1/v law to reproduce the NJOY results. This difference affects the Doppler broadened elastic scattering cross-sections at the low energy region.
4. The NJOY mode uses the fixed incident neutron energy grid to calculate the incoherent inelastic scattering cross-section. The number of energy grid points is 117 from 1.0×10^{-5} to 10 eV to calculate the incoherent inelastic scattering cross section and secondary energy and angular distributions. The incoherent inelastic scattering cross section at the other energy grid points are interpolated using the fifth order Lagrange interpolation and secondary energy and angular distributions are not calculated. This difference affects some materials, *e.g.*, H in ZrH, for which the incoherent inelastic scattering cross-section oscillates.
5. The NJOY mode uses discrete random numbers to calculate the chi-squared random numbers with k degrees of freedom $R_{\chi^2}(k)$. This difference has an impact on the probability table

generation.

Users run “compile_all.csh” or “make” command in “frendy/main_njoy_mode” directory if they want to compile with this calculation mode. The executable file named “frendy_njoy_mode.exe” is generated in “frendy/main_njoy_mode” directory.

9.3 How to Execute FRENDY

The execution command is as follow:

frendy.exe “input file name”

The input file name is set as a command line argument.

9.4 Test Calculation with Samples

The FRENDY suite includes test programs for fast and thermal ACE file generations in the “sample” directory. The “run_frendy.csh” shell script in “sample/run” directory automatically runs all the test programs.

9.5 Test Programs for Boost test Library

For the quality assurance, the test programs are included to verify the capabilities. The Boost test library¹⁸⁾ is used for the test programs. Using the Boost test library, comparison of the calculation results and confirmation of the run-time errors are easily done.

The source files for Boost test library are contained in the “test” directory. Users have to run the “run_all_class.csh” shell script in the “test” directory if they want to compile and run all the test programs. The source file name and the directory structure correspond to those of FRENDY sources in the “frendy” directory. Users must recompile and run the test programs when they modify the source files.

The test programs start with the following message

Running X test cases...

where X is the number of test cases. If the test programs successfully finish, the following message is written on the display

***** No errors detected**

If the test programs find errors, the following message is written on the display

***** Y failures detected in test suite "Master Test Suite"**

where **Y** is the number of errors.

Acknowledgements

The authors especially wish to thank Mr. Kenji Yokoyama, Mr. Tomoyuki Jin, Dr. Yosuke Iwamoto, Dr. Chikara Konno, Dr. Kenya Suyama, Dr. Teruhiko Kugo, and Dr. Tokio Fukahori for their helpful suggestions and continuous encouragements. This study could not be completed without their helps.

References

- 1) K. Shibata, O. Iwamoto, T. Nakagawa, N. Iwamoto, A. Ichihara, S. Chiba, K. Furutaka, N. Otuka, T. Ohsawa, T. Murata, H. Matsunobu, A. Zukeran, S. Kamada, J. Katakura, “JENDL-4.0: A New Library for Nuclear Science and Engineering”, *J. Nucl. Sci. Technol.*, 48(1), pp.1-30 (2011).
- 2) Y. Nagaya, K. Okumura, T. Mori, M. Nakagawa, “MVP/GMVP II: General Purpose Monte Carlo Codes for Neutron and Photon Transport Calculations based on Continuous Energy and Multigroup Methods”, *JAERI 1348* (2004) 388p.
- 3) K. Yokoyama, T. Jin, Y. Hirai, T. Hazama, “Development of the Versatile Reactor Analysis Codes System, MARBLE2”, *JAEA-Data/Code 2015-009* (2015) 120p (in Japanese).
- 4) T. Sato, Y. Iwamoto, S. Hashimoto, T. Ogawa, T. Furuta, S. Abe, T. Kai, P. Tsai, N. Matsuda, H. Iwase, N. Shigyo, L. Sihver, K. Niita, “Features of Particle and Heavy Ion Transport code System (PHITS) version 3.02”, *J. Nucl. Sci. Technol.*, 55(6), pp.684-690 (2018).
- 5) T. Tone, S. Katsuragi, “PROF GROUCH-G; A Processing Code for Group Constants for a Fast Reactor”, *JAERI 1192* (1970) 22p.
- 6) N. Yamano, T. Minami, K. Koyama, Y. Naito, “RADHEAT-V4; A code system to generate multigroup constants and analyze radiation transport for shielding safety evaluation”, *JAERI 1316* (1989) 307p.
- 7) R. E. MacFarlane, D. W. Muir, “The NJOY Nuclear Data Processing System, Version 91”, *LA-12740-M*, Los Alamos National Laboratory (1994).
- 8) A. C. Kahler, Ed., “The NJOY Nuclear Data Processing System, Version 2016”, *LA-UR-17-20093*, Los Alamos National Laboratory (2016).
- 9) D. E. Cullen, “PREPRO 2017, 2017 ENDF/B Pre-processing Codes (ENDF/B-VII of proposed VIII Tested)”, *IAEA-NDS-39*, Rev.17, International Atomic Energy Agency (2017).
- 10) M. B. Chadwick, et. al., “Special Issue on ENDF/B-VII.1 Library”, *Nucl. Data Sheets*, 112(12), pp.2887-3152 (2011).
- 11) A. Koning, C. Dean, U. Fischer, R. Mills, “Validation of the JEFF-3.1 Nuclear Data Library”, *JEFF-Report 23* (2013).
- 12) C. M. Mattoon, B. R. Beck, N. R. Patel, N. C. Summers, G. W. Hedstrom, D. A. Brown, “Generalized Nuclear Data: A New Structure (with Supporting Infrastructure) for Handling Nuclear Data”, *Nucl. Data Sheets*, 113 (12), pp.3145-1371 (2012).
- 13) A. Trkov, M. Herman, D. A. Brown, “ENDF-6 Formats Manual”, Report *BNL-203218-2018-INRE* (2018).
- 14) K. Tada, Y. Nagaya, S. Kunieda, K. Suyama, T. Fukahori, “Development and verification of a new nuclear data processing system FRENDY”, *J. Nucl. Sci. Technol.*, 54(7), pp.806-817 (2017).
- 15) X-5 Monte Carlo Team, “MCNP – A General Monte Carlo N-Particle Transport Code, Version

- 5”, *LA-UR-03-1987* (2003).
- 16) J. Leppänen, M. Pusa, T. Viitanen, V. Valtavirta, T. Kaltiaisenaho, “The Serpent Monte Carlo Code: Status, Development and Applications in 2013”, *Ann. Nucl. Energy*, 82, pp.142-150 (2015).
 - 17) S. Chacon and B. Straub, *Pro Git SECOND EDITION*, Apress, New York (2014).
 - 18) P. Hamill, *Unit Test Frameworks*, O’ Reilly Media, California (2014).
 - 19) G. Breit, E. Wigner, “Capture of Slow Neutrons”, *Phys. Rev.*, 49, pp.519-531 (1936).
 - 20) D. B. Adler, F. T. Adler, “Neutron Cross-sections in Fissile Elements”, Proc. Conf. on Breeding Economics and Safety in Large Fast Power Reactors, Argonne, Monograph *ANL-6972* (1963).
 - 21) F. T. Adler, D. B. Adler, “Interpretations of Neutron Cross-sections of the Fissionable Materials for the Resolved Resonance Region”, Conf. on Neutron Cross-section Technology, Washington, D. C., *CONF-660303*, 2, pp.873-893 (1966).
 - 22) C. W. Reich, M. S. Moore, “Multilevel Formula for the Fission Process”, *Phys. Rev.*, 111(3), pp.929-933 (1958).
 - 23) M. S. Moore, “Fundamentals and Approximations of Multilevel Resonance Theory for Reactor Physics Applications”, *Nuclear Theory for Applications*, *IAEA-SMR-43*, pp.31-57 (1980).
 - 24) K. Yagi, “Genshikakubutsurigaku”, Asakura-shoten, Tokyo, pp.257-263 (1971) (in Japanese).
 - 25) A. M. Lane, R. G. Thomas, “R-Matrix Theory of Nuclear Reactions”, *Rev. Mod. Phys.*, 30(2), pp.257-353 (1958).
 - 26) K. Kobayashi, “Genshirobutsuri”, Corona-sha, Tokyo, pp.1-80 (1996) (in Japanese).
 - 27) S. Kunieda, “Status of the R-matrix Code AMUR toward a consistent cross-section evaluation and covariance analysis for the light nuclei”, *EPJ Web of Conferences*, 146, pp.12029_1-12029_4 (2017).
 - 28) N. M. Larson, “Updated Users’ guide for SAMMY: Multilevel R-Matrix Fits to Neutron Data Using Bayes’ Equations”, *ORNL/TM-9179/R8, ENDF-364/R2*, p.9 (2008).
 - 29) F. H. Frohner, “Applied Neutron Resonance Theory”, Nuclear Theory for Applications, *IAEA-SMR-43*, pp.59-95 (1980).
 - 30) H. Henryson II, B. J. Toppel, C. G. Stenberg, “MC2-2: A Code to Calculate Fast Neutron Spectra and Multigroup Cross-sections”, *ANL-8144* (1976).
 - 31) C. E. Porter, R. G. Thomas, “Fluctuations of Nuclear Reaction Width”, *Phys. Rev.*, 104(2), pp.483-491 (1956).
 - 32) R. N. Hwang, H. Henryson II, “Critical Experimentation of Low-Order Quadratures for Statistical Integrations”, *Trans. Am. Nucl. Soc.*, 22, pp.712-713 (1975).
 - 33) N. M. Steen, G. D. Byrne, E. M. Gelbard, “Gaussian Quadratures for the Integrals”, *Math. Comp.*, 23(107), pp.661-671 (1969).
 - 34) R. E. MacFarlane, “Neutron Slowing Down and Thermalization”, *Handbook of Nuclear*

- Engineering*, 3, Springer, Berlin (2010).
- 35) D. E. Cullen, “Program SIGMA1 (version 79-1) Doppler broaden evaluated cross-sections in the evaluated nuclear data file/version B (ENDF/B) format”, *UCRL-50400*, 17, Part B, Rev. 2 (1979).
- 36) D. E. Cullen, “Nuclear Data Preparation”, *Handbook of Nuclear Engineering*, 1, pp.282-425, Springer, Berlin (2010).
- 37) W. Haeck and A. Trkov, “Nuclear Data Processing”, *INDC(NDS)-0748* (2018).
- 38) H. D. Lemmel, C. H. Westcott, “Fission and Absorption g-factors of ^{241}Pu ”, *J. Nucl. Energy*, 21(5), pp.417-424 (1967).
- 39) R. Pynn, “neutron scattering A PRIMER”, Los Alamos Science Summer 1990 (1990).
- 40) R. E. MacFarlane, A. C. Kahler, “Methods for Processing ENDF/B-VII with NJOY”, *Nucl. Data Sheets*, 111(12), pp.2739-2890 (2010).
- 41) R. W. Richards, J. L. Thomason, “Small-Angle Neutron Scattering Study of Block Copolymer Morphology”, *Macromolecules*, 16(6), pp.982-992 (1983).
- 42) J. I. M. Damian, J. R. Granada, D. C. Malaspina, “New thermal neutron scattering kernels for light and heavy water based on molecular dynamics simulations”, *Phisics Procedia*, 60, pp.300-309 (2014).
- 43) A. Yamamoto, N. Sugimura, “Improvement on multi-group scattering matrix in thermal energy range generated by NJOY”, *Ann. Nucl. Energy*, 33(6), pp.555-559 (2006).
- 44) R. D. Mosteller and R. C. Little, “Impact of MCNP Unresolved Resonance Probability-Table Treatment on Uranium and Plutonium Benchmarks”, *Proc. ICNC'99*, Sep. 20-24, 1999, Versailles, France (1999).
- 45) L. B. Levitt, “The Probability Method for Treating Unresolved Resonances in Monte Carlo Criticality Calculation”, *Trans. Am. Nucl. Soc.*, 14, p.648 (1971).
- 46) I. I. Bondasrenko, Ed., Group Constants for Nuclear Reactor Calculations, Consultants Bureau, New York (1970).
- 47) D. M. Green and T. A. Pitterle, “ETOE, A Program for ENDF/B to MC2 Data Conversion”, *APDA-219*, Atomic Power Development Associates, Inc. (1968).
- 48) J. M. Otter, R. C. Lewis, L. B. Levitt, “U3R A Code to Calculate Unresolved Resonance Cross-section Probability Tables”, *AI-AEC-13024*, Atomics International (1972).
- 49) T. Yotsuji, Probability Distribution Random Number Generating Method for Calculator Simulation, Pleiades Publishing (2010) (in Japanese).
- 50) G. Marsaglina and W. Tsang, “A Simple method for generating gamma variables”, *ACM Trans. Math. Softw.*, 26(3), pp.363-372 (2000).
- 51) D.M. O’Shea and H.C. Thacher, Jr. “Computation of Resonance Line Shape Function”, *Trans. Am. Nucl. Soc.*, 6, pp.36-37 (1963).
- 52) G.P.M. Poppe and C.M.J. Wijers, “More Efficient Computation of the Complex Error Function”,

- ACM Trans. Math. Softw.*, 16(1), pp.38-46 (1990).
- 53) O. Shcherbakov and H. Harada, “Resonance Self-Shielding Corrections for Activation Cross-section Measurements”, *J. Nucl. Sci. Technol.*, 39(5), pp.548-553 (2002).
- 54) P. Martin, G. Donoso, J. Zamudio-Cristi, “A modified asymptotic Pade method. Application to multipole approximation for the plasma dispersion function Z”, *J. Math. Phys.*, 21(2), pp.280-285 (1980).
- 55) K. Tada, “Improvement of Probability Table Generation Using Ladder Method for a New Nuclear Data Processing System FRENDY”, *Proc. Physor2018*, Cancun, Mexico, Apr. 22-26, 2018 (2018).
- 56) E. Anderson, Z. Bai, C. Bischof, S. Blackford, J. Demmel, J. Dongarra, J. D. Croz, A. Greenbaum, S. Hammarling, A. McKenney, D. Sorensen, *LAPACK Users' Guide Third Edition*, Society for Industrial and Applied Mathematics, Philadelphia (1999).

国際単位系 (SI)

表1. SI 基本単位

基本量	SI 基本単位	
	名称	記号
長さ	メートル	m
質量	キログラム	kg
時間	秒	s
電流	アンペア	A
熱力学温度	ケルビン	K
物質量	モル	mol
光度	カンデラ	cd

表2. 基本単位を用いて表されるSI組立単位の例

組立量	SI組立単位	
	名称	記号
面積	平方メートル	m ²
体積	立方メートル	m ³
速度	メートル毎秒	m/s
加速度	メートル毎秒毎秒	m/s ²
波数	毎メートル	m ⁻¹
密度、質量密度	キログラム毎立方メートル	kg/m ³
面積密度	キログラム毎平方メートル	kg/m ²
比體積	立方メートル毎キログラム	m ³ /kg
電流密度	アンペア毎平方メートル	A/m ²
磁界の強さ	アンペア毎メートル	A/m
量濃度 ^(a) 、濃度	モル毎立方メートル	mol/m ³
質量濃度	キログラム毎立方メートル	kg/m ³
輝度	カンデラ毎平方メートル	cd/m ²
屈折率 ^(b)	(数字の) 1	1
比透磁率 ^(b)	(数字の) 1	1

(a)量濃度(amount concentration)は臨床化学の分野では物質濃度(substance concentration)ともよばれる。

(b)これらは無次元あるいは次元をもつ量であるが、そのことを表す単位記号である数字の1は通常は表記しない。

表3. 固有の名称と記号で表されるSI組立単位

組立量	SI組立単位		
	名称	記号	他のSI単位による表し方
平面角	ラジアン ^(b)	rad	1 ^(b)
立体角	ステラジアン ^(b)	sr ^(c)	1 ^(b)
周波数	ヘルツ ^(d)	Hz	1/s
力	ニュートン	N	m kg s ⁻²
圧力、応力	パスカル	Pa	N/m ²
エネルギー、仕事、熱量	ジュール	J	m ² kg s ⁻²
仕事率、工率、放射束	ワット	W	m ² kg s ⁻³
電荷、電気量	クーロン	C	s A
電位差(電圧)、起電力	ボルト	V	m ² kg s ⁻³ A ⁻¹
静電容量	ファラード	F	C/V
電気抵抗	オーム	Ω	m ² kg s ⁻³ A ⁻²
コンダクタンス	ジーメンス	S	A/V
磁束密度	ウェーバ	Wb	Vs
磁束密度	テスラ	T	Wb/m ²
インダクタンス	ヘンリー	H	kg s ² A ⁻¹
セルシウス温度	セルシウス度 ^(e)	°C	Wb/A
光照度	ルーメン	lm	cd sr ^(e)
放射性核種の放射能 ^(f)	ベクレル ^(d)	Bq	lm/m ²
吸収線量、比エネルギー分与、カーマ	グレイ	Gy	m ² s ⁻²
線量当量、周辺線量当量、方向線量当量、個人線量当量	シーベルト ^(g)	Sv	J/kg
酸素活性	カタール	kat	m ² s ⁻²

(a)SI接頭語は固有の名称と記号を持つ組立単位と組み合わせても使用できる。しかし接頭語を付した単位はもはやコヒーレントではない。

(b)ラジアンとステラジアンは数字の1に対する単位の特別な名称で、量についての情報をつたえるために使われる。実際には、使用する時には記号rad及びsrが用いられるが、習慣として組立単位としての記号である数字の1は明示されない。

(c)測光学ではステラジアンという名称と記号srを表し方の中に、そのまま維持している。

(d)ヘルツは周期現象についてのみ、ベクレルは放射性核種の統計的過程についてのみ使用される。

(e)セルシウス度はケルビンの特別な名称で、セルシウス温度を表すために使用される。セルシウス度とケルビンの単位の大きさは同じである。したがって、温度差や温度間隔を表す數値はどちらの単位で表しても同じである。

(f)放射性核種の放射能(activity referred to a radionuclide)は、しばしば誤った用語で“radioactivity”と記される。

(g)単位シーベルト(PV,2002,70,205)についてはCIPM勧告2(CI-2002)を参照。

表4. 単位の中に固有の名称と記号を含むSI組立単位の例

組立量	SI組立単位		
	名称	記号	SI基本単位による表し方
粘度	パスカル秒	Pa s	m ¹ kg s ⁻¹
力のモーメント	ニュートンメートル	N m	m ² kg s ²
表面張力	ニュートン毎メートル	N/m	kg s ⁻²
角速度	ラジアン毎秒	rad/s	m ⁻¹ s ⁻¹ =s ⁻¹
角加速度	ラジアン毎秒毎秒	rad/s ²	m ⁻¹ s ⁻² =s ⁻²
熱流密度、放射照度	ワット毎平方メートル	W/m ²	kg s ⁻³
熱容量、エンントロピー	ジュール毎ケルビン	J/K	m ² kg s ² K ⁻¹
比熱容量、比エンントロピー	ジュール毎キログラム毎ケルビン	J/(kg K)	m ² s ⁻² K ⁻¹
比エネルギー	ジュール毎キログラム	J/kg	m ² s ⁻²
熱伝導率	ワット毎メートル毎ケルビン	W/(m K)	m kg s ⁻³ K ⁻¹
体積エネルギー	ジュール毎立方メートル	J/m ³	m ¹ kg s ⁻²
電界の強さ	ボルト毎メートル	V/m	m kg s ⁻³ A ⁻¹
電荷密度	クーロン毎立方メートル	C/m ³	m ³ s A
表面電荷密度	クーロン毎平方メートル	C/m ²	m ² s A
電束密度、電気変位	クーロン毎平方メートル	C/m ²	m ² s A
誘電率	ファラード毎メートル	F/m	m ³ kg s ⁻⁴ A ²
透過率	ヘンリー毎メートル	H/m	m kg s ⁻² A ²
モルエネルギー	ジュール毎モル	J/mol	m ² kg s ⁻² mol ¹
モルエントロピー、モル熱容量	ジュール毎モル毎ケルビン	J/(mol K)	m ² kg s ² K ⁻¹ mol ¹
照射線量(X線及びγ線)	クーロン毎キログラム	C/kg	kg ⁻¹ s A
吸収線量率	グレイ毎秒	Gy/s	m ⁻² s ⁻³
放射強度	ワット毎メートル毎ステラジアン	W/sr	m ² kg s ⁻³ =m ² kg s ⁻³
放射輝度	ワット毎平方メートル毎ステラジアン	W/(m ² sr)	m ² m ² kg s ⁻³ =kg s ⁻³
酵素活性濃度	カタール毎立方メートル	kat/m ³	m ⁻³ s ⁻¹ mol

表5. SI接頭語

乗数	名称	記号	乗数	名称	記号
10 ²⁴	ヨータ	Y	10 ⁻¹	デシ	d
10 ²¹	ゼータ	Z	10 ⁻²	センチ	c
10 ¹⁸	エクサ	E	10 ⁻³	ミリ	m
10 ¹⁵	ペタ	P	10 ⁻⁶	マイクロ	μ
10 ¹²	テラ	T	10 ⁻⁹	ナノ	n
10 ⁹	ギガ	G	10 ⁻¹²	ピコ	p
10 ⁶	メガ	M	10 ⁻¹⁵	フェムト	f
10 ³	キロ	k	10 ⁻¹⁸	アト	a
10 ²	ヘクト	h	10 ⁻²¹	ゼット	z
10 ¹	デカ	da	10 ⁻²⁴	ヨクト	y

表6. SIに属さないが、SIと併用される単位

名称	記号	SI単位による値
分	min	1 min=60 s
時	h	1 h=60 min=3600 s
日	d	1 d=24 h=86 400 s
度	°	1°=(π/180) rad
分	'	1'=(1/60)°=(π/10 800) rad
秒	"	1"=(1/60)'=(π/648 000) rad
ヘクタール	ha	1 ha=1 hm ² =10 ⁴ m ²
リットル	L	1 L=1 l=1 dm ³ =10 ³ cm ³ =10 ⁻³ m ³
トン	t	1 t=10 ³ kg

表7. SIに属さないが、SIと併用される単位で、SI単位で表される数値が実験的に得られるもの

名称	記号	SI単位で表される数値
電子ボルト	eV	1 eV=1.602 176 53(14)×10 ⁻¹⁹ J
ダルトン	Da	1 Da=1.660 538 86(28)×10 ⁻²⁷ kg
統一原子質量単位	u	1 u=1 Da
天文単位	ua	1 ua=1.495 978 706 91(6)×10 ¹¹ m

表8. SIに属さないが、SIと併用されるその他の単位

名称	記号	SI単位で表される数値
バール	bar	1 bar=0.1MPa=100 kPa=10 ⁵ Pa
水銀柱ミリメートル	mmHg	1 mmHg≈133.322Pa
オングストローム	Å	1 Å=0.1nm=100pm=10 ⁻¹⁰ m
海里	M	1 M=1852m
ノット	n	1 n=100fm ² =(10 ⁻¹² cm) ² =10 ⁻²⁸ m ²
ノット	kn	1 kn=(1852/3600)m/s
ネバール	Np	SI単位との数値的な関係は、対数量の定義に依存。
デシベル	dB	

表9. 固有の名称をもつCGS組立単位

名称	記号	SI単位で表される数値
エルグ	erg	1 erg=10 ⁻⁷ J
ダイーン	dyn	1 dyn=10 ⁻⁵ N
ボアズ	P	1 P=1 dyn s cm ⁻² =0.1Pa s
ストークス	St	1 St=1cm ² s ⁻¹ =10 ⁴ m ² s ⁻¹
スチルブ	sb	1 sb=1cd cm ⁻² =10 ⁴ cd m ⁻²
フォート	ph	1 ph=1cd sr cm ⁻² =10 ⁴ lx
ガル	Gal	1 Gal=1cm s ⁻² =10 ⁻² ms ⁻²
マックスウェル	Mx	1 Mx=1G cm ² =10 ⁸ Wb
ガウス	G	1 G=1Mx cm ⁻² =10 ⁻⁴ T
エルステッド ^(a)	Oe	1 Oe≈(10 ³ /4)π A m ⁻¹

(a)3元系のCGS単位系とSIでは直接比較できないため、等号「≈」は対応関係を示すものである。

表10. SIに属さないその他の単位の例

名称	記号	SI単位で表される数値
キュリ	Ci	1 Ci=3.7×10 ¹⁰ Bq
レントゲン	R	1 R=2.58×10 ⁻⁴ C/kg
ラド	rad	1 rad=1cGy=10 ⁻² Gy
レム	rem	1 rem=1cSv=10 ⁻² Sv
ガンマ	γ	1 γ=1nT=10 ⁻⁹ T
フェルミ	f	1 フェルミ=1 fm=10 ⁻¹⁵ m
メートル系カラット	Torr	1 Torr=(101 325/760) Pa
標準大気圧	atm	1 atm=101 325 Pa
カロリ	cal	1 cal=4.1858J (15°Cカロリー), 4.1868J (ITカロリー), 4.184J (熱化学カロリー)
ミクロ	μ	1 μ=1μm=10 ⁻⁶ m

